VYSOKÉ UČENÍ TECHNICKÉ V BRNĚ

BRNO UNIVERSITY OF TECHNOLOGY

FAKULTA STROJNÍHO INŽENÝRSTVÍ
ÚSTAV STROJÍRENSKÉ TECHNOLOGIE

FACULTY OF MECHANICAL ENGINEERING
INSTITUTE OF MANUFACTURING TECHNOLOGY

VYSOKORYCHLOSTNÍ VRTÁNÍ PLECHŮ Z HLINÍKOVÝCH SLITIN

HIGH SPEED DRILLING OF ALUMINIUM PLATES

DIPLOMOVÁ PRÁCE
MASTER'S THESIS

AUTOR PRÁCE — Bc. LUKÁŠ PILNÝ
AUTHOR

VEDOUCÍ PRÁCE — prof. Ing. MIROSLAV PÍŠKA, CSc.
SUPERVISOR

BRNO 2011

Vysoké učení technické v Brně, Fakulta strojního inženýrství

Ústav strojírenské technologie
Akademický rok: 2010/2011

ZADÁNÍ DIPLOMOVÉ PRÁCE

student(ka): Bc. Lukáš Pilný

který/která studuje v **magisterském navazujícím studijním programu**

obor: **Strojírenská technologie (2303T002)**

Ředitel ústavu Vám v souladu se zákonem č.111/1998 o vysokých školách a se Studijním a zkušebním řádem VUT v Brně určuje následující téma diplomové práce:

Vysokorychlostní vrtání plechů z hliníkových slitin

v anglickém jazyce:

High speed drilling of aluminium plates

Stručná charakteristika problematiky úkolu:

Specifikace mechanizmu tvorby otřepů při procesu vrtání, přehled doporučených procesních parametrů a nástrojů. Experimentální vyhodnocení tvorby otřepů a vizuální jednotnosti vrtaných děr při vrtání 2 mm tenkých plechů ze slitiny A5205 vrtáky o průměru 1,8 – 2,2 mm. Analýza jednotlivých parametrů.

Cíle diplomové práce:

Specifikace mechanizmu tvorby otřepů při procesu vrtání, přehled doporučených procesních parametrů a nástrojů. Experimentální vyhodnocení tvorby otřepů a vizuální jednotnosti vrtaných děr při vrtání 2 mm tenkých plechů ze slitiny A5205 vrtáky o průměru 1,8 – 2,2 mm. Analýza jednotlivých parametrů.

Seznam odborné literatury:

1. SHAW, M.C. Metal Cutting Principles. Oxford University Press, 2nd ed., 2005, pp. 651, ISBN 0-19-514206-3.
2. AURICH, J. C., DORNFELD, D., ARRAZOLA, P. J., FRANKE, V., LEITZ, L., & MIN, S. (2009). Burrs-Analysis, control and removal
3. KO, S., & LEE, J. (2001). Analysis of burr formation in drilling with a new-concept drill. Journal of Materials Processing Technology, 113(1-3), 392-398.
4. LEOPOLD, J., SCHMIDT, G. (2004) Methods of Burr Measurement and Burr Detection. VDI-Berichte 1860:223-229.
5. TURKOVICH, V. Influence of very high cutting speed on chip formation mechanics, in: Proceedings of the 7th NAMRC, Society of Manufacturing Engineers, Dearborn, Michigan, 1979, pp. 241-247.
6. HAMADEA, R.F.ISMAILB, F. A case for aggressive drilling of aluminium, aDepartment of Mechanical Engineering, American University of Beirut (AUB), b Mechanical Engineering Department, University of Waterlo, July 2004
7. International Standard ISO 13715:2000, Technical drawings - Edges of undefined shape, Vocabulary and indications.

Vedoucí diplomové práce: prof. Ing. Miroslav Píška, CSc.

Termín odevzdání diplomové práce je stanoven časovým plánem akademického roku 2010/2011.

V Brně, dne 8.12.2010

L.S.

prof. Ing. Miroslav Píška, CSc.
Ředitel ústavu

doc. RNDr. Miroslav Doupovec, CSc.
Děkan fakulty

Abstract

Optimization of the metal drilling process requires creation of minimum amount of burrs and uniform appearance of the drilled holes. The goal was to understand the role of various key factors such as cutting conditions, clamping conditions and drill geometry on burr formation when 2 mm sheets of wrought aluminium alloy Al99.7Mg0.5Cu-H24, using 1.6 and 2 mm diameter drills, so that the burr formation could be minimized and an uniform hole surface obtained for a great number of holes drilled on a single workpiece.

This goal was approached by three subsequent investigations. First, an experimental test was performed to investigate the effect of cutting speed and feed per revolution, as the most recognized drilling parameters influencing burr formation, on the resulting burr size and drilled hole uniformity. Second, a vacuum clamping system, used to hold the aluminium sheet and restrict the space for burr formation at the drill exit, was constructed and tested for its influence on burr formation. Third, the effect of different drill geometries on burr formation and the uniformity of hole appearance was evaluated.

Results from the first experiment showed that burr height and width is reduced at both the entry and exit sides of a sheet when a higher cutting speed is used. With greater feed rates, it was found that burr height and width increase on both sides, with the exception of the height of burrs on the entry side, which may be minimally decreased. The second experiment showed that a properly designed vacuum clamp fixture can be used to significantly reduce exit-side burr formation. In the third experiment, a three flute drill with a properly constructed vacuum clamp was found to eliminate both entry and exit burrs, the demand on the uniform appearance of drilled holes was fulfilled as well as high productivity achieved. Such optimized process requiring no additional deburring results in a noticeable production cost reduction. Furthermore, recommendations for further research into improvements of the production process are made.

Keywords: Burr minimizing, burr, measurement, high speed drilling, vacuum clamping, hole uniformity

Rozšířený abstrakt

Úvod

Vrtání je nejpoužívanější obráběcí operace [5, 6], kterou se zhotovují nebo zvětšují již předvrtané díry. Vrtání je často použito jako hrubovací operace předcházející vyhrubování, vystružování a broušení, aplikovaných pro dosažení finálních rozměrů a požadované struktury povrchu vrtaných děr. Tento fakt jasně ukazuje, jak je vrtání a jeho optimalizace důležité v obráběcích procesích. Optimalizace procesu vrtání kovových materiálů zahrnuje, mimo jiné, minimální výskyt otřepů a vizuální jednotnost vrtaných děr.

Předmětem této diplomové práce byla optimalizace procesu vrtání pro výrobu mřížek reproduktorů určených pro luxusní automobily. Nejnovější design je vyroben z 2 mm tenkých plechů tvářené hliníkové slitiny Al99,7Mg0,5Cu - H24 v různých desénových variacích a otvory o průměru 0,8 až 2,2 mm rozmístěných dle přání zákazníka. Veškeré vrtané díly s frézovaným vnějším tvarem jsou následně anodizovány, pro dosažení povrchu odolnému proti poškrábání, a tvářeny do požadovaného finálního tvaru. Na povrch těchto mřížek jsou kladeny vysoké dekorativní požadavky. Jelikož po procesu vrtání a frézování následuje pouze anodizace bez jakékoliv přídavné operace, je velice důležité, aby vrtané otvory byly jednotného vzhledu, bez vad a otřepů. Projekt byl vypracován ve spolupráci Vysokého učení technického v Brně (VUT — Česká republika), Denmark technical university (DTU — Dánsko) a firmy Bang & Olufsen A/S (Dánsko).

Identifikace problémů

Otřepy

Během procesu vrtání, otřepy jsou tvořeny na hranách vrtaných otvorů z vstupní, stejně tak i výstupní strany vrtáku z materiálu obrobku (viz. Figure 1.2). Otřepy jsou tvořeny malým množstvím plasticky zdeformovaného materiálu obrobku, který je typicky tvrdší než materiál obrobku z důvodu deformačního zpevnění. Takovéto otřepy představují nepřijatelný defekt, vyžadující přídavné operace pro odstranění a následné leštění povrchu pro dosažení požadovaného dekorativního povrchu. Tyto přídavné operace jsou časově a finančně náročné, nepřidávající hodnotu finální součásti. Podle [14], náklady spojené s odstraněním otřepů pro vysoce precizní komponenty dosahují až 30 % výrobních nákladů a pro středně komplexní dílce v rozmezí 15 až 20 % z celkových výrobních nákladů. Mimoto, otřepy mohou způsobit malá řezná zranění dělníků při manipulaci, montáži a mnoho dalších problémů. Optimalizace a kontrola výrobního procesu je proto tou nejlepší strategií pro minimalizování či kompletní eli-

minaci tvorby otřepů. Tato kontrola procesu vyžaduje dobrou znalost ve všech výrobních stádiích, od konstrukce dílce skrze plánování výroby, s ohledem na mechanismus tvorby otřepů na obráběném dílci. Úspěšná kontrola a optimalizace všech stádii ve výrobním procesu může vést k produkci komponentů bez otřepů, splňující kvalitativní požadavky, nebo může vést k významnému snížení nákladů potřebných k odstranění vzniklých otřepů.

Vizuální jednotnost děr

Jelikož se samotná mřížka reproduktoru sestává z velkého počtu vrtaných děr (viz. Figure 1.4), jakýkoliv defekt způsobující nejednotný vzhled děr představuje nepřijatelný desénový defekt a tudíž vadný díl. Takovýto defekt byl ve společnosti interně nazván „star effect at hole entry“, představující lesknoucí se prstenec okolo hrany vstupní strany otvoru. V případě, že se takovýto defekt objeví u několika vrtaných děr, odraz světla od těchto děr je v porovnáním s rádně vrtanými dírami v odlišném směru, způsobující nejednotný vzhled vrtaného vzoru.

Cíle práce

Přestože kompletní eliminace tvorby otřepů během procesu vrtání může být nedosažitelná, jakákoliv redukce velikosti vzniklých otřepů může vést k snížení nákladů na nezbytnou přídavnou operaci pro jejich odstranění. Vizuální jednost vrtaných děr musí být dosažena společně s maximální možnou výrobní produktivitou.

Identifikace parametrů ovlivňující tvorbu otřepů

Mnoho různých parametrů a jejich vzájemné kombinace ovlivňují mechanismus tvorby otřepů (viz Figure 3.9). Předešlé studie zkoumající vliv různých parametrů pro jejich vliv na tvorbu otřepů při vrtání prokázaly, že hlavní ovlivňující parametry jsou posuv na otáčku, geometrie vrtáku a vlastnosti materiálu obrobku. Velikost vzniklých otřepů může být významně redukována vhodnou volbou těchto procesních parametrů.

Posuv na otáčku je nejčastěji měněný parametr mezi parametry ovlivňující tvorbu otřepů. Majoritní většina výzkumů ukázala, že vyšší posuv zapříčiňuje vznik většího objemu vzniklých otřepů. Toto je běžně vysvětlováno zvyšující se posuvovou silou s větším posuvem. Posuvová síla určuje objem materiálu obrobku, který podstoupí plastickou deformaci na výstupní straně vrtáku z materiálu obrobku a končí ve vyhnutí tohoto materiálu ve formě otřepů. Okolo 50 až 75 % posuvové síly pochází z příčného ostří vrtáku [6]. Tato centrální část na špici vrtáku neposkytuje dobré podmínky pro řezný proces, kvůli nepříznivé geometrii a velmi malé či nulové řezné rychlosti, a spíše poskytuje tvářecí proces. Pro minimalizaci tohoto jevu jsou aplikovány modifikace a redukce příčného ostří vrtáku. V dnešní době je na trhu dostupná široká škála geometrií vrtáků s modifikací příčného ostří, poskytující lepší samostředící vlastnosti, odvod tepla a mnoho dalších výhodných vlastností s ohledem na obráběný materiál.

Mechanismus tvorby otřepů byl shledán významně závislým na mezi kluzu a mezi pevnosti obráběného materiálu. Tyto materiálové vlastnosti se výrazně mění se vzrůstající teplotou [30]. Chlazení vede k menší tvářitelnosti materiálu obrobku, materiál se stává křehčím, vedoucím k redukci vzniklých otřepů. Způsob upnutí obrobku

také významně ovlivňuje výskyt otřepů. Redukce tvorby otřepů může být dosaženo skrze omezení deformace materiálu obrobku ve směru posuvové síly či omezení prostoru pro vznik otřepu.

Plánování experimentů

Výběr testovaných parametrů ovlivňujících tvorbu otřepů a jednotnost vrtaných děr byl založen na předchozích experimentálních výzkumech. Rozdílné procesní parametry, geometrie nástrojů a vliv upínacího systému byly vyhodnoceny pro nalezení vhodného řešení, jak minimalizovat tvorbu otřepů a pro zajištění vizuální jednotnosti vrtaných děr. Experimenty byly provedeny v následujících třech krocích:

- Přípravný test
- Testování upínacího systému
- Testování různých geometrií nástrojů

První test byl proveden za účelem nalezení mechanismu tvorby otřepů pro zkoumaný materiál, vyhodnocení vlivu řezných parametrů (posuvu na otáčku a řezné rychlosti) na tvorbě otřepů a ověření způsobilosti experimentálního vybavení pro následující testy.

V druhém experimentálním testu byl zkonstruován upínací systém poskytující omezení prostoru pro tvorbu otřepů na výstupní straně vrtání a jeho efektivnost byla vyhodnocena.

V posledním, třetím testu, byl pozorován vliv rozdílných geometrií vrtáků na tvorbu otřepů s použitím speciálního upínacího systému a stroje zamýšleného pro finální výrobu mřížek reproduktorů.

Měření byly provedeny pro řezné síly (posuvová síla a eventuálně moment), velikosti vzniklých otřepů (výška a šířka) a vizuální vyhodnocení jednotnosti vrtaných děr.

Experimentální aparatura

První (přípravný) test byl proveden na vertikální CNC frézce Cincinnati Sabre 750 s implementovaným elektrickým vysokorychlostním vřeteníkem HES-BT 40 H poskytujícím maximální otáčky n = 50 000 min^{-1} s omezeným výkonem (viz. Figure 6.2). Vrtaný 2 mm plech z hliníkové slitiny byl upnut přímo na dynamometr, bez podpory výstupní strany vrtáku z materiálu obrobku, a vrtán dvoubřitým vrtákem o průměru 1,6 mm s vybroušenou „split-point“ geometrií špičky o krátké délce vrtáku 4 mm. K chlazení byla použita 7 % vodou ředitelná emulze, aplikovaná v malém množství ručním rozstřikovačem. Řezné síly byly měřeny za použití dvoukomponentního piezoelektrického dynamometru KISTLER 9271A, vyhodnocující posuvovou sílu a kroutící moment, a zesilovačů měřeného signálu KISTLER 5051. Měřené signály byly následně digitalizovány a zaznamenány s využitím PC s programem LabView 8.0.

Druhý test, vyhodnocující efektivnost konstruovaného vakuového upínacího přípravku na redukci otřepů na výstupní straně vrtání, byl opět proveden na vertikální CNC frézce s implementovaným vysokorychlostním vřeteníkem, jako v prvním testu.

Rozdíl v experimentální aparatuře byl pouze ve smyslu upnutí obrobku, kde v předchozím prvním testu nebyla poskytnuta podpora obrobku z výstupní strany vrtání, zatímco použitý vakuový systém poskytl eliminaci prostoru pro tvorbu otřepů z výstupní strany vrtání na obrobku. Jako vakuové těsnění bylo užito 2 NBR O-kroužků umístěných v obdélníkových drážkách. Geometrie použitého vrtáku, chlazení a měřící aparatura byly totožné s předchozím, přípravným testem.

Třetí test zkoumající vliv rozdílných geometrií vrtáků byl proveden ve společnosti Bang & Olufsen z důvodů nedostatečného poskytovaného kroutícího momentu a výkonu elektrického vysokorychlostního vřetene použitého v předešlých testech. Touto cestou byla navíce zaručena opakovatelnost výsledků testu pro zamýšlenou aplikaci do výrobního procesu. Pro test bylo použito dvou vřetenové obráběcí centrum Chiron DZ 12K W, chlazení proudem 7 % vodou ředitelné emulze, 4 různých geometrií vrtáků o průměru 2 mm, tříkomponentního piezoelektrického dynamometru KISTLER 9257BA společně s PC vybavený programem DynoWare pro zobrazení a zaznamenání měřených sil. S ohledem na výsledky druhého provedeného testu, ukazující možnou eliminaci otřepů na výstupní straně vrtání v případě použití vhodně konstruovaného upínacího přípravku, bylo požito vakuového upínání s měkkým neoprenovým vakuovým těsněním umístěným v rybinových drážkách. Takováto konstrukce poskytla těsným kontaktem s upínacím přípravkem eliminaci prostoru pro tvorbu otřepů na výstupní straně vrtání obrobku.

Pracovní postup

V prvním testu byl testován vliv řezné rychlosti a posuvu na tvorbu otřepů a jednotnost vrtaných děr. V prvním experimentálním nastavení pro vyhodnocení vlivu řezné rychlosti bylo použito fixní hodnoty posuvu f = 0,035 mm, doporučeného výrobcem použitého vrtáku, a 5 různých řezných rychlostí (v_c = 80 až 221 m $\cdot$ min^{-1}, představující otáčky vřetene n = 16 000 až 44 000 min^{-1}). Oblast testovaných řezných rychlostí byla zvolena s ohledem na doporučení výrobce vrtáku pro minimální testovanou hodnotu a limitována možnostmi použitého experimentálního zařízení pro maximální hodnotu. Pro každou testovanou řeznou rychlost bylo provedeno 6 opakování (6 vrtaných děr). V druhém experimentálním nastavení pro vyhodnocení vlivu posuvu na tvorbu otřepů a jednotnost děr bylo použito fixní hodnoty řezné rychlosti a 5 různých posuvů na otáčku. Vzhledem k výsledkům měření sil z předešlého nastavení bylo rozhodnuto nepoužít elektrického vysokorychlostního vřeteníku pro toto nastavení, pro podezření z nedostatečného kroutícího momentu a výkonu zařízení pro vysoké posuvy. Proto bylo použito hlavního vřeteníku stroje s fixní hodnotou řezné rychlosti limitované možnostmi použitého stroje (v_c = 35 m $\cdot$ min^{-1}, představující otáčky vřetene n = 6 963 min^{-1}) a 5 různých posuvů (f = 0,035 až 0,150 mm). Vyhodnocení bylo provedeno s ohledem na měřené řezné síly, rozměry vzniklých otřepů na vstupní a výstupní straně vrtáku do/z obrobku a vizuální vyhodnocení jednotnosti vrtaných děr.

Pro vyhodnocení efektivnosti vakuového upínacího přípravku na eliminaci otřepů na výstupní straně vrtáku z obrobku bylo použito stejných řezných parametrů, jako v předchozím prvním testu. Následné porovnání výsledků získaných v prvním testu, bez vlivu upínacího přípravku, a tohoto testu s užitím vakuového upínání, umožnilo vyhodnocení vlivu upínacího přípravku na redukci otřepů na výstupní straně vrtání obrobku. Měření velikostí vzniklých otřepů bylo v tomto testu provedeno pouze pro

výstupní stranu, jelikož vstupní strana vrtáku na obrobku nebyla použitým upínacím přípravkem ovlivněna.

V třetím testu pro vyhodnocení vlivu 4 rozdílných geometrií vrtáků bylo použito 5 různých řezných rychlostí a 5 různých posuvových rychlostí. Pro nalezení optimálního nastavení pro výrobu vzhledem k utvořeným otřepům, maximální možné produktivitě a zkoumání výskytu defektů způsobujících nejednotný vzhled vrtaného vzoru bylo použito 22 kombinací z možných 25 kombinací řezné rychlosti a posuvové rychlosti. 3 kombinace byly před zahájením testu vyřazeny pro příliš velké či naopak příliš malé zatížení nástroje, poskytující nevhodné podmínky pro řezný proces. Oblasti testovaných řezných a posuvových rychlostí byly opět voleny vzhledem k doporučením výrobců vrtáků pro nejnižší testované podmínky a maximální hodnoty byly limitovány možnostmi použitého strojního vybavení pro dosažení maximální produktivity. Pro každou kombinaci řezných parametrů a každou testovanou geometrii vrtáku bylo vyvrtáno 200 děr pro důkladné vyhodnocení výskytů jakýchkoliv defektů v jednotnosti vrtaných děr. Přestože materiál testovaného obrobku obsahoval pouze minimální množství křemíku, tudíž poskytující minimální brusné opotřebení nástrojů, nejdůležitější nastavení řezných parametrů zajištujících maximální produktivitu (maximální vytížení stroje = max. otáčky spolu s maximálním posuvem) bylo testováno jako první nastavení pro veškeré testované geometrie vrtáků. Toto bylo provedeno pro eliminaci vlivu možného opotřebení nástroje, pro ostatní kombinace řezných parametrů bylo zvoleno náhodné pořadí. Vyhodnocení měřené posuvové síly a velikosti otřepů bylo provedeno pouze pro nastavení zajišťující vysokou produktivitu výroby, tudíž maximální řezné rychlosti (v_c = 226 m · min^{-1}, představující otáčky vřetene n = 35 969 min^{-1}) a 4 různých posuvů (f = 0,035 až 0,190 mm). Vizuální vyhodnocení vzniklých otřepů a defektů způsobujících nejednotný vzhled vrtaných děr byl proveden pro všechny vrtané vzorky.

Měření velikosti otřepů

Dle standardu ISO 13715 [15] je velikost otřepu definována pouze jednou hodnotou, jakožto odchylka od ideálního geometrického tvaru. Předchozí provedené experimentální studie ovšem prokázaly, že tloušťka plasticky zdeformovaného materiálu otřepů představuje důležitější roli v nákladech na odstranění otřepů v porovnání s jejich výškou [22]. Proto byly měřené rozměry otřepů zvoleny s drobnými úpravami dle návrhu z předešlé studie na výskytu otřepů v [22] a měřeny byly výšky, tloušťky a tloušťky kořene otřepů z vstupní, tak i výstupní strany vrtáku na obrobku. Tloušťka kořene otřepů představuje šířku plasticky zdeformované oblasti materiálu obrobku od povrchu vrtané díry.

Výška otřepů byla měřena za použití optického autofokusního mikroskopu (Alicona Infinite focus). Použití optického zařízení poskytuje měření otřepů, které nejsou deformovány kvůli kontaktu s měřidlem. Měřící princip tohoto zařízení je založen na variaci zaostření. Tento princip spojuje malé hloubky zaostření s vertikálním skenováním. Výsledkem tohoto skenování je kompletní 3D rekonstrukce skenovaného otřepu, umožňující rychlé a detailní měření zahrnující celý obvod vzniklého otřepu. Výhodou oproti použití profil-projektoru tkví v tom, že měření není zkresleno v případě výskytu malé přesahující části otřepů pocházející z místa oddělení tzv. „dril cap“ — materiálu obrobku vytlačeným na špičce vrtáku. Při použití profil-projektoru by tato nerepresen-

tativní malá část otřepu byla vyhodnocena jako maximální hodnota celého vzniklého otřepu. Při zahrnutí celého obvodu otřepů v měření lze vyhodnotit representativní výšku otřepů s povšimnutím přesahující malé části a eliminovat tak zkreslení celého měření.

Tloušťky otřepů bylo rozhodnuto měřit za použití optického souřadnicového zařízení s automatickou detekcí hran založenou na přechodu světlé do tmavé oblasti. Toto měření bylo provedeno v kolmém směru na měřený vzorek, vyhodnocující aktuální vrtaný průměr otvoru a průměry hran vzniklých otřepů. 3D rekonstrukce vzniklého otřepu z předchozí strategie měření pro výšku otřepů poskytuje pouze vnější povrch, ideální pro vyhodnocení výšky. Ale pro vyhodnocení tloušťky je nezbytné do měření zahrnout vrtaný průměr. V případě, že je otřep vyhnut v kuželovitém tvaru způsobeném vibrací vrtáku, měření na 3D rekonstrukci vnějšího povrchu by bylo zkresleno. Další výhodou této měřící strategie je rychlost díky automatické detekci hran a zahrnutí celého obvodu otřepu, měřením průměrů hran otřepů.

Závěry a shrnutí výsledků z experimentů

Měřená data z prvního testu prokázala, že výška i tloušťka otřepů z vstupní i výstupní strany vrtání na obrobku byla redukována s použitím vyšší řezné rychlosti. Naopak, se zvyšujícím posuvem se rozměry vzniklých otřepů zvětšovaly po určitou maximální hodnotu, kde byly stabilizovány a nadále nenarůstaly i přes nadále zvyšující se posuv. Variace ve výsledných rozměrech utvořených otřepů byla redukována se zvyšující řeznou rychlostí, vedoucí ke stabilizaci procesu. Z měřené posuvové síly byl viděn zřejmý efekt zvyšující se teploty řezného procesu na snižující pevnost materiálu obrobku, vyžadující menší řezné síly při použití vyšších řezných rychlostí. Maximální kroutící moment a výkon elektrického vysokorychlostního vřeteníku byl shledán nedostatečným pro následující testy.

Druhý provedený test odhalil, že vhodně konstruovaný upínací přípravek může významně redukovat tvorbu otřepů na výstupní straně vrtání na obrobku. Použité O-kroužky jako vakuové těsnění byly prokazatelně nedostatečně stlačeny, poskytující vůli mezi vrtaným plechem a upínacím přípravkem a tudíž prostor pro tvorbu otřepů.

V třetím, posledním testu vyhodnocujícím vliv rozdílných geometrii vrtáků byl vrták mající 3 břity viděn jako překonávající zbylé testované vrtáky, jak ve vyžadovaných řezných silách během vrtání, tak i velikosti vzniklých otřepů. Za použití vhodně konstruovaného vakuového upínacího přípravku s použitým měkkým neoprenovým vakuovým těsněním a rybinových drážek pro udržení těsnění v drážce i při opětovném upínání, maximální možné řezné rychlosti vzhledem k možnostem stroje a vysokém posuvu zajišťujícím vysokou produktivitu, bylo dosaženo eliminace otřepů z obou stran vrtaného plechu a zajištění uniformity vrtaných děr.

Defekt způsobující tzv. „star effect at hole entry“ reprezentovaný lesknoucím se prstencem okolo obvodu díry z vstupní strany vrtání na obrobku byl vyhodnocen jako způsobený kuželovým defektem na vstupní straně otvoru. Tento defekt byl způsoben vyhnutím vrtáku z osy vrtání při počátečním kontaktu vrtáku s povrchem obrobku při iniciaci vrtání a může být eliminován použitím krátkých vrtáků, vysokých posuvů a použitím vrtáků s dobrou samostředící geometrií.

Hlavní závěr a aplikovatelnost v praxi

Použitím vrtáku s 3 břity, vhodně konstruovaným upínacím přípravkem, aplikovaným vydatným chlazením 7 % vodou ředitelné emulze a následujících řezných parametrů bylo dosaženo eliminace otřepů z obou stran vrtaného plechu hliníkové slitiny Al99,7Mg0,5Cu-H24: řezná rychlost v_c = 226 m $\cdot$ min^{-1}, za použití 2 mm vrtáku představující otáčky vřetene n = 36 000 min^{-1}, posuv f = 0,190 mm. Požadavky na jednotný vzhled vrtaných děr byly splněny společně s dosažením maximální možné produktivity pro použité 2 vřetenové obráběcí centrum. Takovýto optimalizovaný proces vrtání nevyžaduje žádnou přídavnou operaci pro odstranění otřepů a poskytuje významnou redukci v nákladech na produkci vyráběného produktu mřížek reproduktorů.

Klíčová slova

Minimalizace otřepů, otřepy, měření, vysokorychlostní vrtání, vakuové upínání, vizuální jednost otvorů

REFERENCE

PILNÝ, Lukáš. *Vysokorychlostní vrtání plechů z hliníkových slitin: Diplomová práce*. Brno: Vysoké učení technické v Brně, Fakulta strojního inženýrství, 2011. 128 s., 10 příloh. Vedoucí práce prof. Miroslav Píška CSc.

STATEMENT

I declare that the present diploma thesis with its name Vysokorychlostní vrtání plechů z hliníkových slitin was carried out only by me with the help of literature and sources stated in the reference list which is a part of this diploma thesis.

27. 5. 2011 .....

Bc. LUKÁŠ PILNÝ

ACKNOWLEDGEMENT

I am really thankful to my supervisor prof. Miroslavovi Píškovi for allowing me to carry out my master thesis abroad and fruitful discussions concerning the topic. Thanks to Brno University of Technology, my home university, for the international exchange program and financial support during that time.

Special thanks to prof. Leonardo De Chiffre for being my project advisor at Technical University of Denmark, guidance, discussions and for giving me the great opportunity of this interesting project at DTU, in cooperation with the company Bang & Olufsen A/S.

Thanks to M. Sc. Morten Frank Villumsen, technology specialist from Bang & Olufsen A/S, for his constant aid and advices, for being available for me and providing me the great experience at international company. Also thanks to the company Bang & Olufsen A/S for supporting me with material and tools for the experimental work.

Great thanks are due to the staff at DTU. To laboratory engineer Mr. Peter Sanderhoff for helping me with constructing of the vacuum clamping system and regulation, drilling force measurements and providing me with the necessary accessories for the project. To Mr. Lars Peter Holmbæck for practical guidance with the experimental work at the machining laboratory. I also thank to technician Mr. Jakob Rasmussen for his guidance with measuring instruments and to Mr. Rene Sobiecki for the discussions dealing with the measurements.

Contents

Chapter 1

Introduction

1.1 Background and motivation

This project was done in cooperation with the company Bang & Olufsen a/s, which is world renowned for its distinctive range of quality audio, video and multimedia products. The company has an important role in the automotive audio market in partnership with world-renowned car manufacturer BMW, Mercedes-AMG, Audi and Aston Martin.

Figure 1.1: Bang & Olufsen music speakers system integrated in BMW 6-Series Coupé [2].

The work done in this thesis was aimed on the production of sound speaker grilles by a drilling process. Demand on sound system for exclusive cars is constantly increasing. Aluminium is used as a design feature to express excellence in high-end audio products. The surface of the parts is very essential in expressing this. The newest grilles design is made of two millimetres thin aluminium plates in a myriad

of designs available with custom-made hole patterns. The grilles have high demands on the decorative finish. It is therefore very important that the holes are burr free and uniform. All parts with surfaces produced by drilling and milling of outer shape are subsequently anodized in order to obtain scratch-resistant surface, and subsequently formed into desired final shape. The metal cutting processes such as drilling and milling produce surfaces without any additional after-treatment operation other than the anodizing process. Therefore it is of utmost importance that surface errors are reduced to an absolute minimum.

1.2 Problem identification

Burrs

During the drilling process, burrs form on both the hole entry and exit side as a result of plastic deformation of the workpiece material. Burrs consist of small amount of attached material that protrude from the entry and exit surface around the drilled hole. The entry burr is usually of smaller size than the exit burr. An illustration of burr formation during drilling process is shown in Figure 1.2.

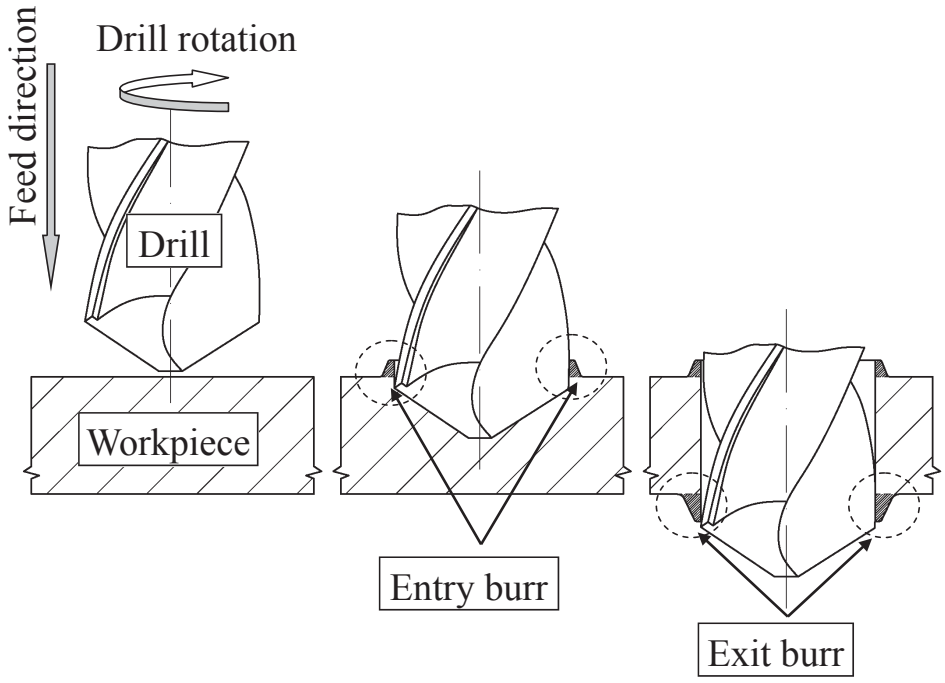

Figure 1.2: Entry and exit burr formation during drilling process.

These unwanted burrs formed are typically harder than the original workpiece material because of strain-hardening effect [3], making difficulties with possible removing by subsequent anodizing process. The anodizing process is not used as deburring operation, but it is applied in order to gain scratch-resistant surface on the workpieces. However, small burr volume can be removed in this way. These hardened burrs represent inadmissible surface defect requiring an additional deburring processes for removing, which are very time consuming, costly and non-value-adding operations. Moreover the burrs can cause small injuries of assembly

workers through cuts and many other problems. See Figure 1.3 for a photograph of burrs on a drilling exit side of the workpiece.

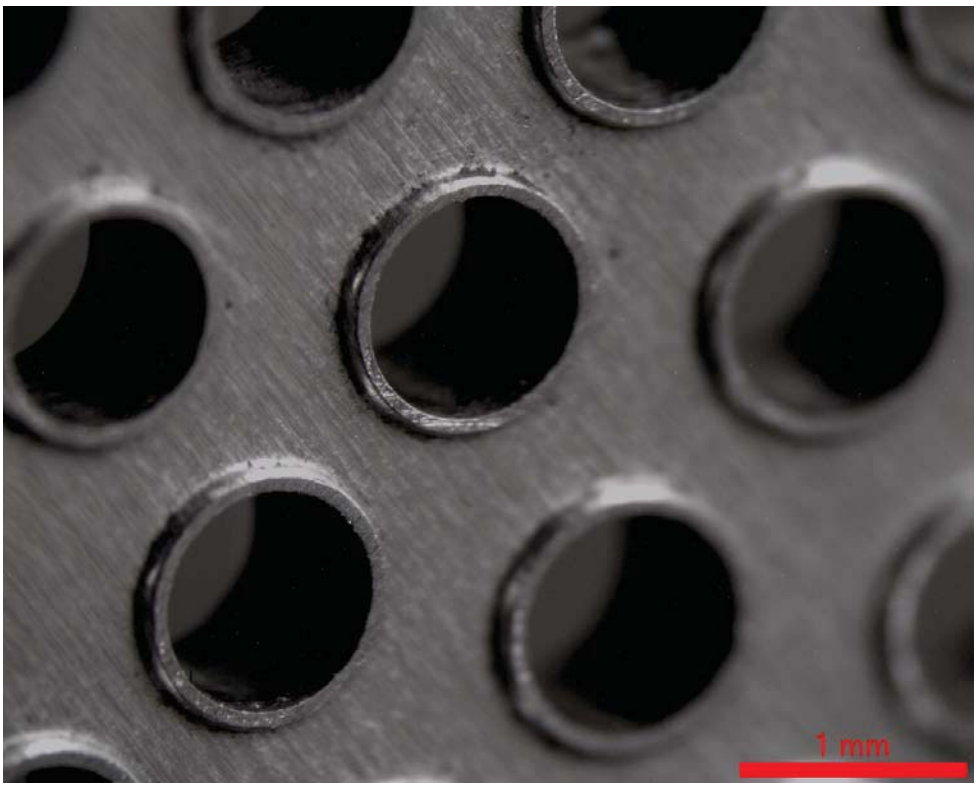

Figure 1.3: Hole exit burrs.

Uniformity of the holes drilled

Since one part of the sound speaker grille contains a great number of holes drilled, any defect in hole quality resulting in different appearance represents non-permissible design defect. Such a defect was experienced at the company and internally called, hereinafter, "Star effect at hole entry". This defect presents a shiny ring around the circumference of the hole entry. If such a defect appears at a few holes among the holes drilled, it causes different light reflection than other holes resulting in non-uniform hole pattern appearance.

1.3 Project goals

Although it may not be attainable to eliminate burr occurence completely, any reduction in burr size could reduce expenses on deburring operations. Or else, even to eliminate the need for any deburring operation in case that the proportion of burr formed can easily and completely be removed by subsequent anodizing operation in order to reach decorative surface finish. The uniformity of the hole pattern drilled have to be gained at the same time. Keeping this ultimate goal in mind, the following items are of interest to the present thesis:

- Reduction of hole entry and exit burrs
- Uniform appearance of the holes drilled
- Drilling time reduction
- Selection of processes/methods for further study

Figure 1.4: Bang & Olufsen speaker from a 2008 Audi S5 [4].

1.4 Thesis outline

In the interest of gaining necessary background knowledge about drilling operation, literature survey on drilling is presented in Chapter 2. Chapter 3 details burr formation mechanisms and lists an overview of previous researches pertinent to the project goals listed above. To draw meaningful conclusions from the experimental data, the statistical approach of design and analysis of experiments is briefly introduced in Chapter 4. Chapter 5 describes a planning of the experimental work, goals and approaches of individual tests, and workpiece material used during the tests. The experimental work investigating the influence of process parameters recognized as the most influencing burr formation, according to literature survey (cutting speed and feed per revolution), is described in Chapter 6. Subsequent Chapter 7 describes work done to construct clamping system, in order to restrict the room for burr formation at hole exit side, and to evaluate its influence. Chapter 8 presents an investigation on different tool geometries in the interest of gaining project goals. The last Chapter 9 summarizes the key conclusions of the project and lists recommendations for future work to be done.

Chapter 2

Literature survey on drilling

The following literature survey was conducted in order to gain necessary background knowledge about the drilling operation. This chapter deals with introduction of the drilling operation in general, drilling characteristics, presents twist drill geometry investigation as the representative and widely used drilling tool, review recommended parameters and an overview of the twist drill materials.

2.1 An Introduction to drilling

Drilling is a highly efficient machining method by cutting, in order to produce or enlarge holes by means of single or multi-edged tools called drill. The cutting tool, the workpiece, or both may rotate with tool generally being fed.

The fact that drilling is by far the most common machining operation [5, 6] shows clearly how important the operation is in metal cutting. Drilling is frequently preliminary roughing operation to reaming, boring or grinding to meet final dimensions and surface finish of the holes produced. While modern drilling tools provide to solid drilling being carried out in a single operation without previous drilling of centre and pilot holes and to a hole quality where subsequent machining to improve accuracy and surface texture often is eliminated. With today's tools, tolerances of IT9 can be obtained, which is sufficient in most of the finishing operations [5].

Table 2.1: Capabilities of drilling and boring operations[7]

	Diameter range	Hole depth/ diamater [mm]	
Tool type	[mm]	Typical	Maximum
Twist	0.5–150	8	50
Spade	25–150	30	100
Gun	40–250	100	300
Trepanning	40–250	10	100
Boring	3–1200	5	8

Several different drilling methods exist, including conventional, deep hole, and small-hole drilling. There is a wide variety of drill types and geometries, when the most common are helically fluted twist drills with various tip geometries. In present

case of drilled hole range 0.8 to 2.2 mm, the twist drill is used exclusively [5, 6, 7] (for the overview of drilling tools depending on drilled diameter see Table 2.1). For this reason, following sections in the present chapter are only dealing in more detail with the twist drill geometry.

2.2 Drilling characteristics

The primary cutting movement is rotational, usually performed by the tool. Secondary cutting movement is rectilinear, in the feed direction, usually also by means of the tool.

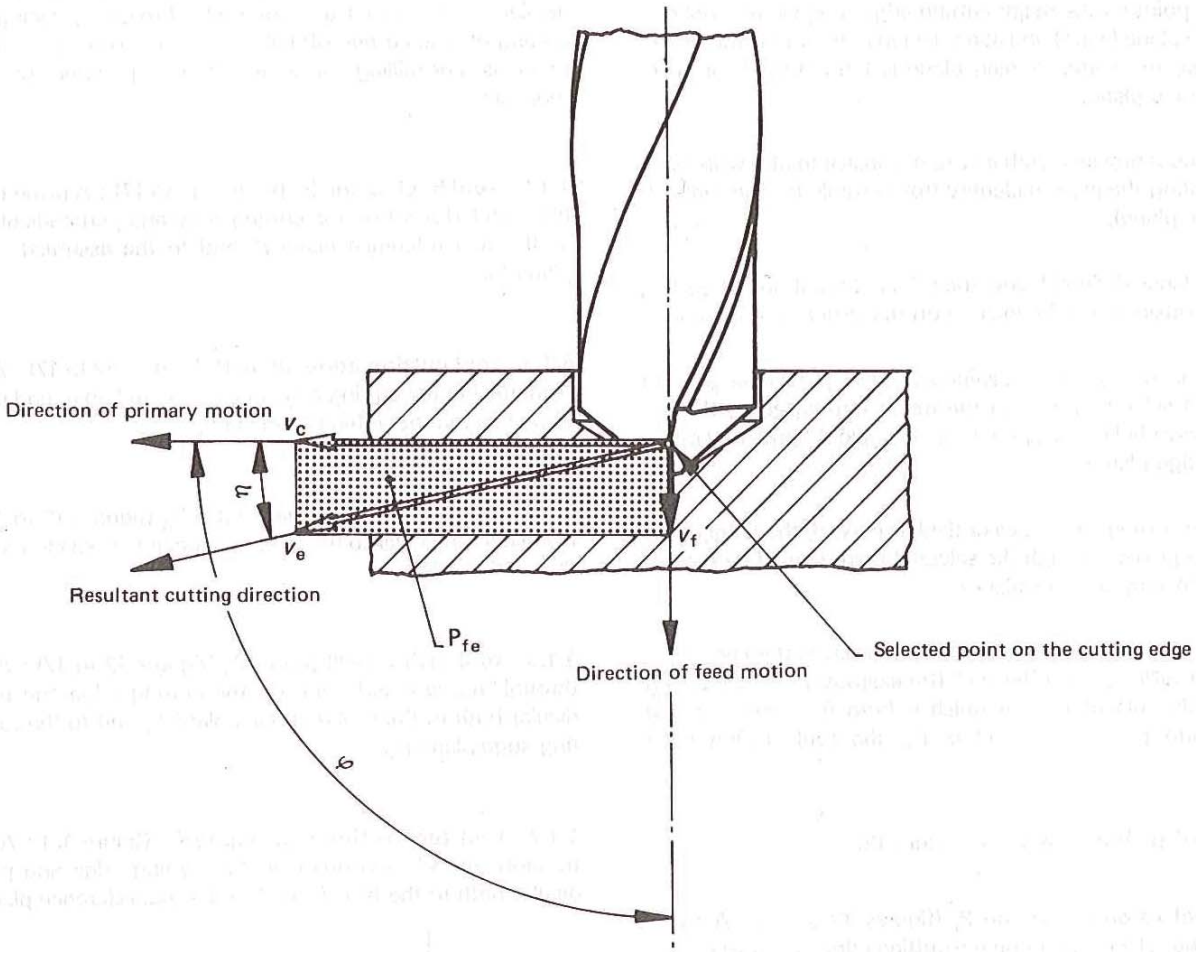

Figure 2.1: Tool and workpiece motions — twist drill[8].

To each point on the cutting edge of the tool, depending on the distance from the rotational axis D_i [mm] and revolutions of the tool n [min^{-1}], corresponds a different peripheral speed v_{ci}, and is determined by:

$$v_{ci} = \frac{\pi \cdot D_i \cdot n}{1000} \qquad [\mathrm{m \cdot min^{-1}}] \tag{2.1}$$

Hence, the actual peripheral speed varies along the cutting edge of the tool point from zero to a maximum value measured on the outer drill diameter, and it is called by a term cutting speed v_c, which is widely used in practice, as a single value defined

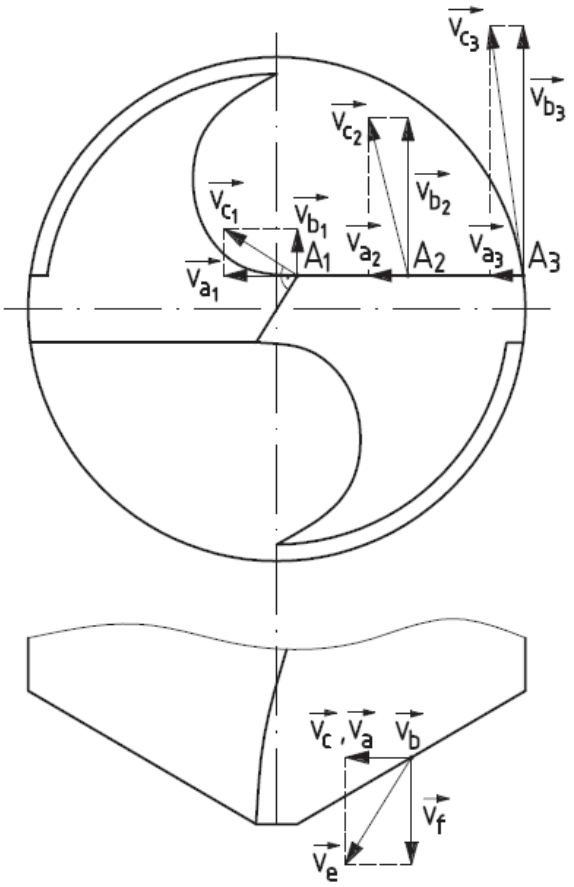

Figure 2.2: Directions of the primary and secondary movement when drilling with two-flute twist drill[9].

by:

$$v_c = \frac{\pi \cdot D \cdot n}{1000} \quad [\text{m} \cdot \text{min}^{-1}] \tag{2.2}$$

Where D [mm] is drill diameter.

The rectilinear speed of the tool motion is defined by the term feed speed v_f, which is determined by revolutions of the tool n [min^{-1}] and feed of the drill f [mm]:

$$v_f = \frac{f \cdot n}{1000} \quad [\text{mm} \cdot \text{min}^{-1}] \tag{2.3}$$

Since the drill can have multiple edges, the feed per tooth (edge) is defined as:

$$f_z = \frac{f}{z} \quad [\text{mm}] \tag{2.4}$$

Where z [-] designates the number or cutting edges of the tool.

Cutting width or radial cutting depth a_p:

$$a_p = \frac{D - d}{2} \quad [\text{mm}] \tag{2.5}$$

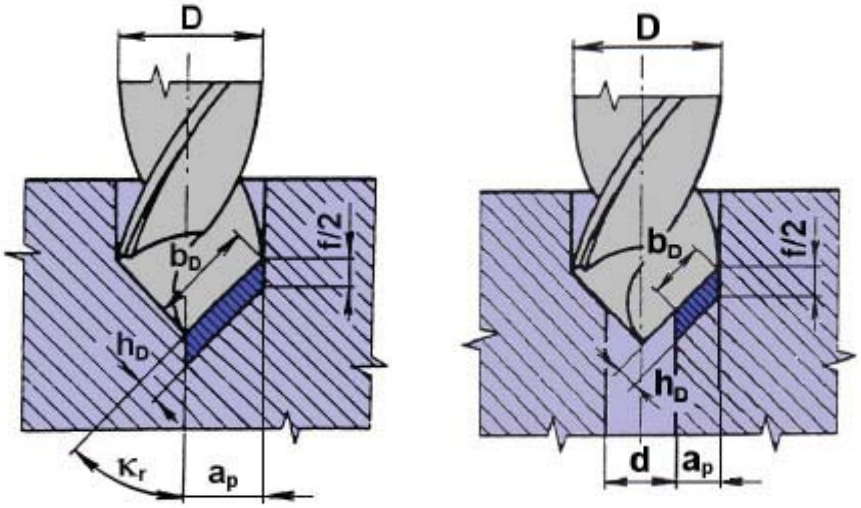

Figure 2.3: Geometrical elements of the undeformed chip: in plain drilling (left), in secondary drilling (right)[9].

Thickness of the undeformed chip h_d to be removed by each lip:

$$h_D = f_z \cdot sin\kappa_r = \frac{f}{2} \cdot sin\kappa_r \qquad \text{[mm]} \tag{2.6}$$

Undeformed chip width b_D in plain drilling:

$$b_D = \frac{D}{2 \cdot sin\kappa r} \qquad \text{[mm]} \tag{2.7}$$

The total transverse cross-sectional area of the undeformed chip in drilling:

$$A_D = h_d \cdot b_D = \frac{(D \cdot f)}{4} \qquad \text{[mm}^2\text{]} \tag{2.8}$$

Undeformed chip thickness b_D in secondary drilling:

$$b_D = \frac{(D - d)}{2 \cdot sin\kappa_r} \qquad \text{[mm}^2\text{]} \tag{2.9}$$

Where d [mm] is diameter of primary hole antecedent to secondary drilling (see Figure 2.3).

The total cross-sectional area of undeformed chip in secondary drilling:

$$A_D = \frac{(D - d) \cdot f}{4} \qquad \text{[mm}^2\text{]} \tag{2.10}$$

Drilling time

Drilling time is determined by:

$$t = \frac{L}{f \cdot n} \qquad \text{[min]} \tag{2.11}$$

Where: L – total drill travel [mm], f – feed [mm], n – revolutions of the tool [min^{-1}]

The length of drill travel can be expresses by:

$$L = l_a + l_o \qquad \text{[mm]} \tag{2.12}$$

Where: l_a – minimum length of approach, l – length of the drilled hole (cutting length) [mm], l_o – overrun (see Figure 2.4 for the sketch with description)

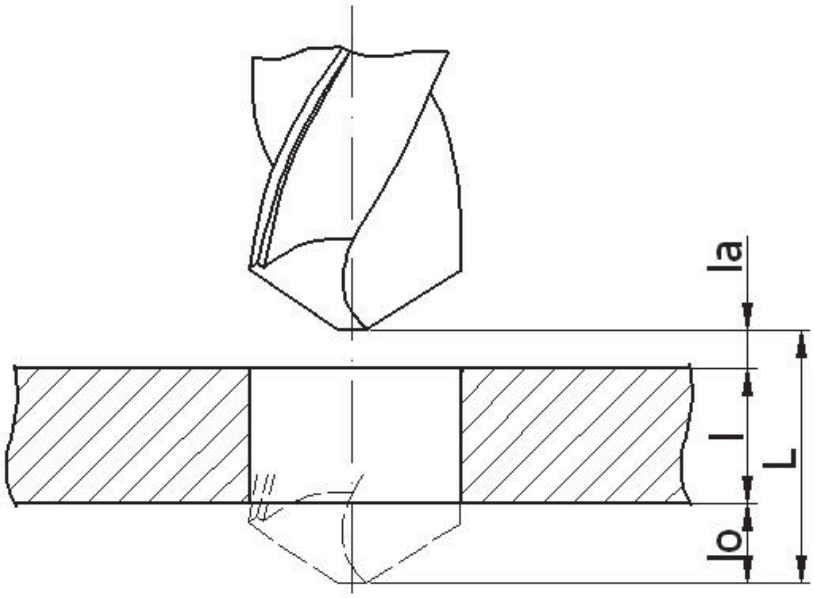

Figure 2.4: Tool approach, overrun and cutting length.

2.3 Twist drill description

As previously mentioned, the most common drilling tool is helically fluted twist drill with various tip geometries. In present case of drilled hole range 0.8 to 2.2 mm, the twist drill is used exclusively [5, 6, 7] (for the overview of drilling tools depending on drilled diameter see Table 2.1). For this reason, following sections in the present chapter are only dealing in more detail with the twist drill geometry.

The twist drill is a complex cutting tool with one or more cutting edges designed to produce identical chips and one or more helical or straight flutes for admission of coolant and passage of chips. Four major actions take place at the point of a drill:

- A small hole is pierced by the rotating web (chisel edge)
- Chips are formed by rotating cutting edges (cutting lips)
- Chips are evacuated out of the hole by a screw conveyor in the form of flutes provided in the drill
- The drill is guided in the hole by the margins

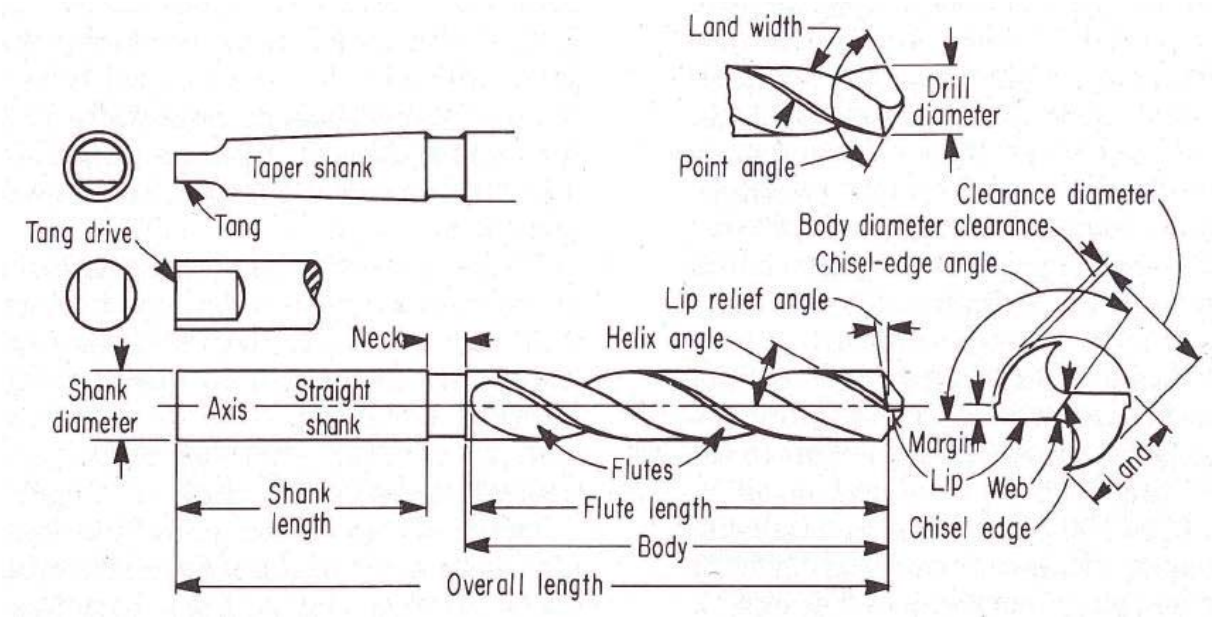

Figure 2.5: Drill nomenclature [10].

The geometry provided on a drill (Figure 2.5) represents a compromise of several conflict requirements as follows:

- A small web to reduce feed force (thrust) on the drill but a large web for greater resistance to chipping and torsional rigidity
- Large flutes to provide space for chip evacuation but small flutes in the interest of torsional rigidity
- Great helix angle to quickly remove chips but a decrease in helix angle in the interest of greater strength of cutting edges

The significant drill parameters from the analytical point of view are:

- Point angle $(2\kappa_r)$
- Helix angle (δ)
- Web thickness (w)
- Clearance angle (α)

Drill point geometry is very complicated inasmuch as the quantities of interest vary with radial position across the cutting edge.

Helix angle (δ)

A helix angle without any additional specifications refers to the helix angle at the drill circumference and varies with the radius (r) to any particular point on the cutting edge of the drill (see Figure 2.6). The quantity depends upon the workpiece material to be drilled and drilling method.

Conventional drills have helix angles (25 to 33°). High helix angle — fast spiral (35 to 40°) is designed for drilling deep holes in materials having low tensile strength, such as aluminium, magnesium, copper, die cast metals, some plastics and soft steels and free machining brasses and bronzes. Low helix angle — slow spiral (15 to 20°) is made for drilling plastics, brass and is also successful in applications for shallow drilling of some aluminium and magnesium alloys. The wide, ground and (or) polished flute surface assists in clearing chips from the holes.

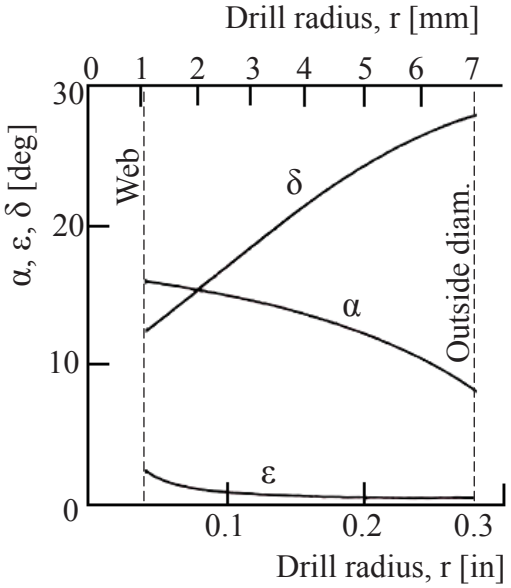

Figure 2.6: Variation of helix angle δ, clearance angle α, and feed angle ε, across the cutting edge of a representative 14.3 mm diameter drill. Helix angle, $28°$; clearance angle, $8°$; point angle $118°$; chisel edge angle, $120°$; web thickness, 2.03 mm, feed rate, 0.23 mm [10].

The helix angle has the greatest influence at the periphery of the drill (see Figure 2.6). An increase in helix angle causes a great increase in both γ_n and γ_e at the periphery of the drill and a smaller increase near the centre. Therefore increased helix angle results in freer cutting but in less support all across the cutting edge particularly at the drill circumference. A large helix angle with small point angle having thin web would be indicated for weak materials and the reverse for strong metals.

Point angle $(2\kappa_r)$

Point angle or cutting edge angle (κ_r) also depends on workpiece material to be drilled. Recommended quantities for aluminium and its alloys when HSS drills used vary in range of 90 to 140 ° among different literatures. For general recommendation for different materials to be drilled see Table 2.2. Commonly used conventional twist drills have point angle of 120°. When elongation and toughness of the workpiece material become large, the point angle is designed to be bigger to facilitate chip ejection. For AL alloy is the point angle designed to be 140 to 170° according to [11]. When increase in point angle, the effective rake angle is increased near the drill centre with corresponding amount to the normal rake angle. This provides freer cutting at the point but less support at the cutting edge. The much smaller change at the periphery

of the drill leads to slightly stronger edge but slightly greater forces. Therefore, a small point angle would be indicated for the drilling of softer metals such as aluminium alloys, where support of the cutting edge can be sacrificed in order to decrease forces at the periphery. Drills with flatter points (135 to 140°) are generally used to produce holes in harder, tougher materials, and they usually minimize burring [6].

There are many various drill point geometries in order to reduce forces, wear, friction and heat generation for specific workpiece materials to be drilled, closely detailed in Section 2.4.

Table 2.2: General recommendations for drill geometry for High-speed Twist drills [7].

Workpiece material	Point angle [deg]	Lip–relief angle [deg]	Chisel–edge angle [deg]	Helix angle [deg]	Point
Aluminum alloys	90–118	12–15	125–135	24–48	Standard
Magnesium alloys	70–118	12–15	120–135	30–45	Standard
Cooper alloys	118	12–15	125–135	10–30	Standard
Steels	118	10–15	125–135	24–32	Standard
High-strength steels	118–135	7–10	125–135	24–32	Crankshaft
Stainless steels, low strength	118	10–12	125–135	24–32	Standard
Stainless steels, high strength	118–135	7–10	120–130	24–32	Crankshaft
Heigh-temp. alloys	118–135	9–12	125–135	15–30	Crankshaft
Refractory alloys	118	7–10	125–135	24–32	Standard
Titanium alloys	118–135	7–10	125–135	15–32	Crankshaft
Cast irons	118	8–12	125–135	24–32	Standard
Plastics	60–90	7	120–135	29	Standard

Clearance angle (α)

The clearance angle at the centre of a drill is considerably greater than the value at the periphery of the drill and it may be as much as 100 %. The matter of clearance angles of the drills is in that a drill is fed downward upon the cut surface along a spiral path which inclines the feed angle (ε) and the effective rake angle on engagement (γ_e) will increase:

$$\gamma_e = \gamma + \varepsilon \quad \text{[deg]} \tag{2.13}$$

Whereas the effective clearance angle α_e on engagement is reduced.:

$$\alpha_e = \alpha - \varepsilon \quad \text{[deg]} \tag{2.14}$$

The feed angle is seen to play rather insignificant role when normal drilling conditions are used (see Figure 2.6), and becomes to be important only on large drills and drills that are fed with abnormally high feed rates. The feed angle in terms of the feed per revolution at any point on the cutting edge at radius r of the drill may be obtained as:

$$\varepsilon = tang^{-1}\frac{f}{2\pi r} \quad \text{[deg]} \tag{2.15}$$

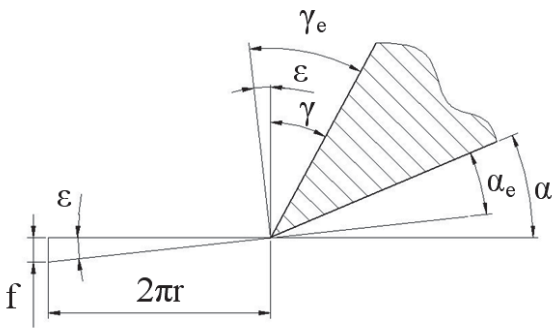

Figure 2.7: Feed angle during cutting.

With increased feed, the feed angle ε increases and the effective clearance angle is reduced. This means that the clearance angle should increase from the periphery towards the centre of the drill to avoid abrasion between the tool and the walls of the hole. The quantity and distribution along the cutting edge depends on type of grinding of the drill point (see Figure 2.8). For small drill diameters either a plain flank grinding or a cylindrical flank grinding is widely used. These grinding methods are the simplest but their disadvantage is decreasing clearance angle towards the centre of the drill. The most widely used grinding method is cylindrical one. Axis and top of the cylinder are situated in a way to obtain smaller radius of the flank and thereby greater clearance angle. Helical flank grinding is performed by simultaneous rotational movement of the drill and axial movement of grinding wheel, providing favourable clearance angle close to the centre of the drill. This method provides better centring and smaller feed force to the drill [9].

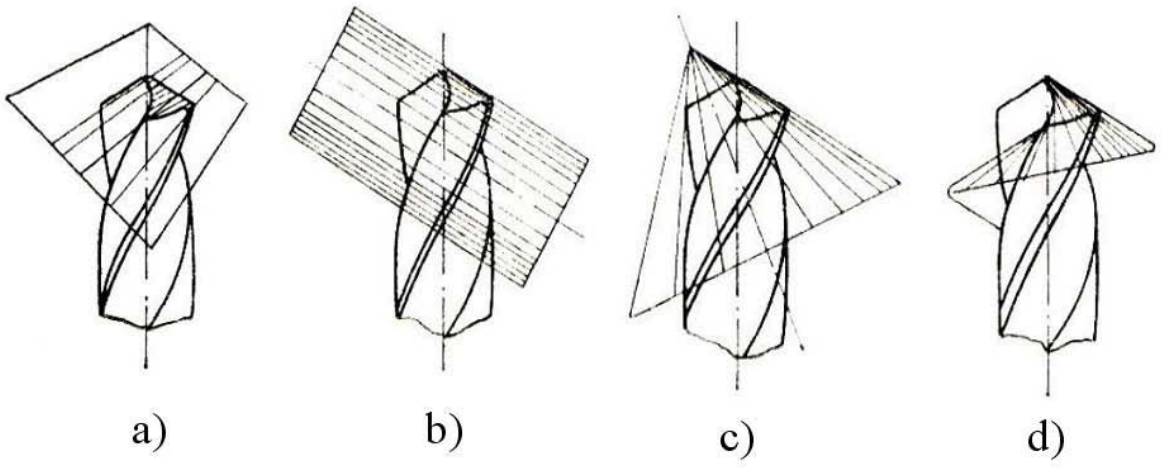

Figure 2.8: Point grinding methods for twist drill: a) Plain flank grinding, b) Cylindrical flank grinding, c) Conical flank grinding, d) Helical flank grinding [9].

The inclination angle (λ_s) (for tool angles description see Appendix A) is seen to increase towards the centre of the drill, while the normal rake angle (γ_n) decreases and even assumes negative values (see Figures 2.10, 2.9). Nevetheless, the effective rake angle (γ_e) does not become negative as a consequence of the large inclination angles near the centre of the drill. The action of the drill near the web might be described as

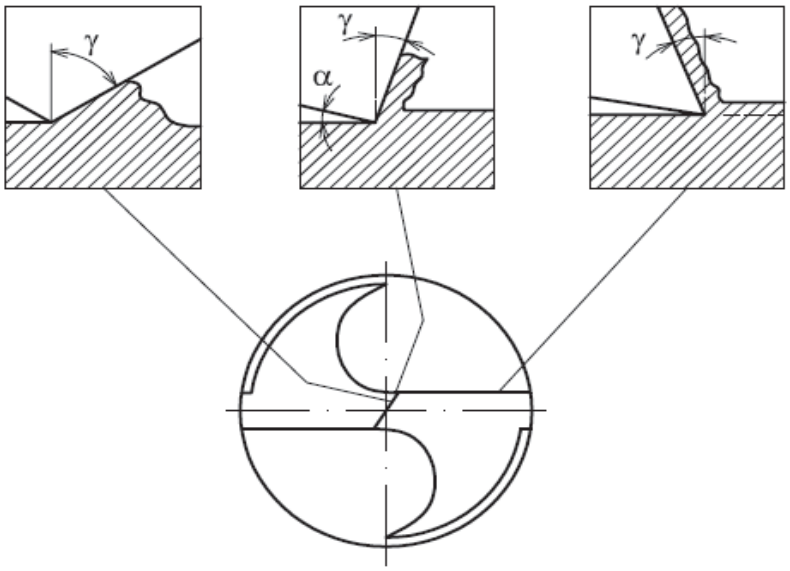

Figure 2.9: Chip formation depending on a rake angle along the cutting edge of the drill [6].

slicing action due to large inclinations. The support at the cutting edge varies inversely with magnitude of γ_n and is seen to be greatest near the point of the drill. This is favourable since the action at its very centre might rather be described as extrusion that cutting [10].

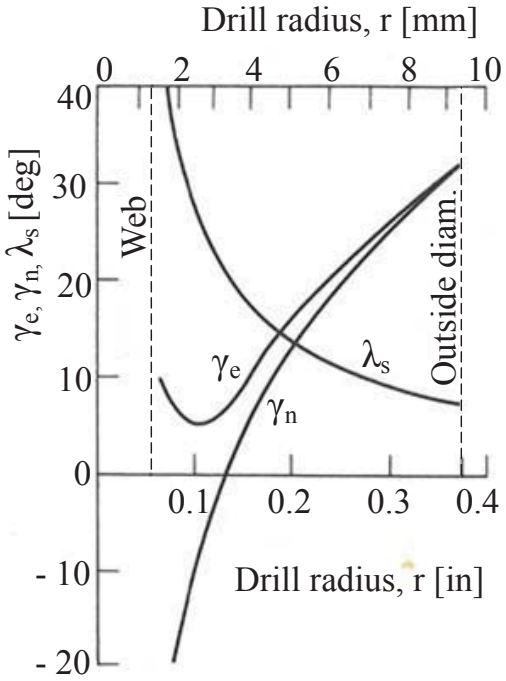

Figure 2.10: Variation of inclination angle λ_s, normal rake angle γ_n, and effective rake angle γ_e, across cutting edge of representative 19 mm drill. Helix angle, $32°$; point angle, $118°$; web thickness, 2.79 mm [10].

Web thickness (w)

Web thickness (w) is the metal column in the drill, which separates the flutes. It is measured at the drill point and increases towards to shank as much as 50 % in order to obtain greater torsional rigidity of the drill.

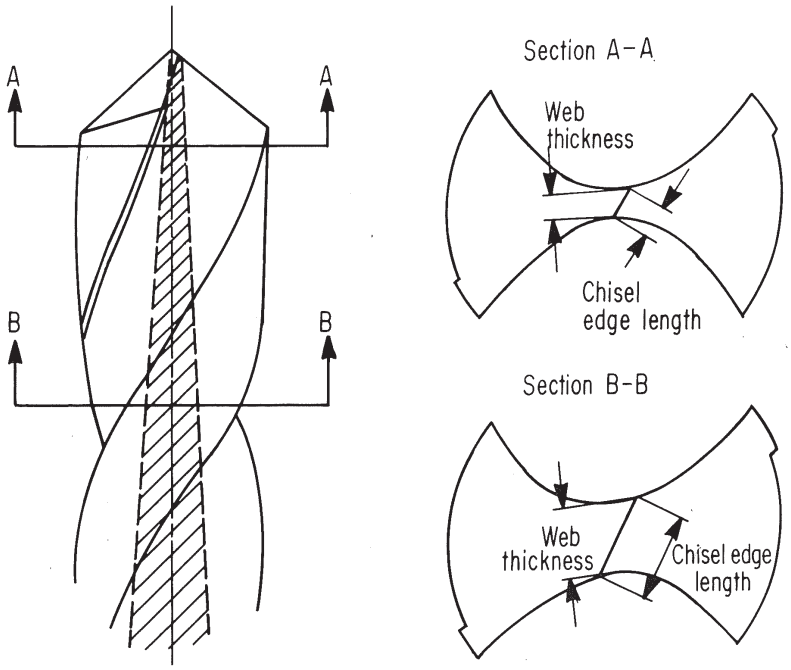

Figure 2.11: Progressively increased the web thickness and chisel edge length of the twist drill [6].

An increase in web thickness results in strengthening of the cutting edge near the point (decrease in γ_n) and small increase in effective rake angle. This would be indicated for strong materials to be drilled since under such conditions failure at the drill point is common. As was already discussed, with increasing web thickness the chisel edge increases (see Figure 2.11), greater power is required, additional heat is generated, resulting in shorter drill life. Web thickness as percentage of the drill diameter is for standard drills at about 15 to 20 %, for very small or heavy-duty drills can reach as much as 50 %. For a standard drill of regular proportions, about 15% of the torque comes from web because most of the torque results from outer portions of the drill lips where most of the material removal occurs. Of about 50 % of the total thrust is caused by the web (the central part of the drill), which does not provide cutting action but rather an extruding action. If the web thickness is doubled, the thrust force is increased by more than 60 % and then, about 75 % of the total thrust is caused by the web [6].

For minimizing this action, web thinning or chisel edge modifications of the drill points are applied. Perhaps the most commonly used methods are shown in Figure 2.3 and split-point geometry described further (see Figure 2.16). Length A in Figure 2.3 is usually one-half to three-fourths the length of the cutting lip so that an abrupt wedge is not formed at the extreme point. In order to change the shape of the chip, a positive rake angle can be maintained along the full length of the cutting edge (Fig.2.3 , b)

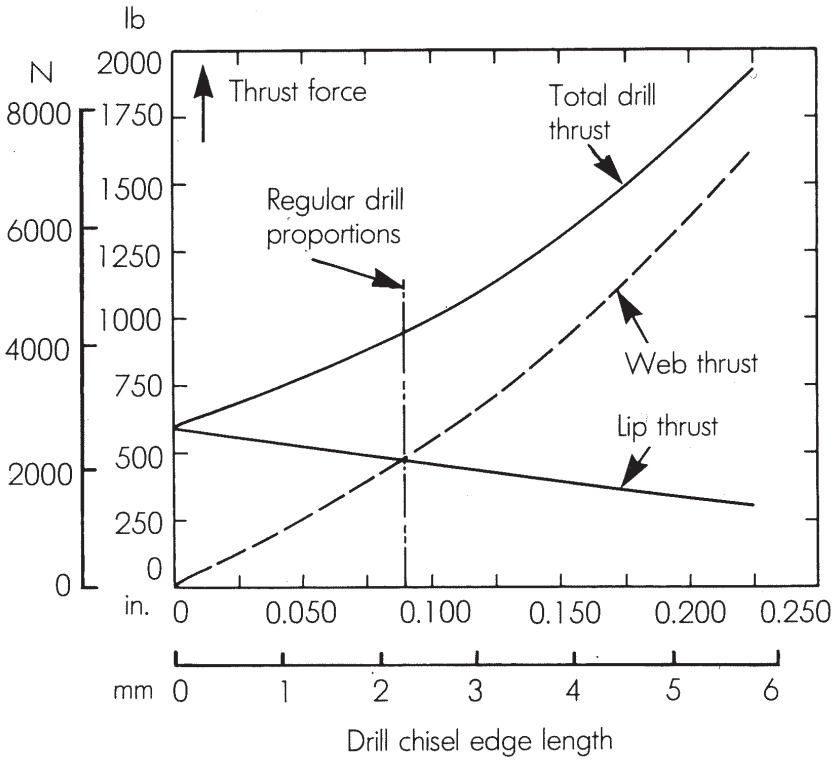

Figure 2.12: Effect of chisel edge length on thrust force [6].

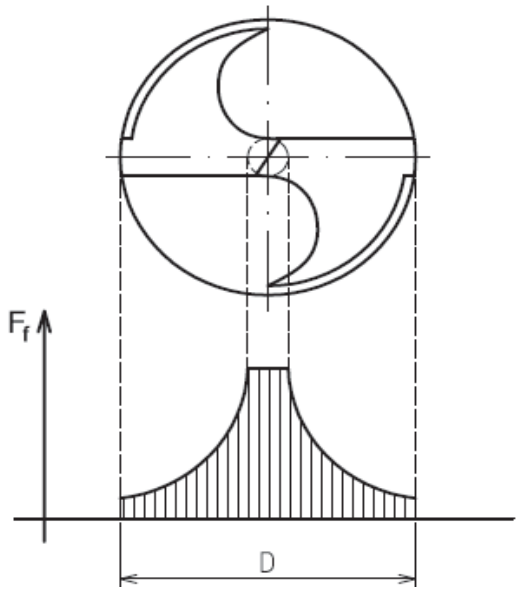

Figure 2.13: Feed force distribution along the drill diameter [6].

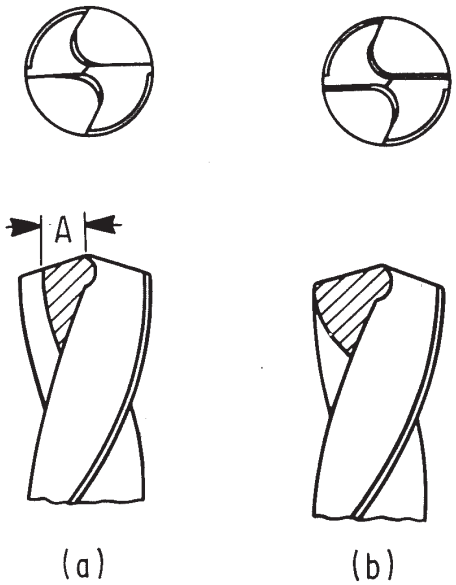

Figure 2.14: Types of web thinning: a) at chisel edge and b) undercut thinned point [6].

2.4 Drill point geometries

Since drill points form the cutting edges, their geometries are crucial to the tool performance.

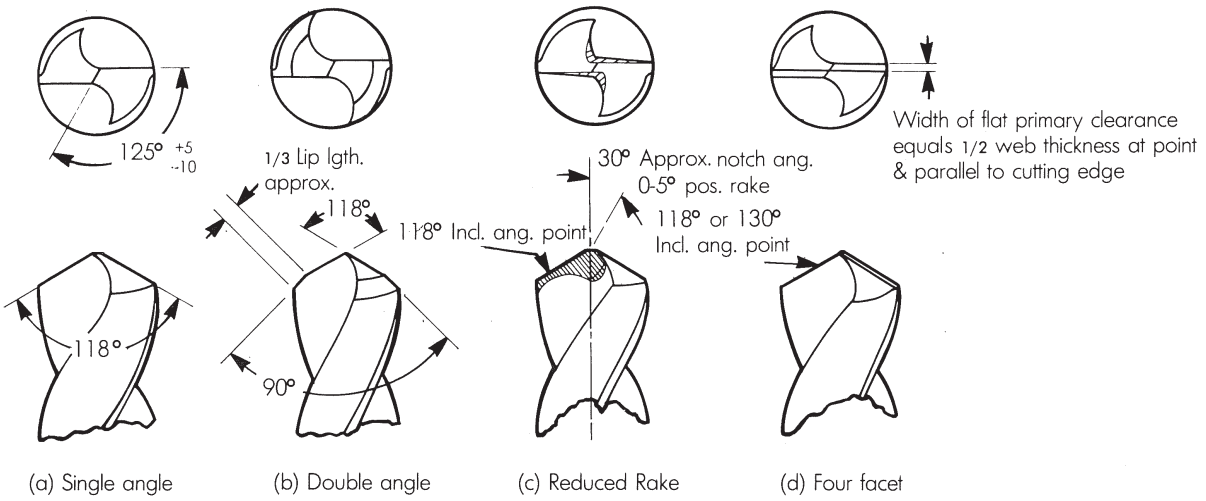

Figure 2.15: Four types of drill point geometries used for different application [6].

Single-angle points

This type of drill point is most commonly used because they provide satisfactory results in drilling a large variety of materials. A possible limitation is that its straight chisel edge contributes to wandering of the point, often requiring to first use a center drill for improved hole accuracy. Also, the sharp corners tend to break down more rapidly, and there is more of tendency to produce burrs on breakthrough [6].

Double-angle (double-cone) points

Double angle points are generated by first grinding a larger included angle (118 to 135°) and consequently a smaller included angle (typically 90°) providing the effect of chamfers and reducing abrasive wear on the corners. Initial applications were in drilling materials such as medium and hard cast irons with low heat conductivity as well as very abrasive materials to decrease the temperature accumulation as well as wear at the outer cutting edge providing burr free edge at the drill exit [11]. Also, the clearance angle is greater than conventional drills to reduce frictional forces and heat generation. More recent applications include improving hole sizes and finishes and drilling very hard materials reducing chipping of the corners of the lips. This geometry is frequently used for the same applications as drills with rounded-edge (radial lip) points [6], detailed later in this section.

Reduced-rake points

Both cutting edges are flatted on their flute faces from the cutting lip corner towards the chisel edge, as illustrated in Figure 2.15 c). This type of point reduces the effective axial rake angle to positive 0 to 5°, causing a plowing or pushing of material rather

than shearing. Reduced sharing action prevents the tool from digging in when low tensile strengths materials are drilled. It also strengthen the cutting lips, therefore it is often used in operations where chipping of the lips has been a problem [6].

Four and six-facet points

The geometry of a four-facet point is made by grinding flat primary relief (10 to 18°) and secondary clearance angles (25 to 35°) on the end of flutes. The width of primary relief flat is one-half of web thickness, resulting in four facets on the end of the drill which subtend at a point of the drill axis and entirely remove the chisel edge. This provides self-centering, require less power and thrust and permits increased feed rates to the drill. Drills with these points, on the other hand, are subjected to more wear on their margins and another disadvantage is the cost of resharpening with special machine. This geometry has found the greatest use for solid carbide drills used to produce holes in printed circuit board materials such as fiberglass-epoxy [6].

Split-points (crankshaft point)

This type of geometry was originally developed for use on drills producing small-diameter, deep holes in automotive crankshafts. Since then it has gained use for drilling a wide variety of hard and soft materials. In producing split points on drills, the clearance face of cutting edges is given sharp (typically 55°) secondary relief to the center of the chisel edge, thus creating a secondary cutting lip. The angle between these lip segments acts as chip breaker, producing smaller chips. This reduction of the original chisel edge reduces thrust at about 25 to 30 % compared to conventional drill and improves centering. A disadvantage is the need for a point splitting grinding machine [6].

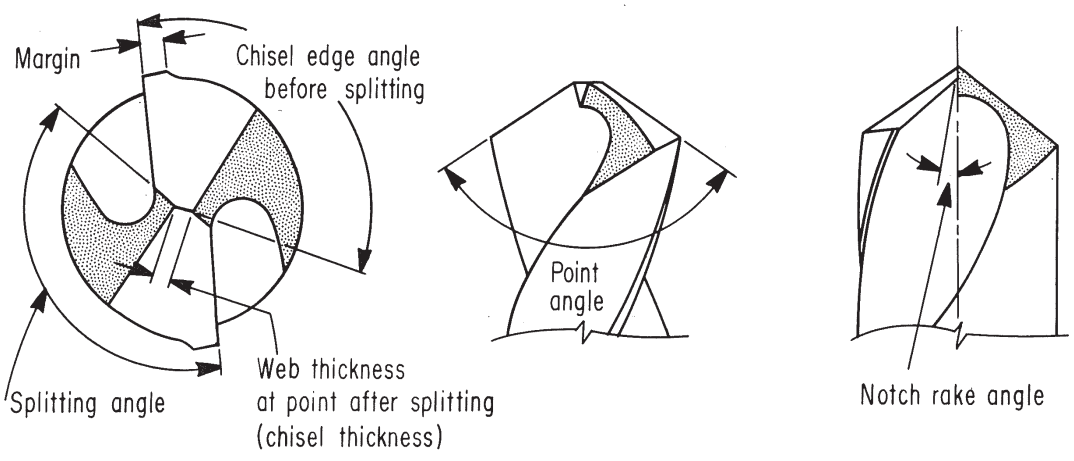

Figure 2.16: Geometry of split-point twist drill [6].

Helical (spiral) points

Helical point is generated by reducing the drill point from chisel edge to a spiral point (see Figure 2.17). This produces an S-shaped chisel providing continuous cutting across the web. Advantages are in a selfcentering capability of the drill and some

reduction of thrust. A possible disadvantage is that burrs are sometimes produced at hole breakthrough [6].

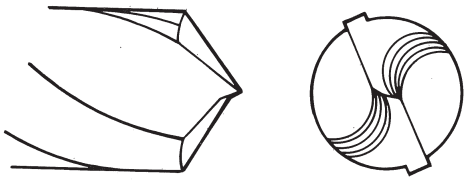

Figure 2.17: Helical (spiral) point with an S-shaped point rather than straight-line chisel edge [6].

Rounded edge (radiused-lip) points

This point is generated by grinding a blended, rounded edge (radiused corner or lip) on conventional points, as illustrated in Figure 2.18. Continuously varying point angle is provided, with the lips and margins blended by a smoothed curve. Since the drill cuts on long, curved lips, there is less chip load per unit area and less heat is generated. Because the corners are eliminated, margin wear is reduced. Burrs at breakthrough are eliminated, and tool life can increases in compare to conventional pointed drills when cast iron is drilled. This geometry is used when drill life is most important. A disadvantage is that these points are not self-centering and are best applied with guide bushing. When used on NC machines, prior center drilling is required. Also special grinding machines are required to produce these points [6].

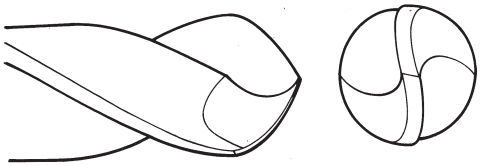

Figure 2.18: Rounded-edge point which has lips and margins blended by smooth curves [6].

Combined helical/rounded-edge points

The point produced (see Figure 2.19) combines features both the helical and rounded-edge points providing the self-centering capability of helical point and the long life, burr-free exit, and higher feed capacity of rounded-edge points. These features make this geometry capable of producing accurate holes on NC machines without prior center drilling [6].

Multifacet points (MFD)

There are more than 20 types of MFD drill points geometries dealing with various workpiece materials and drilling conditions. This geometry is more complicated and thus costly to produce than geometries mentioned before. The design of MFD is conditioned for: cutting force reduction, strenghtening the center of the drill, speeding

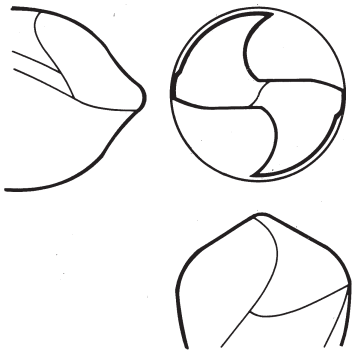

Figure 2.19: Combined helical/rounded-edge point [6].

up heat transfer, improving centering tendency and facilitating chip ejection [11]. For MFD geometry designed for drilling of aluminum alloys see Figure 2.20.

Special MFD drill for thin sheets is depicted in Figure 2.4. A sharp tip in the centre gives a good centering on the workpiece, and two sharp corners cut the sheet to form a hole [11]..

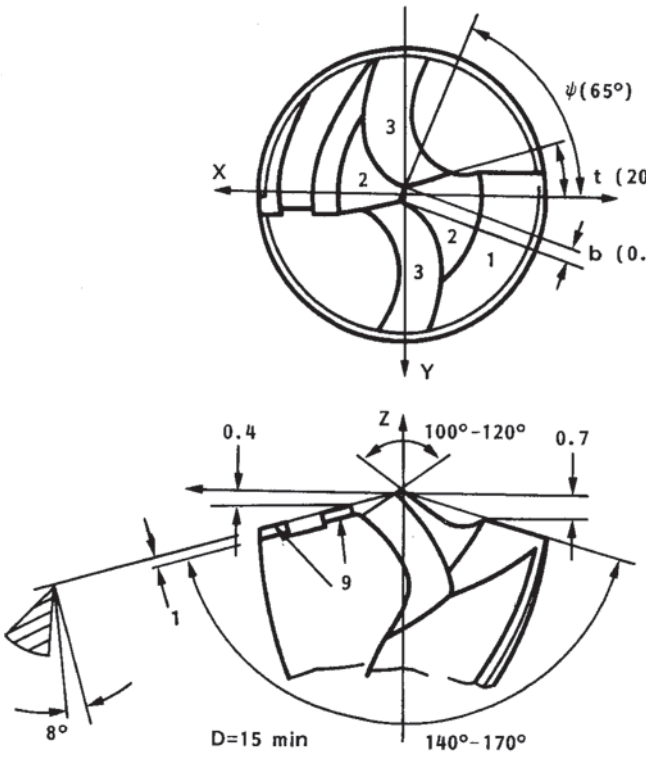

Figure 2.20: MFD for drilling aluminum alloys [11].

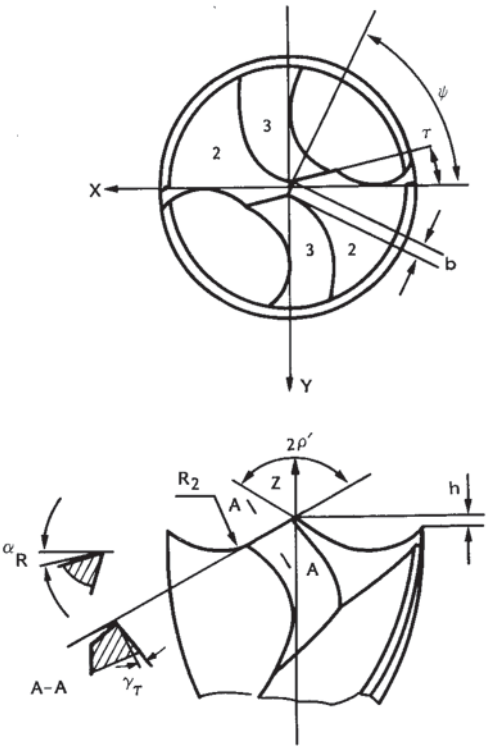

Figure 2.21: MFD for drilling thin sheets [11].

Step drills

Step drill has two or more diameters grounded into the lands of the drill used to perform two or more operations in a single feed stroke. It can be made by grinding

down and stepping the conventional drills. Significant reductions in machining costs are often possible by multi-diameter drills instead of various diameter drills. This geometry is also seen to reduce burr formation at the breakthrough side [6, 12].

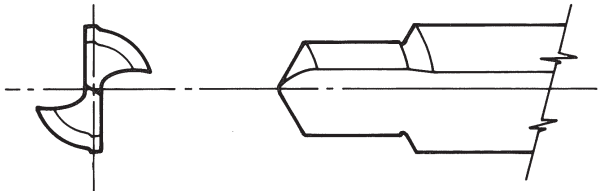

Figure 2.22: Step drill geometry [6].

2.5 Drill materials

Materials used for the manufacture of standard industrial quality drills are chosen on the basis of possessing the following characteristics: high hardness, retention of high hardness at elevated temperatures, toughness and abrasion resistance. The most commonly used materials which meet this criteria are high-speed steel and sintered tungsten carbide [6, 7, 10].

High-speed steels. Twist drills intended for general industrial applications are most commonly made from molybdenum-based high-speed steels: M1, M2, M7, and M10. These drills are effective in drilling a majority of materials. In case of more difficult operations in which increased hot hardness is requested because of greater heat generated, cobalt containing HSS types as M33, M35, M36, M42, and T15, are often used. Cobalt-containing HSS drills permit faster process in compare with regular HSS drills, but they are more expensive. Therefore, they are generally only employed when necessary, or when productivity can be improved.

Heat treatment (hardening, quenching, and tempering) of HSS drills is vital to the quality and performance of the drill. Twist drills made from M1 and M7 HSS for general purpose use are usually heat threated to a hardness of 64 to 66 HRC.

Surface treatments are applied to HSS drills in order to either increase hardness of the outer surface or to reduce the friction between the drill and workpiece or chips in the flute. The treatments are generally applied after the drills have been finish grounded. The treatments producing a thin hard layer includes nitriding, cyaniding, and eventually carbonitriding and carburizing. These processes are done a liquid or gaseous media at elevated temperatures in order to accelerate the absorption of the element(s) into the outer surface. These layers produced are hard, but also brittle. Therefore they are kept thin to reduce the probability of chipping.

Surface treatments for reduction of friction or improving lubrication include the limited penetration of oxygen or sulfur into drill surfaces in a controlled atmosphere furnace with an elevated temperature, and vapor or liquid processing. The development of a thin surface oxide acting as a solid lubricant and preventing welding of chips to the drill is the most widely used surface treatment on drills. Various oxide films can be produced in air at temperatures above 204 C°, most advantageous films for improved performance are created in a dry or superheated steam atmosphere at temperatures of 427 to 566 C°. Oxides created in salt baths are less effective than those

produced by steam. Drills having dark gray to blue-black surface oxide layers created in this way are often used for drilling ferrous materials [6, 7].

Carbide drills have a much higher hardness and greater resistance to abrasive wear, permit higher stock removal rates and remain sharper longer, but they have lower transverse strength. Limiting characteristics is brittleness, requiring rigid and accurate setup and machines. They are recommended for drilling in cast irons, aluminum and other soft nonferrous materials, highly abrasive materials such as reinforced plastics, steels harder than 48 HRC and softer ceramics [6, 7, 10].

Coatings are frequently applied to the outside surface of the drill in order to improve their wear resistance. There is a large number of different coatings and their combinations at this time. However, since the used workpiece material in present work has only very small silicon content and thus doesn't evoke substantial wear, coatings are not detailed in present work.

Polished flutes are required for soft alloys to prevent chip packing and material build-up [6].

Chapter 3

Literature survey on burrs

The following chapter details literature survey on burr formation. Based on the main goals of this work, the chapter includes burr formation mechanisms in general, closer focuses on drilling burr formation process, detail burr geometry and measuring methods for evaluation, influencing drilling parameters and their impact on burr occurrence.

3.1 An Introduction regarding burrs

Burrs are according to ISO 13715 defined as "Rough reminder of material outside the ideal geometrical shape of an external edge, residue of machining or of a forming process" (see Figure 3.1) [13]. An ideally shaped edge of a workpiece would be with zero material-overhang as have the workpiece models either in technical drawings or CAD models of produced parts. Despite this demand, burrs occur in most cases of machining or forming process. Burrs occurrence can cause many problems such as functional problems, small injuries of assembly workers, assembly issues, etc. There are many papers dealing with different kinds of deburring processes, but subsequent deburring process is costly, very time consuming and non-value-adding operation. Therefore there is more work focused on burr formation process and how to control or minimize this unwanted phenomena by variation of process variables in recent time. The costs associated with removing these burrs as a percentage of manufacturing cost varies up to 30 % for high precision components such as aircraft engines, etc. In automotive components, the total amount of deburring cost for a part of medium complexity is in the range of 15 to 20 % of manufacturing expenses [14].

Therefore it is very important and the best strategy how to minimize or prevent burrs from occurrence by controlling the process at all stages of "the process chain". This control requires good knowledge from the design of the component through production planning according to burrs creation on the workpiece. The successful control at all production stages can result in producing of burr-free components or significant deburring cost breakdown.

3.2 Burr formation mechanisms

According to [3], a burr forms always when the material escapes the cutting process and occurs at both, tool entry and exit surfaces, in machining processes. Following

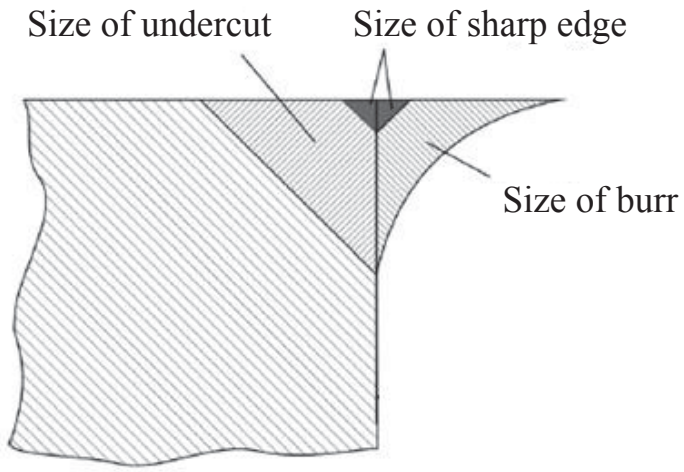

Figure 3.1: Definition of burrs according to ISO 13175, where: undercut — deviation inside the ideal geometrical shape of an internal edge, sharp edge — external or internal edge of a part with almost zero deviation from the ideal geometrical shape [13].

findings were concluded:

- Larger and more burrs occur with increasing ductility of workpiece material.
- Lower burr formation is achieved if the material is restricted to deform in force direction.For instance due to workpiece geometry and machining conditions.

Following, a burr formation model in cutting processes developed by Beier is described. If one body (cutting edge) penetrates into another body, a three-dimensional compression (stress) cone forms. If the range of elastic deformation is exceeded, lasting deformations in all three spatial directions even at the cutting edge occur. These permanent plastic deformations form preferably in the direction of lowest resistance. This leads to enduring material formation at the machined workpiece, at the face where no material has been removed by the tool. The burr forms beyond the contact area of tool and workpiece [3].

Hashimura, [15] citted in [3], considers the burr formation mechanism to be affected not only by cutting conditions including the geometry of the workpiece and tool, but also by the mechanical properties of the workpiece. Figure 3.2 shows schematic views of burr formation mechanisms as described by Hashimura. He classifies eight stages in the burr formation process. From a certain stage of burr formation, the process has to be considered separately for ductile and brittle materials. This is necessary as crack propagation and the deformation before crack propagation are important for the final burr shape and are different when machining ductile or brittle materials.

Stage 1 describes continuous cutting with flow type chip for ductile materials and either shear or crack type chip for brittle materials. In stage 2, called pre-initiation, the deformation and stress distribution are affected by the workpiece edge. The elastic deformation zone intersects the workpiece edge or appears at the workpiece edge as elastic bending. The plastic deformation zone around the primary shear zone is

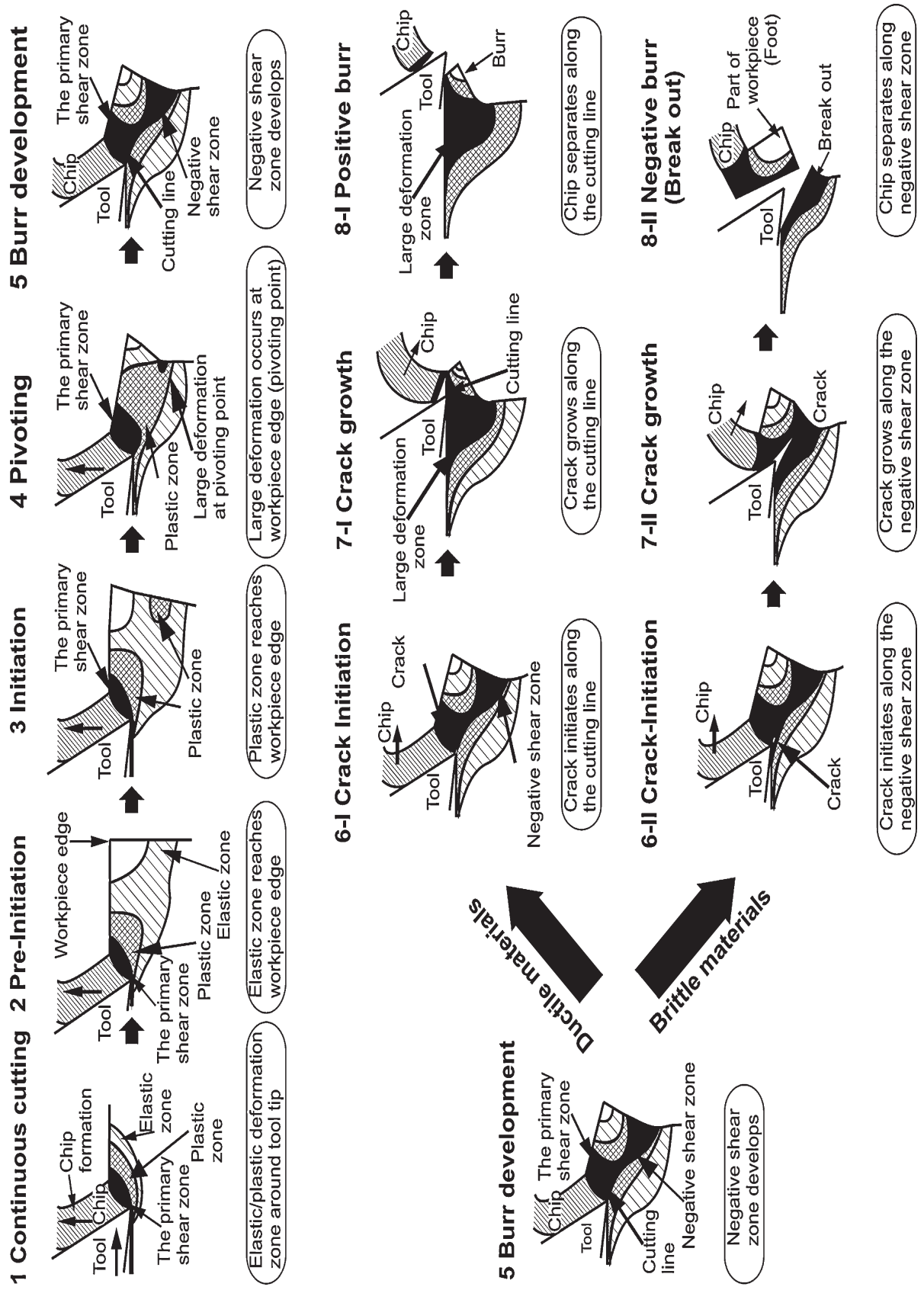

Figure 3.2: Schematic of burr formation [15] depicted in [3].

also considered to be extended toward the edge. Burr initiation is starting in step 3. The plastic deformation occurs at the workpiece edge as plastic bending. The plastic deformation zone around the primary shear zone and the primary shear zone are also considered to be extended. Step 4 describes pivoting. A large catastrophic deformation occurs at the workpiece edge. A pivoting point where the large deformation is visually apparent can be observed. A negative shear zone develops in stage 5. The burr develops and the large deformation at the pivoting point expands to connect with the deformation in the primary shear zone. The large deformation zone below the cutting line is called the negative shear zone. As the tool moves toward the workpiece edge, the workpiece corner continues to pivot with the chip and the burr size increases [3].

Stages 1 to 5 are explaining burr development without crack formation. Stages 6 to 8 are describing chip separation by crack propagation for ductile and brittle materials. Stage 6-I describes crack initiation for ductile materials. The crack initiates at the tool tip in the primary shear zone in a direction along the cutting line. This occurs because ductile materials have a large critical fracture strain. The crack grows along the primary shear zone (stage 7-I). Moving along the cutting line, the tool not only leads to a growing crack but also deforms the workpiece. As a result, the crack appears to grow along the cutting line. Stage 8-I indicates the end of burr formation. The crack causes separation of the chip along the cutting line and a positive burr remains on the corner of the workpiece. For brittle materials the crack initiates at the tool tip in the negative shear zone and its propagation direction is toward the pivoting point (stage 6-II) [3].

The chip is separated from the workpiece by the crack in the secondary shear zone. In stage 7-II the crack grows along the negative shear zone. Moving along the cutting line, the tool induces crack growth and the crack mode may change from shearing mode to opening mode. The workpiece edge also deforms slightly due to crack propagation. Stage 8-II again indicates the end of burr formation. The crack separates the chip along with the part of the workpiece above the negative shear line. As a result, an area consisting of the fractured surface and a small amount of deformed material remains on the workpiece edge. In this case, the burr breaks out and is called a negative burr [3].

All cutting processes have similar mechanics of burr formation with small differences. According to goal of this work, burr formation in drilling process is described in more detail later on.

3.3 Types of burrs

Gillespie as one of the first who laid fundamental work concerning burr formation described four different kinds of burrs [16]: poisson burr, roll over burr, tear burr and cut-off burr depending on the formation mechanism during manufacturing process (see Figure 3.3). The Poisson burr is a result of the material's tendency to bulge to the sides when it is compressed until permanent plastic deformation occurs [17]. The rollover burr is essentially a chip which is bent rather than sheared resulting in a comparatively large burr. This type of burr is also known as an exit burr because it is usually formed at the end of a cut. The tear burr is the result of material tearing loose from the workpiece rather than shearing clearly. It is similar to the burr formed

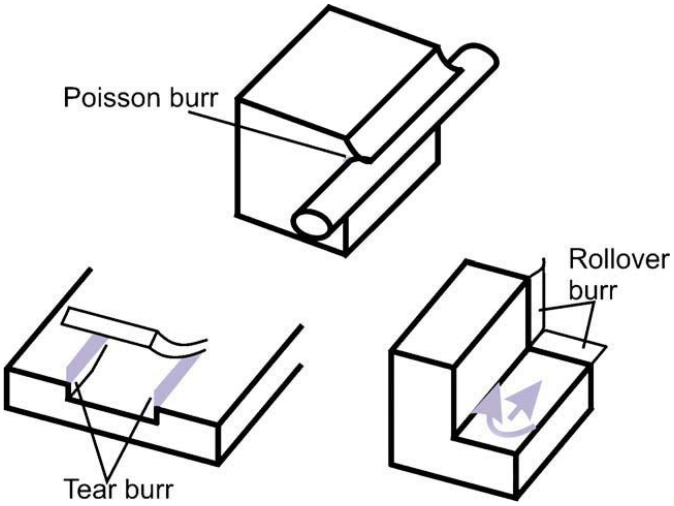

Figure 3.3: Schematic of poisson, tear and rollover burr [16].

in punching operations. The cut-off burr is the result of workpiece separation from the raw material before the separation cut is finished [16].

3.4 Burr formation in drilling operations

In drilling, the burr that forms at the entrance of the hole can be a result of tearing, a bending action followed by clean shearing, or lateral extrusion. The burr that is formed when a sharp drill exits the workpiece is a Poisson burr resulting from rubbing at the margins of the drill. When a normal or worn out drill exits the uncut chip rolls, resulting in a rollover burr [18]. Typical drilling burr types were described by Kim in [19] as uniform burr with or without cap, transient burr and crown burr according to different formation mechanisms (Fig. 3.4).

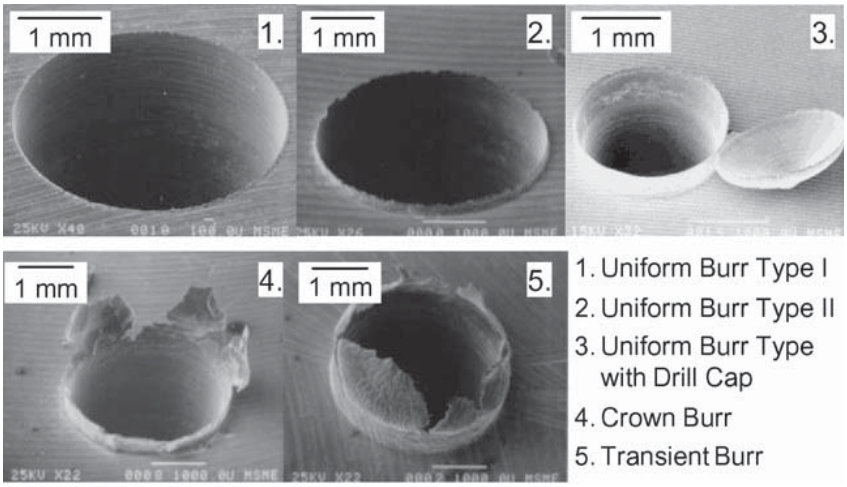

Figure 3.4: Typical drilling burr types by CODEF [19].

The above burr types are observed under different cutting conditions, different drill geometry, material properties, feed rate and cutting velocity. At the exit stage

in drilling, many kinds of burrs are formed according to different mechanisms as the result of the plastic deformation and fracture. The final geometry of the burr is determined by the amount of plastic deformation, directly dependent on the ductility of the material, which is represented as elongation and fracture strain. The fracture location is determined by the fracture strain of the material and the tool geometry. Therefore most burr formations are highly dependent on the material properties, the drill geometry and the cutting conditions [20].

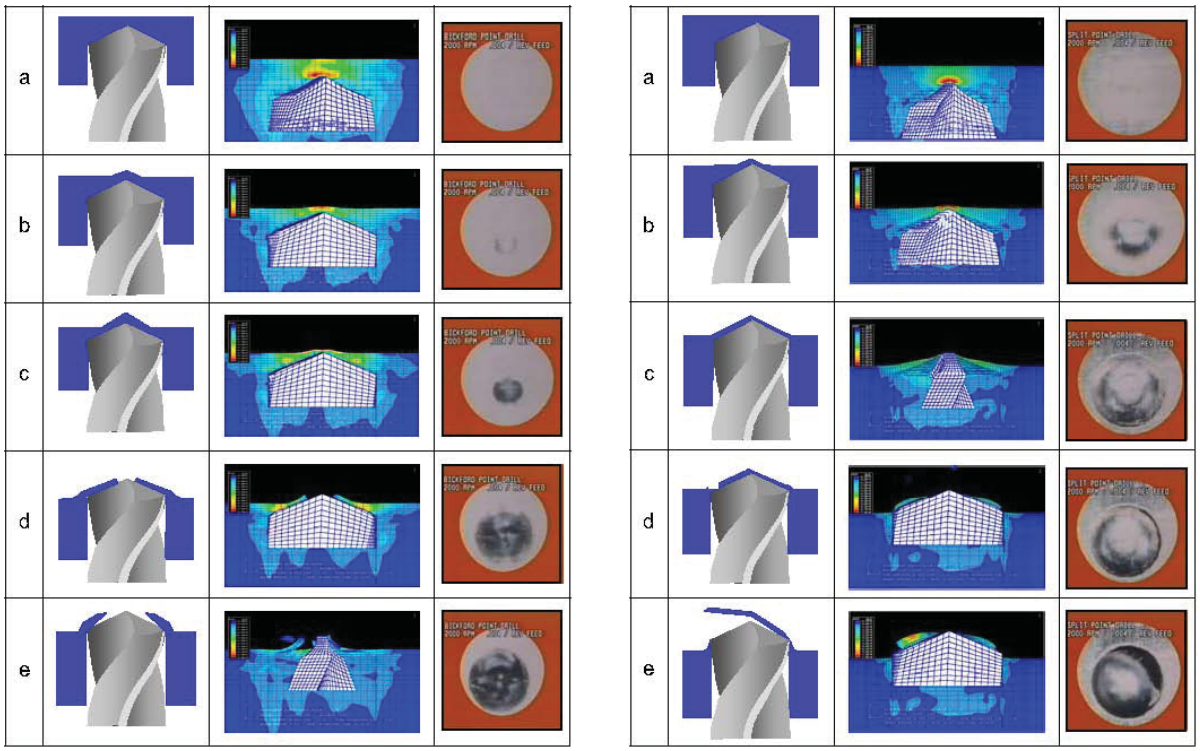

Figure 3.5: Burr formation mechanism of a crown burr — left picture, an unifirm burr with a drilling cap — right picture [21].

In Fig.3.5, five locations of the drill during burr formation are depicted. First column in each picture shows proposed burr formation mechanism by the author [21], second one is represented by FEM simulation and the last one shows images captured by high-speed camera during drilling process.

In the left side picture, the mechanism of a crown burr formation is shown. The first step (a) shows steady-state cutting followed by state (b) when the drill approaches the exit of the hole and the thicker layer of the plastic zone enables to be cut during the formation and allows only little expanding of the plastic zone to the edges of the drill (c). If the initial crack occurs at the centre of the drill (d), the cap is torn into several pieces (e) and forms crown burr which is very large and irregular.

The right side figure shows formation of an uniform burr with a drilling cap. Step (a) again shows steady-state cutting following by step (b) when the drill approaches the exit of the hole and the plastic deformation occurs. The thin layer would rather be formed by the thrust force than to be cut, because there is not enough support to be entirely cut by the drill. The initially formed plastic zone near the drill point area in the center of the drill expands to the edges of the drill in (c). The thin layer of

the deformed material pushed out without being cut will be a cup or a burr. If the remaining plastically deformed material cannot sustain the deformation, a crack at the edges of the hole or at the drill point can be initiated. In step (d) the initial crack occurs at the edge of the drill and a cap is consequently formed (e).

3.5 Burr geometry

According to ISO 13715 standard [13], only one value defines the deviation from the ideal geometrical edge, see Figure 3.6. This value "a" is termed as the size of the burr measured from the burr tip perpendicular to the surface from which the burr is overhanging.

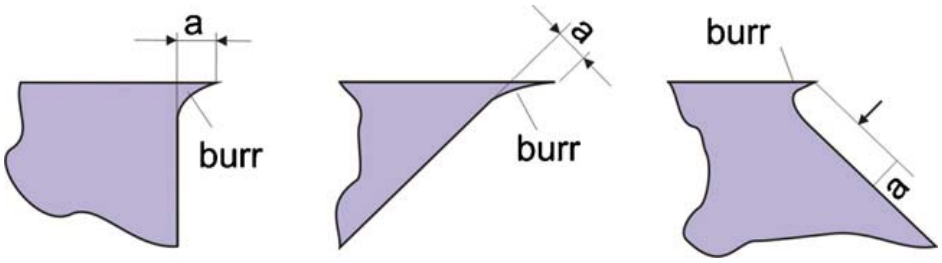

Figure 3.6: Burr geometry according to ISO 13715 [**?**], picture from [3].

But burrs are so variable that for proper investigations it is required to enlarge the number of measured burr dimensions and to perform a large number of measurements to be statistically accurate [22]. Schäfer [23] cited in [3] describes basic burr parameters with using a random cross-section and states that each burr can be characterized its cross-sectional and longitudinal profile. He defines the following burr description:

- The burr root thickness bf is the thickness of the burr root area measured in the cross-section.
- The burr height h_0 is defined by the distance between the ideal edge of the workpiece and the highest point in the cross-sectional area.
- The burr root radius r_f as shown in Figure 3.7 is determined by positioning a circle to the burr root.
- The burr thickness b_g describes the thickness parallel to the burr root area at a distance of r_f, as measured in the cross-section [3].

In spite of the most common measured characteristic is burr height, it has been revealed that burr thickness contributes more to deburring costs than a burr height [22]. Schäfer establish burr value "g" (see Figure 3.7) including different weighting factors of the four geometric burr parameters according to impact of the individual burr parameters on the deburring process. It is apparent that such detailed burr characteristic is very time demanding and not all measuring methods are capable to evaluate these characteristics. Hence the most recognized characteristics are burr heigh and thickness.

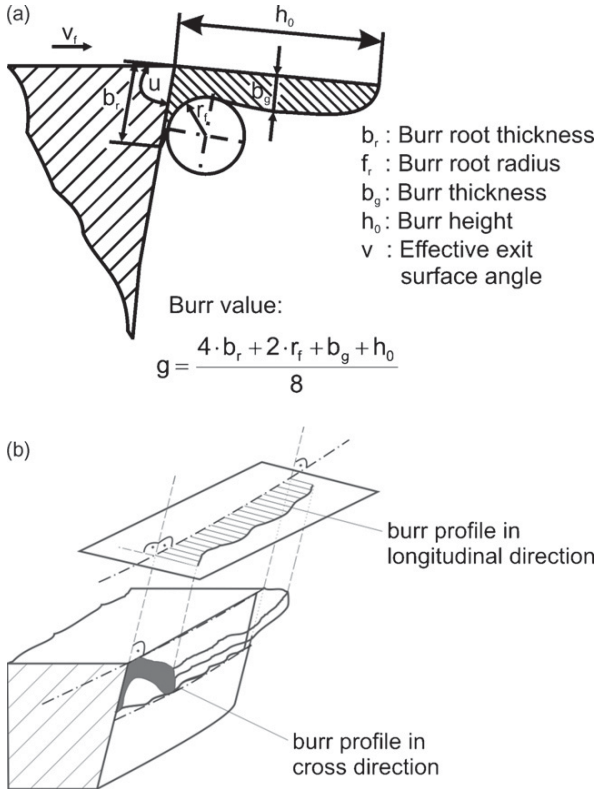

Figure 3.7: Measurement values of a burr according to Schäfer [3].

3.6 Measurements of burrs

Measuring of burr geometry is necessary for any research aiming to avoid or minimize the burr occurrence. In production, it is essential to securely detect the remaining burrs in parts. Burrs form along the edge periphery, generally non-uniform and usually contain thin and sharp peaks. Such burr geometry with large measurement range makes it difficult to find proper methods for burr measurement [24]. The choice of an appropriate system depends on application conditions, requested measuring accuracy and burr characteristics to be measured like burr height, thickness, burr volume or hardness of the burr, though burr height and thickness are the most often and easily measured burr values [25] cited in [3].

The main division according to various criteria:

- One-, two-, three-dimensional
- Destructive or non-destructive
- With or without contact [25] cited in [3].

3.6.1 Destructive methods

To analyze a burr accurately, a metallographic cross-section of the burr is necessary. This allows measuring overall burr values as defined by Schäfer. Also hardness of the

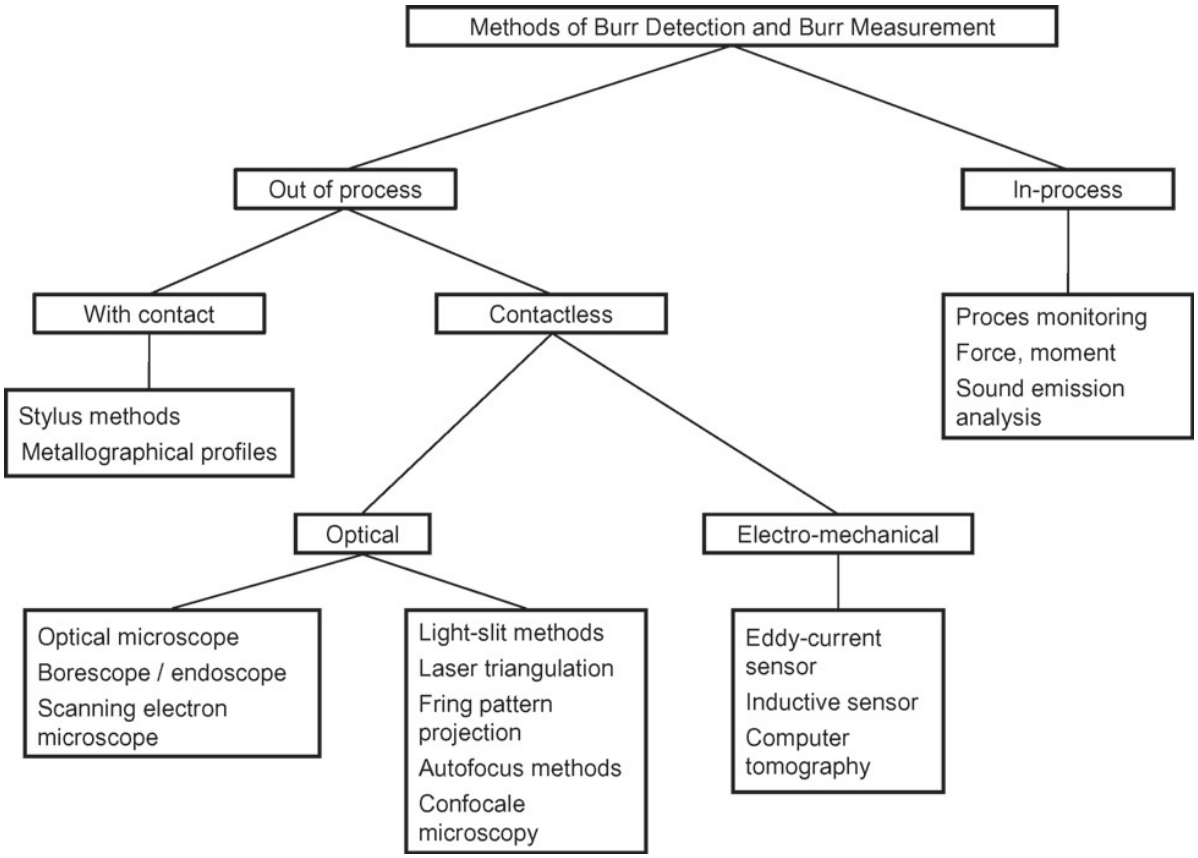

Figure 3.8: Methods of burr detection and measuring [25] cited in [3]

burr and structural changes in the material which result from cutting process can be measured in the metallographic cross-section. Moreover, it is only method to measure burr leght and thickness for rolled back and spiral burrs. On the down side, it is very time-consuming to prepare this metallographic cross-section and it allows only the measurement at one specific workpiece position [3]

3.6.2 Mechanical systems

Contact stylus methods are slow and plastic deformation due to the pressure might reduce the real burr height. The real profile of the burr is falsified because of the conical shape of the tracer [24], [25] cited in [3].

3.6.3 Optical systems

A large number of various optical systems to measure or detect burrs are available at this time. Camera, microscope, laser and interferometer systems are among the most important optical systems. It must be considered that optical instruments at micro or nanometer scale have high resolution, but their vertical and lateral measurement ranges are very small [26]. Optical sensors with large scale, on the other hand encounter the difficulty of the burr edges with steep angles which may cause insufficient light intensity or reflection to the detector [27] cited in [24]. More detailed descriptions of the various optical measuring methods are in [26], some of the

in-process implemented optical systems are stated in [3].

3.6.4 Various other systems

There are many other measuring systems as e.g. non-contact electric capacitance gauging sensor, an acoustic emission system, inductive sensor for part inspection at tough industrial conditions like residues of oil, lubricants and other contaminants [3].

3.7 Influencing parameters on drilling burr formation

There are many various parameters affecting burr formation in drilling process. Gillespie in [16] reveals that burrs cannot be prevented only by changes in process parameters as feed, cutting speed, or tool geometry alone. Nevertheless, the burr size can be significantly minimized by appropriate choosing of aforementioned machining parameters. Link [3] points out that burr formation parameters cannot reliably be separated into direct and indirect factors due to the complex connections and relations between a large number of influencing variables (see Figure 3.9) .

Many studies investigating various parameters with influence on burr formation have shown that major effects in drilling process are feed rate followed by drilling geometry and material properties.

3.7.1 Influence of process parameters

Feed rate

The feed per revolution is the most commonly varied parameter among burr formation influencing parameters. Majority of all the studies [29, 19, 3, 30, 12, 31, 32] have all shown that higher feed rates tend to increase burr volume (hight and/or thickness). It is commonly explained by increasing thrust force while increasing feed rate. The thrust force determines the amount of material that experiences plastic deformation at the tool exit side, which ends in shearing out effect of this material and a larger burr formation. In study [32], high feed drilling of three aluminium alloy types (A1050, A2017 and A6061) was performed. Conventional machine tool and 6 mm in diameter TiN coated SKH56 drills having point angle of 118° and 32° helix angle are employed in this study. The thrust force when high feed drilling alloy A1050 at a spindle speed of $1500\,\mathrm{min}^{-1}$ and feed of 0.5 to 1.0 mm is high, resulting in the creation of large burrs. While in the case of alloy A2017 and A6061 is high feed drilling very feasible resulting in smaller burrs.

It has been experimentally found (number of studies cited in [33, 10]) that the specific cutting energy (and thus the cutting forces and torque) generally decays versus increasing feed. One widely accepted explanation is that additional energy is spent to provide for the plowing forces that act on the flank area and on the tool edge. As the drill takes a bigger bite, the cutting efficiency improves as the proportion of plowing force to the cutting force at the tool-workpiece interface decreases [33, 34].

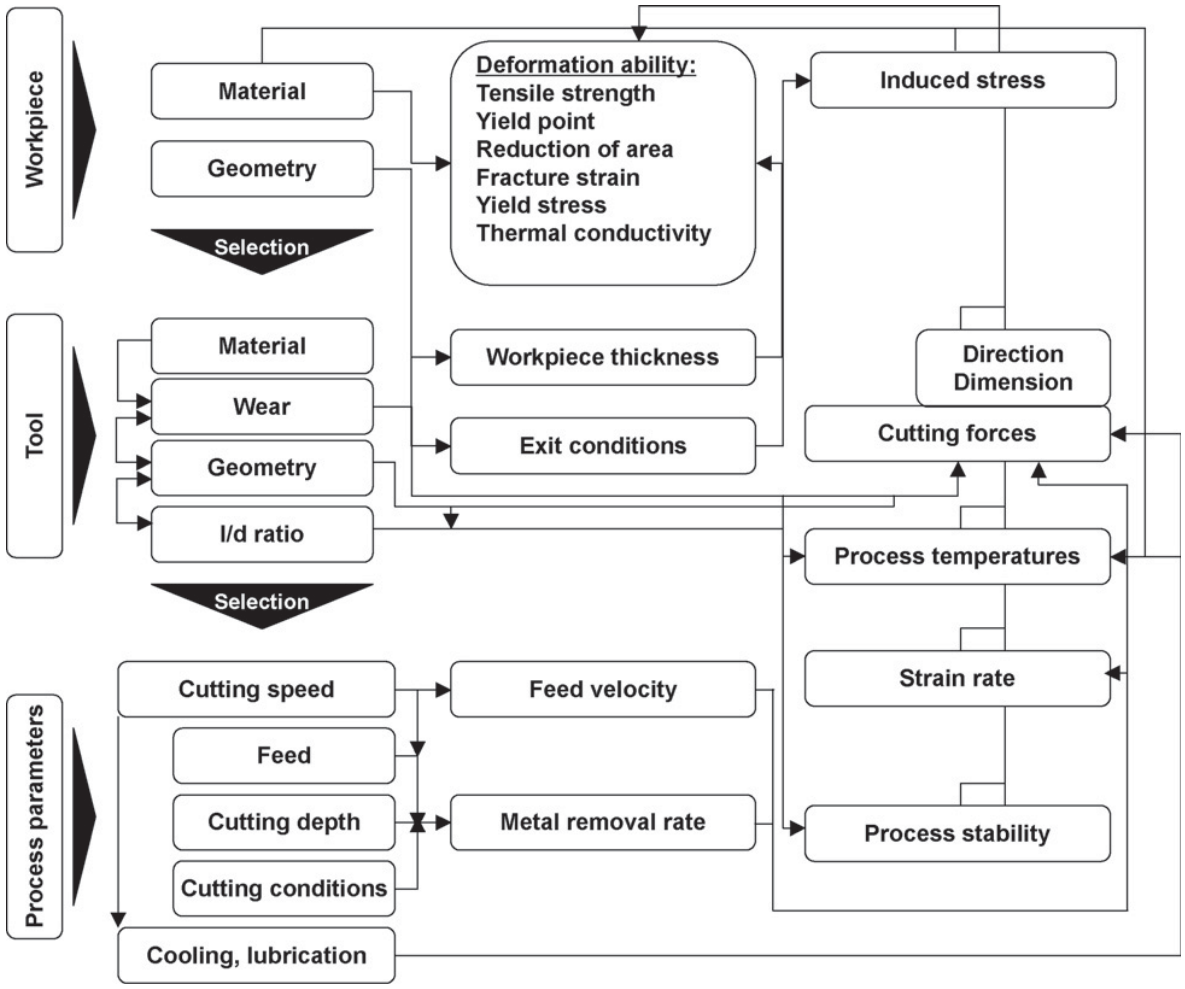

Figure 3.9: Interdependencies of burr formation parameters according to [28] depicted in [3]

An empirical law equation related to adjusted specific cutting energy K_s, to h_D, the uncut chip thickness, is described as [35] in [33]:

$$K_s = K\,(h_D)^{-p} \tag{3.1}$$

where K_s is the "adjusted" specific cutting energy and p is a constant ranging from 0.15 to 0.3. For various wrought aluminums is widely accepted range of this empirical parameter 800–900 W·s·cm^{-3} at a reference uncut chip thickness of 0.25 mm. Figure 3.10 depicts how the adjusted specific cutting energy decreases as a function of increasing uncut thickness (feed) while using three values for the constant p for comparison.
Shaw and Oxford [10] shown that specific cutting energy (u) varies inversely with $(fd)^{0,2}$ in drilling.

Figure 3.11 shows the thrust force for each speed to increase with the feed, which is in line with the fact that the force is proportional to area of the uncut chip (being roughly the product of the feed per tooth and the drill diameter). An interesting observation is that the thrust force is consistently lower at higher speeds than at lower speeds for all values of feed. Reported data on drilling in 15.87 mm thick A390 cast aluminum samples while using 6.35 mm diameter solid carbide drill 119° drill point

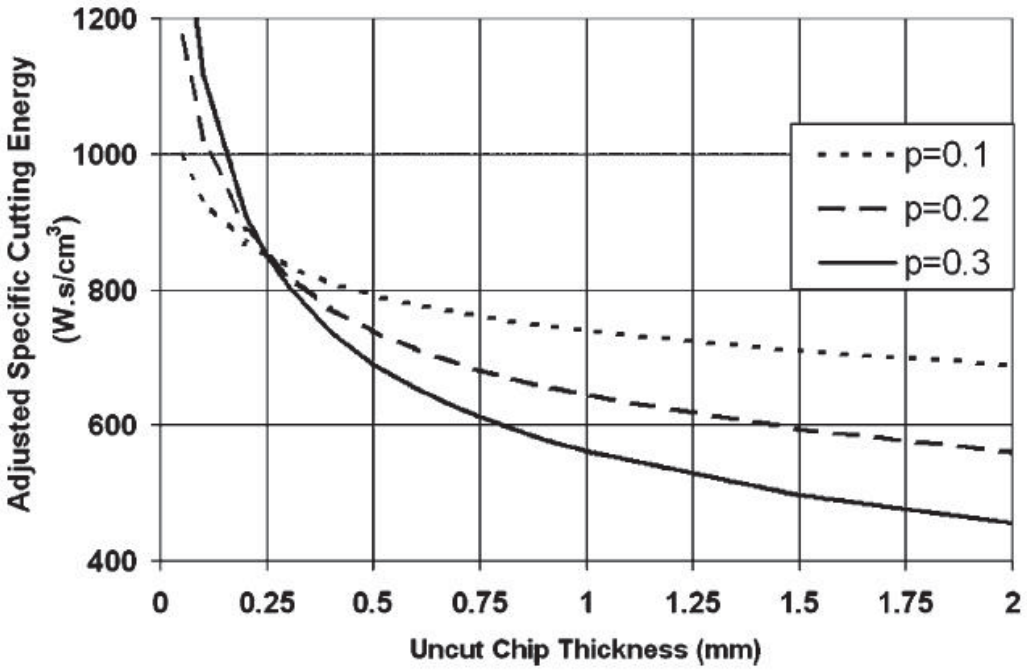

Figure 3.10: Adjusted specific cutting energy vs. uncut chip thickness [35] depicted in [33]

and 33° helix angle. These data reflects the thermal softening behaviour (described forth in section 3.7.3) due to the low melting temperature of aluminum [33].

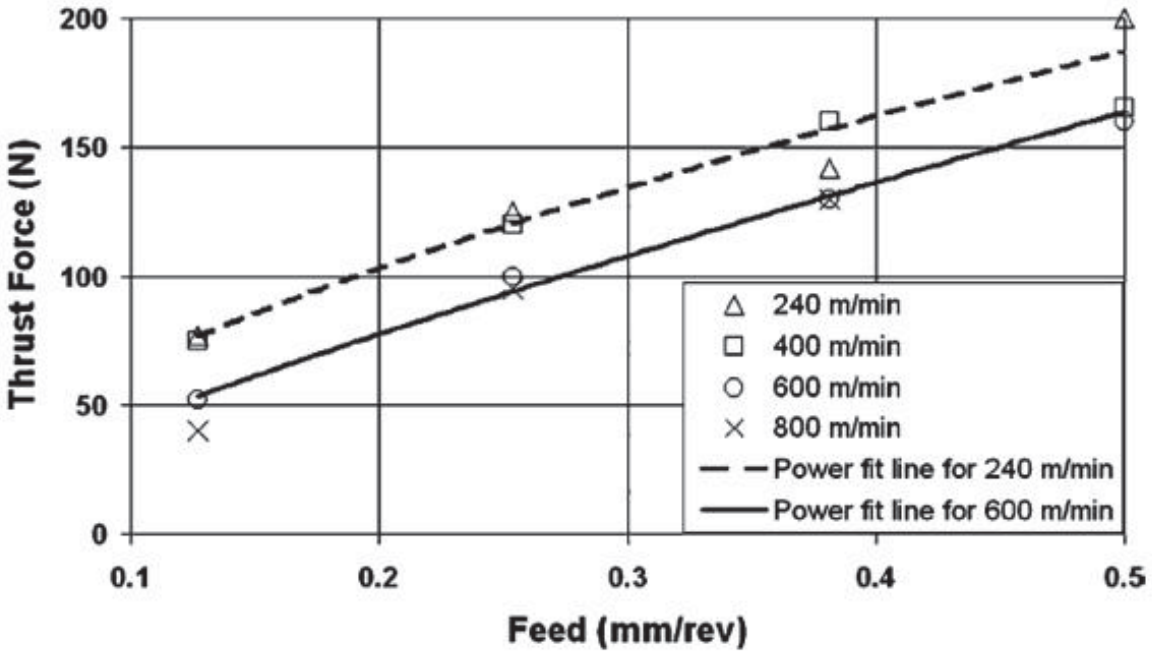

Figure 3.11: Thrust force vs. feed at different speeds [33] based on [36] data.

Cutting speed

Cutting speed is widely recognized as not significantly influencing the burr volume [3]. However, depending on the cutting speed, the heat generation at the cutting edge changes greatly, influencing the workpiece material properties. It also affects the rate of tool wear, especially corner wear, which is seen to have a large influence in drilling burr formation [19]. On the contrary, burr sizes were seen to remained nearly constant with increasing drill wear when drilling aluminium [12].

3.7.2 Influence of tool

Drill geometry

Increasing the chisel edge to diameter ratio increases thrust force on the workpiece and consequently the burr size [30, 19]. Larger drills produce an increased thrust which results in increase of burr height [29, 30]. Point angle was observed to have a significant role too. The lowest burr height occurs at high point angles as 135° in drilling Al 7075 [37] or titanium alloy [3]. Japanese researches summarized and reported by Takazawa [38] citted in [19] claimed that drill with a nick on the cutting lips produces smaller burrs than conventional drill.

3.7.3 Influence of material

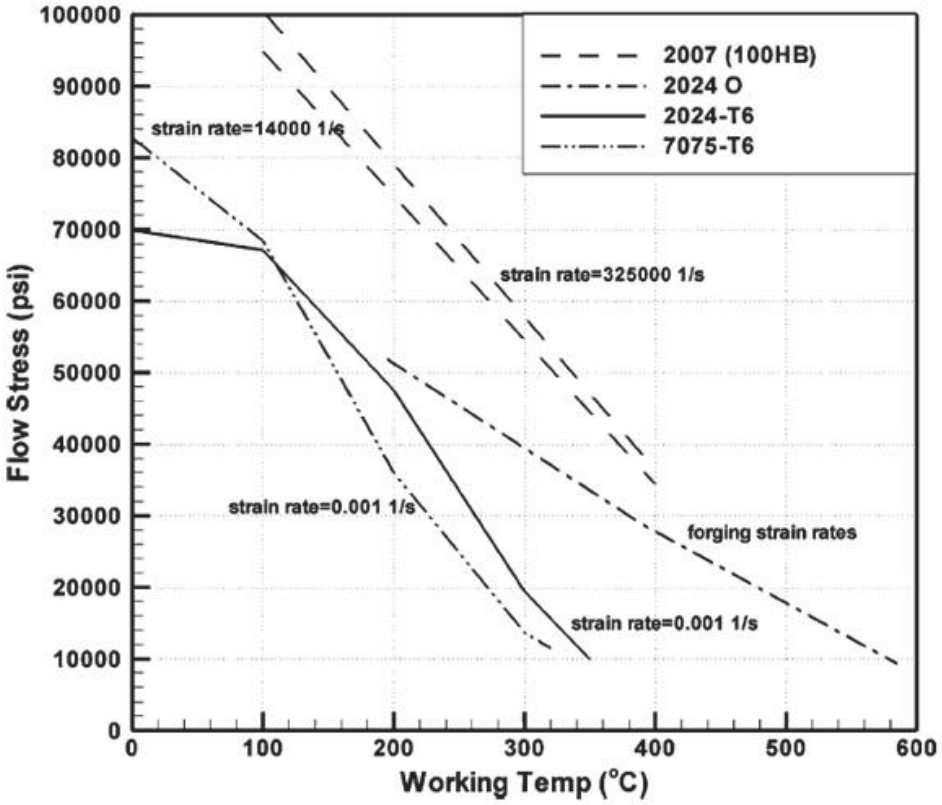

Figure 3.12: Flow stress vs. temperature (various references cited in [33])[1]

[1]For converting from psi (pound per square inch) to Pascal (Pa) use: 1 $psi = 6894.75729$ Pascals (Pa)

Material properties

Burr formation process has been concluded as heavily dependent on yield strength and ultimate strength of the workpiece material. These material properties vary significantly with increasing temperature [30]. Reduction of temperature with using carbon-dioxide was performed [31] resulting in reducing of burr formation. The reduction of flow stress is minimized by cooling and this leads to a lower formability. Material becomes more brittle and this results in a reduced burr formation.

The phenomenon of decreasing thrust force while using higher speeds, shown in influence of feed, could be explained by the aluminum work's strength as being the sum of two competing phenomena:

- Thermal softening of the material thanks to heat generation at the shear plane and the tool-workpiece interface.
- Work hardening associated with high strain rates at the shear plane (proportional to cutting speed)

The work material flow stress decreases as function of the material's working temperature [33].

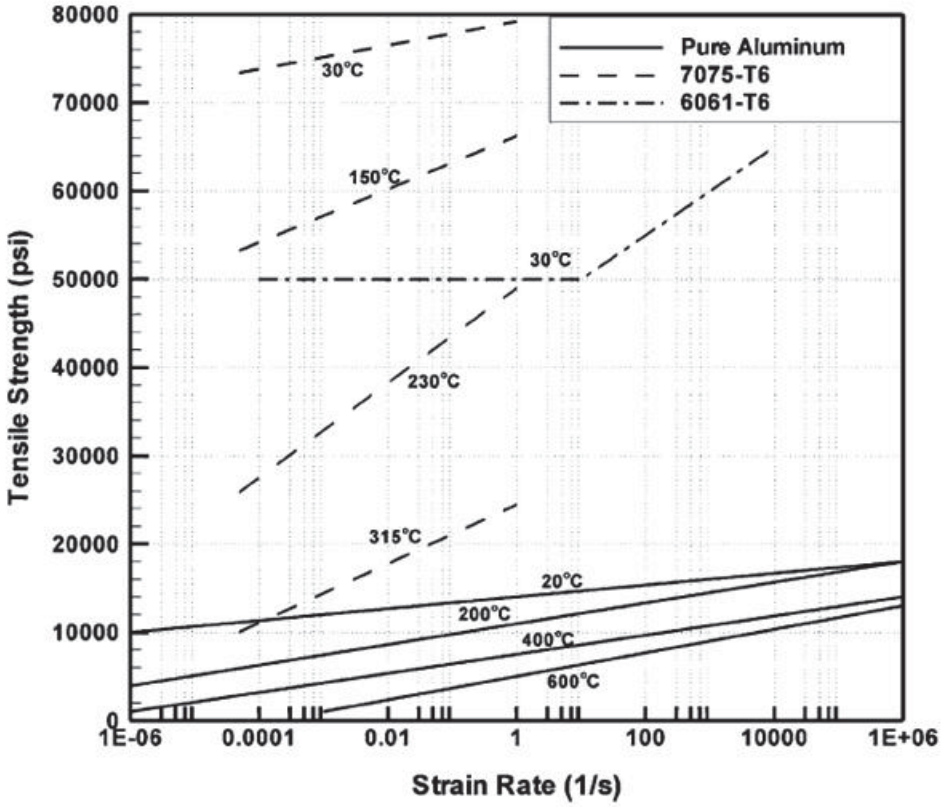

Figure 3.13: Tensile strength vs. strain rate for various aluminums (various references cited in [33])[3]

To demonstrate thermal softening, different heat treatment conditions as well as various strain rates for aluminium materials are depicted in Figure 3.12. For example, the flow stress of aluminum 2007 is reported to decrease as function of increasing working temperature. The flow stress of A2007 is equal to 64 000 psi

(441 MPa) at working temperature of about 260 °C and this stress drops to about 34 000 psi (234 MPa) for working temperature of about 400 °C. This represents halving the strength over temperature increase of 140 °C. Over the same temperature range, small increase of flow stress can be seen as a result of strain rate increase from 14 000 to 325 000 s^{-1}. High spindle speed of 100 000 rpm plus an aggressive feed $0,5\,\mathrm{mm} \cdot \mathrm{rev}^{-1}$ having the strain rate of about $1 \cdot 10^6\,\mathrm{s}^{-1}$ is greater than that at lower strain rates (conventional drilling speeds of about $1 \cdot 10^4\,\mathrm{s}^{-1}$ [33].

Tensile strength versus strain rate of different kinds of aluminium is plotted in Figure 3.13. It can be seen that while for a high purity aluminium, the data indicates comparable values of strength increase due to work hardening (say from $1 \cdot 10^4$ to $1 \cdot 10^6\ s^{-1}$) and softening due to temperature increase (say from 200–620 °C), for Al7075-T6 the data shows loss of the strength of about 70 % over temperature rise of 285 °C in compare with only 6% strengthening over strain rates from $1 \cdot 10^4$ to $1\ s^{-1}$) [33].

Exit surface geometry

The exit surface geometry of the workpiece changes due to the plastic deformation at the end of the cutting process. Already a small negative exit surface angle leads to early initiation of the bending mechanism and results in a large burr. Hence, thinner parts as sheet may have a larger burr resulting from drilling operation. Min [39] cited in [40] developed a burr formation model related to drilling of intersecting holes. An interaction angle defining the interaction between the cutting edge and the exit surface was proposed under assuming constant exit surface geometry (see Figure 3.14). The model can predict the likely burr formation area. The area increases as feed increases, speed decreases and the exit surface angle decreases [40].

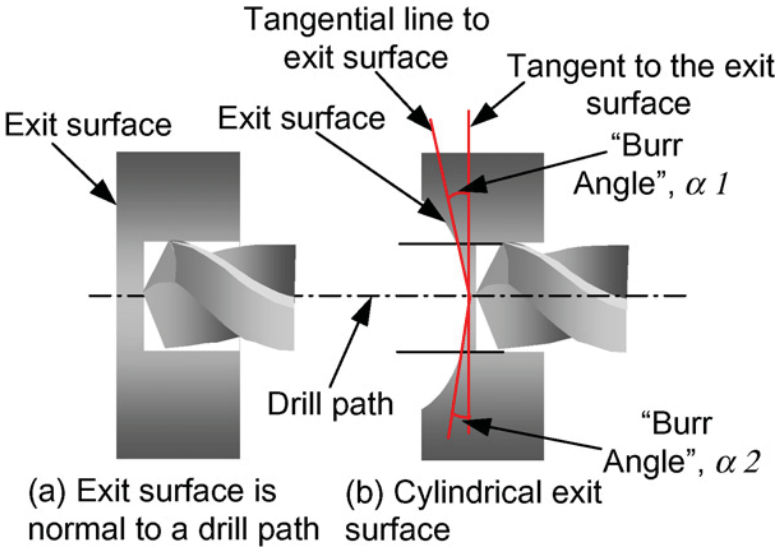

Figure 3.14: Burr formation when drilling intersection holes according to Min [39] depicted in [40].

3.8 Summary and recommendations

Based on literature survey dealing with drilling (see Chapter 2) and burrs (in present Chapter 3), a summary of findings resulting from the previous researches pertinent to the project goals and recommendations for drilling of aluminium alloys are briefly presented.

Drill geometry

- helix angle (30 to 40°)
- point angle (130 to 140°) mostly seen to minimize burring
- web thinning or chisel edge modification — reduction of drill wandering, in order to avoid hole entry defects. Reduction of thrust (feed force), which is determining the amount of workpiece material that experiences plastic deformation at the tool exit side, resulting in shearing out effect of this material and a larger burr formation
- double angle (cone) and rounded-edge (radial lip) point geometries provide burr-free edge at the drill exit (for cast iron workpiece material)
- step drill geometry is seen to reduce burr formation at the breakthrough side
- multifacet points (MFD) designed for drilling in thin sheets and aluminium
- polished flute surface to prevent chip packing and material build-up

Process conditions

- lower feed rates resulting in lower thrust force $\Rightarrow$ less workpiece material that experience plastic deformation at the tool exit side
- higher cutting speed may reduce burring
- lowering the process temperature in the interest of lower formability of the workpiece material
- lubrication in order to avoid material build-up during drilling

Clamping conditions

- restriction of the worpiece material being deformed in drill feed direction

Burr measurements

Burr size defined by single value according to ISO 13715 was found to be insufficient because a burr thickness contributes more to deburring costs than a burr height. Utilization of burr measurement values according to Schäfer [22].

- advantageous utilization of the optical measuring systems (the burr profile is not falsified or deformed due to the contact with measuring instrument)

Chapter 4

Design and Analysis of Engineering Experiments — DOE

To draw meaningful conclusions from the experimental data, the statistical approach of design and analysis of experiments (DOE) was used in planning of the experimental work and it is briefly described in this last chapter of the literature survey.

4.1 Introduction [1]

An experiment is a test or a series of performed tests, usually to discover something about a particular process or system. More formally, the experiment can be defined as a test in which purposeful changes are made to the input variables of a process so that we may observe and identify the reason for changes observed in the output response. For simplification. the design and analysis of engineering experiments is hereinafter referred to the notation —DOE

Experiments are widely used in engineering and science. Experimentation plays an important role in product realization activities as new product design and development, manufacturing process optimization, and process improvement. The process can be usually visualized as a combination of operations, machines, methods, people, and other resources transforming some input (often a material) into a output that has one or more observable response variables. The objectives of experiment may include to:

- Reduce time to design or develop new products and processes
- Improve existing process
- Improve reliability and performance of the products
- Achieve robustness of the product or process
- Evaluation of design alternatives, settings, materials, system tolerances, etc.

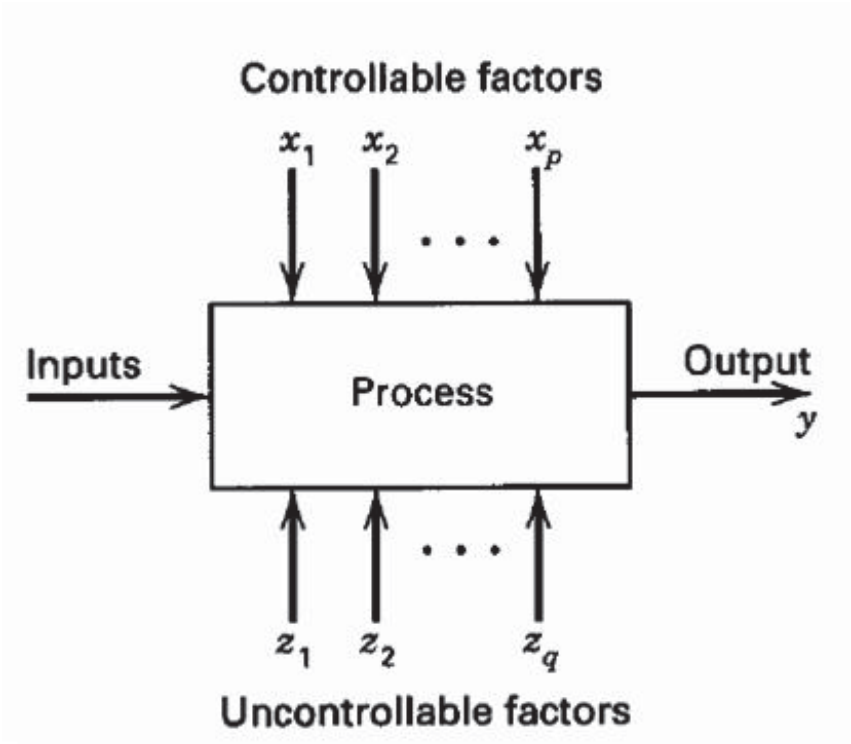

Figure 4.1: General model of process or system [1].

4.2 The basic principles of DOE [1]

The statistical approach to experiment design is necessary to drawn meaningful conclusions from the data. Statistical methods are the only objective approach to analysis, when the problem involves data subjected to experimental errors. There are three basic principles of experimental design:

4.2.1 Randomization

- Randomly determined order of the individual runs or trials of the experiment
- Averaging out the effect of extraneous factors (material irregularity, etc.)

Replication

- An independent repeat of each factor combination
- Estimation of experimental error or background noise, Improving precision of estimation

4.2.2 Blocking

- Technique used to improve precision by reducing or eliminating of the variability transmitted from nuisance factors (factors that may influence the experimental response but in which we are not directly interested)

4.3 Strategy of experimentation [1]

4.3.1 Best-guess approach

To select an arbitrary combination of factors, test them, and see what happens. This strategy is frequently used in practice by engineers and scientists. It often works reasonably well, because the experimenters often have a great technical or theoretical knowledge of the system they are studying, as well as practical experience. But there are at least two disadvantages. First, if the initial best-guess does not produce the desired results, now the experimenter has to take another guess at the correct combination of factor levels. This can continue for a long time, without any guarantee of success. Second, when the initial best-guess produces an acceptable result, the experimenter would tend to stop testing, although there is no guarantee that the best combination (solution) has been found.

4.3.2 One-factor-at-a-time (OFAT)

This strategy is extensively used in practice. The OFAT method consists of selecting a starting point, or baseline set of levels, for each factor. Than successively varying each factor over its range with the other factors held constant at the baseline level. Consequently after performing all the tests, a series of graphs showing how the response variable is affected by varying each factor with all other factors held constant. The major disadvantage of this method is that it fails to consider any possible interactions between factors. Because interactions between factors are very common, this strategy is always less efficient than other methods based on a statistical approach.

4.3.3 Factorial experiment

This statistically designed approach is the correct approach to deal with several factors, in which factors are varied together and make it the most efficient use of the experimental data. The factorial experimental design would enable to investigate the individual effects of each factor levels (or the main effects) and to determine factors interactions. In case there are four to five or more factors, it is usually unnecessary to run all possible combinations of factor levels and a fractional factorial experiment can be used. This is a variation of basic factorial design, where only a subset of the runs are used, providing good information about the main effects of factor levels as well as some information about how these factors interact. This method is extensively used in industrial research and development.

4.4 An application of DOE in this work

All the experiments in the present work were planned with using DOE. In case of complicated linkages of influencing parameters or not very clear data for direct evaluation, this approach would allowed to draw meaningful conclusions based on statistics.

During evaluation of measurement data gained from experimental tests, the correlations were clear, not requiring the usage of statistical approach. Therefore,

throughout the experimental work is DOE used only for planning. This also allows one to use the gained data for further study.

Chapter 5

Planning of the experimental investigations

5.1 Goal and approach

This section of experimental tests describes investigations performed on burr occurrence when drilling aluminium Al99.7Mg0.5Cu–H24 sheets. A number of different process parameters, different tool geometries and influence of clamping system was evaluated in order to find suitable solutions for minimizing burr formation and assuring the hole uniformity during drilling operation. The experimental parameters were selected based on earlier experimental studies discussed in the literature survey on burrs (see Chapter 3.7.1), recommendation of manufacturers of the tools used during the tests and experience already gained by the company Bang & Olufsen.

5.2 Organisation of the work

The experimental work was done in the three subsequent tests as follows:

- Preliminary test (Chapter 6)
- Clamping system investigation (Chapter 7)
- Tool geometry investigation (Chapter 8)

The first experimental test, hereinafter referred by the notation — Preliminary test (Chapter 6), was performed in order to find burr formation mechanism for the particular material used, to choose and evaluate the influence of drilling process parameters, which are generally recognized as heavily influencing the burr occurrence according to previous literature survey (see Chapter 3.7.1). At the same time, it was of interest to verify capability of experimental equipment for consequent tests.

In the second phase test — Clamping system investigation (Chapter 7), a clamping system in the interest of minimizing burr formation was constructed and it's influence on burr formation was evaluated.

The final test, hereinafter referred by the notation — Tool geometry investigation (Chapter 8), observes an influence of different tool geometry on burr formation while the special clamping system and machine tool intended to use at the company work shop for production were used.

Measurements were carried out with respect to cutting forces (thrust and eventually torque), final burr dimensions (height and width) and visual uniformity of the holes. Description of test setups, conditions, data analyses and conclusions are presented forth in particular chapters.

5.3 Workpiece material

Since the workpiece material for production of the sound speaker grilles was a fixed parameter and could not be varied, it's properties are stated in this section. The thickness of the sheets of 2 mm was a fixed parameter too and it was not varied through all the test performed.

Wrought aluminum alloy Al99.7Mg0.5Cu-H24 according to chemical designation DIN 1725–1 from Alcan Singen GmbH, Germany was used. This material is variation of EN AW–5205–H24 in accordance with European Standard EN 573–3 as well as AA 5205–H24 according to Aluminum Association of America, where the Mg content has been reduced to 0.5 % instead of 0.8 %. Prefix H24 is the temper (according to European Standard EN 515). It means that the material was strain hardened and partially annealed, having $\frac{1}{2}$ the ultimate tensile strength of that achieved by a cold reduction of ∼75 %.

Chemical composition (Table 5.1) and mechanical properties of the used material are shown in Table 5.2, according to Alcan specialty sheet in agreement with inspection certificate EN 10204–3.1. Measured mechanical properties are in accordance with tensile test EN 10002–1, Appendix B/, Sample form 1 (12.5 mm x 50 mm).

Table 5.1: Chemical composition of used material Al99.7Mg0.5Cu-H24 according to Alcan specialty sheet from the material producer, Alcan Singen GmbH, Germany

Chemical composition [wt %]							
Si	Fe	Cu	Mn	Mg	Cr	Zn	Ti
0.113	0.160	0.048	0.002	0.476	0.001	0.003	0.019

Table 5.2: Mechanical properties of used material Al99.7Mg0.5Cu-H24 according to Alcan specialty sheet from the material producer, Alcan Singen GmbH, Germany

Specified mechanical properties		
Min. ultimate tensile strength	Min. proof stress	Min. elongation
Rm [MPa]	Rp0.2 [MPa]	A50 [%]
130–170	>= 90	>= 8
Measured Mechanical properties in accordance with EN 10002–1		
Ultimate tensile strength	Proof stress	Elongation
Rm [MPa]	Rp0.2 [MPa]	A50 [%]
150–151	139–141	11–12

Chapter 6

Preliminary test

According to the literature survey in Chapter 3, feed rate was recognized as the most influencing drilling process parameter on burr formation. Influence of cutting speed is mostly recognized as not significantly influencing the burr volume, however there are some studies showing that higher spindle speeds tend to reduce burr thickness. In order to evaluate the influence of the discussed process parameters on burr volume when drilling aluminium (see Chapter 5.3 for details about the material used), varied factors in the preliminary test were cutting speed and feed per revolution while fixed drill geometry was used during the test. In the interest of isolating the influence of cutting speed and feed on burr formation, a simple fixture without supporting the drill exit side was used during the test (for description see Chapter 6.1.5). Since the high speed spindle intended to use in combination with conventional machine tool had a narrow operating range, it's capability for the consequent tests was verified by comparison of theoretically calculated drilling torque and power with the values measured during preliminary drilling test.

Measurements were carried out with respect to cutting forces (thrust and torque), final burr dimensions for hole entry as well as exit side (height and widths) and visual uniformity of drilled holes was evaluated. Description of the test setup, conditions, data analyses and conclusions are presented forth in this chapter.

6.1 Experimental setup

A vertical CNC milling machine with high speed spindle attached was used during preliminary drilling test. Cutting forces were measured using two-component measuring piezo-electric transducer. Burr height measurements were performed on an optical measuring device based on autofocus variation. Burr thicknesses were measured on an optical CMM machine. All equipment used is described forth in this chapter. The basis setup of the drilling test is depicted in Figure 6.1.

6.1.1 Tool

The tool used was 2-flute, 1.6 mm diameter, HSS uncoated twist drill DIXI 1138/18652.04 V2 from the manufacturer DIXI. This drill had grounded split-point geometry, since it is known that the chisel edge length of standard geometries is greater, causing higher thrust force and thus greater burr volume formed. Moreover, this point geometry improves centering capability of the drill. The geometries with reduced chisel length

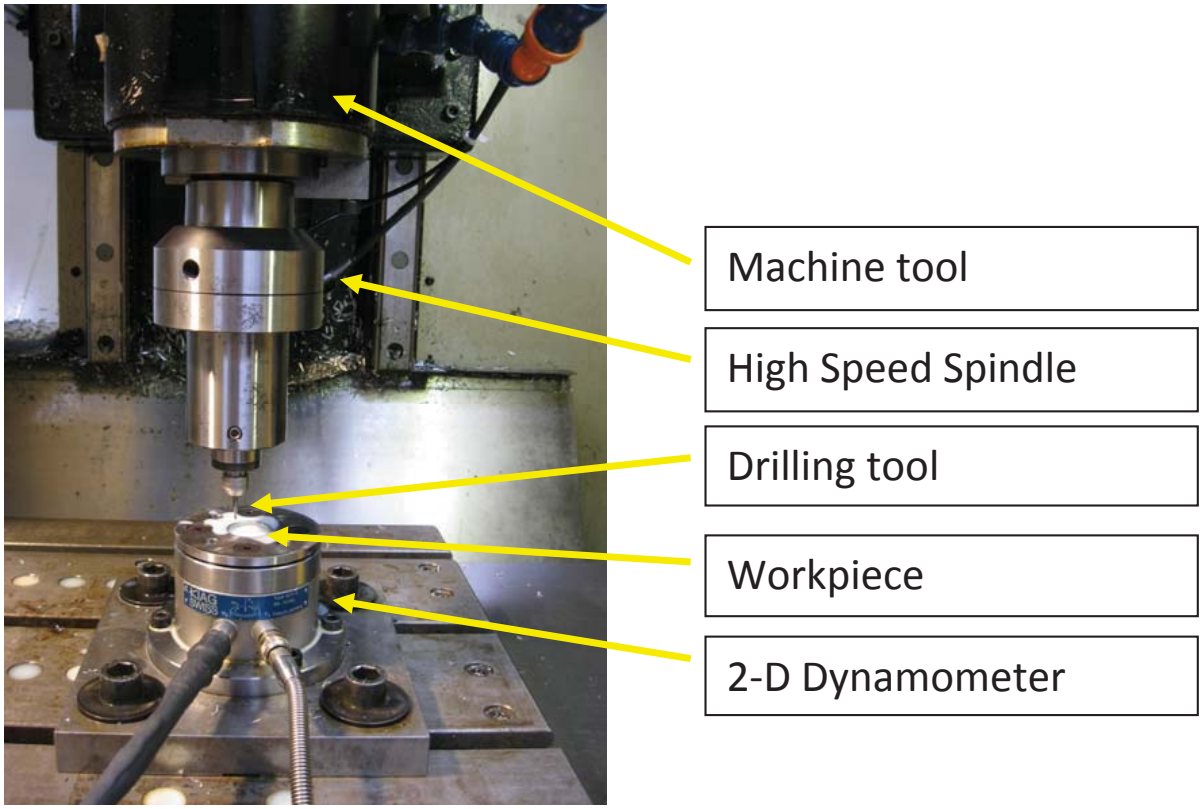

Figure 6.1: Experimental setup of preliminary drilling tests.

are thus of interest and therefore this geometry was chosen as a representative type for this test. The drill was of very short length, in order to avoid drill wandering during initiation of drilling process, slow helix and having polished flutes to prevent chip packing and material build-up. For the summary of the drill geometry see Table 6.1.

Table 6.1: Description of drill DIXI 1138/18652.04 V2 used during the preliminary test

Drill point	Flutes [-]	Material/Coating	Point angle [deg]	Helix angle [deg]	Flute length [mm]
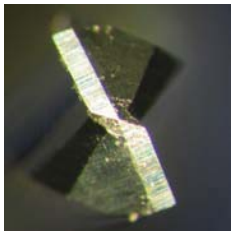	2	HSS/none	140	13	4

6.1.2 Machine tool

The machine tool used for the test was a vertical CNC milling machine Cincinnati Milacron Sabre 750 with 3 CNC controlled axes. The main characteristic of the machine tool are summarized in Table 6.3.

Table 6.3: Cincinnati Milacron Sabre 750 CNC characteristic

Characteristic	Unit	Magnitude
X/Y/Z axis travel	[mm]	762/381/508
Spindle revolutions	[min^{-1}]	60–8000
Feed speed range	[$m \cdot min^{-1}$]	3–15
Rapid traverse speed	[$m \cdot min^{-1}$]	15
Tool stations		12
Motor power	[kW]	11
Machine type		Vertical
Control		Acramatic

6.1.3 Attached high speed spindle

The main spindle of the CNC machine tool was capable to provide a maximum of 8 000 rev $\cdot$ min^{-1} which was insufficient for the purpose of the test. In order to achieve desired rotational speed required for effective machining, when using small drill diameter, an electrically driven high speed spindle HES–BT40 H from the Japanese manufacturer NSK Nakanishi was used. With high speed spindle mounted into the tapper fit of the machine, it was possible to reach rotational speeds of up to 50 000 rev $\cdot$ $min^{-1}$with limited power and torque output (see graph in Figure 6.2 for high speed spindle power characteristics). The high speed spindle consists of a compact brushless motor and spindle assembled together in a steel body which is fitted directly to the tapper fit of the main machine spindle. The spindle is provided with ultra-precision ceramic bearings in order to reduce heat generation by friction and to ensure high rotational accuracy. Moreover the air cooling is applied to prevent heat build-up and allow long, continuous operation. The rotational speed of the spindle is controlled by an external control unit Astro–E 500, model NE52–500 with resolution of 1000 rev $\cdot$ min^{-1}as well as selection of the rotational direction. Spindle run out is declared by manufacturer to be less than 1 μm when measured at the tapered part on the inside diameter of the chuck engaging portion and less than 8 μm after chucking. The main characteristic of the high speed spindle are summarized in Table 6.4.

Table 6.4: High speed spindle NSK Nakanishi HES–BT40 H characteristic

Characteristic	Unit	Magnitude
Spindle type		NSK Nakanishi HES–BT40 H
Control unit		NSK Nakanishi NE52–500
Max. spindle revolutions	[min^{-1}]	50 000
Max. output power	[W]	195
Max. torque	[Nm]	0.06 (for 0$\div$ 30 000 rev $\cdot$ min^{-1}, see Figure 6.2)
Motor cooling pressure	[bar]	Air, 2–5
Spindle run out	[μm]	$<$1
Run out after chucking	[μm]	$<$8

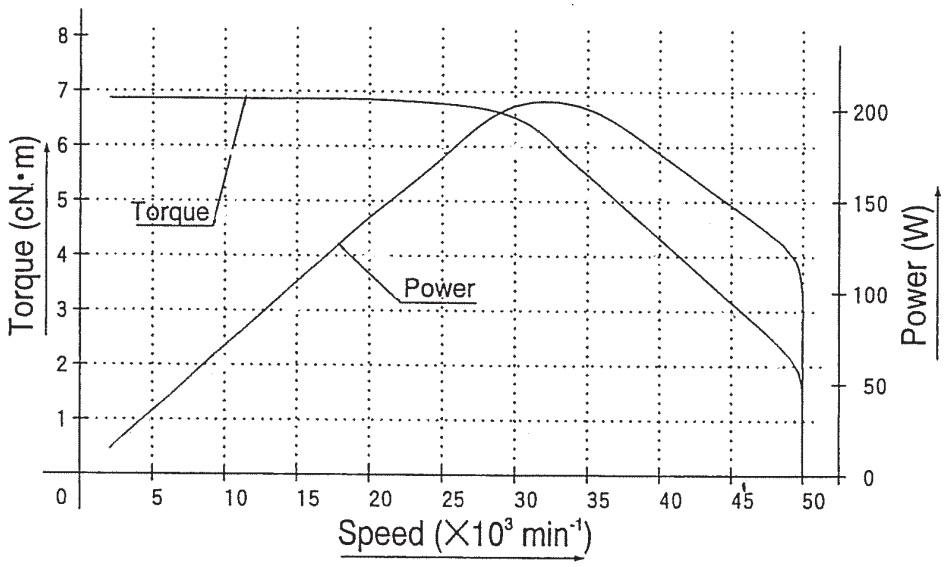

Figure 6.2: Power capabilities of the high speed spindle NSK Nakanishi HES–BT40 H depending on rotational spindle speed used.

6.1.4 Workpiece geometry

All operations were carried out on square specimens (50x50 mm) having thickness 2 mm. The given specimen geometry was chosen in respect to limited operating space of used optical measuring device as well as positioning with respect to axis of the dynamometer to ensure the best measuring accuracy. Sheet thickness of 2 mm was fixed dimension as previously mentioned in Chapter 5.3.

6.1.5 Workpiece clamping system

For evaluation of general behaviour of burr formation for present workpiece material used, a simple clamping system with no support of drilling exit side was used (see Figure 6.3 for sketch of the fixture used). In this way the workpiece was firmly fixed, preventing the thin plate from significant bending in axial direction of drilling feed force.

6.1.6 Thrust and torque measuring device

The two-component measuring piezo-electric transducer Kistler type 9271A, SN 76766 was used for measuring thrust and torque while drilling. This used load cell is capable of measuring simultaneously a force parallel to the load cell axis (drilling thrust) and a moment in the plane normal to the line of application of the force (drilling torque). The inbuilt quartz measuring cell permits working with minimal measuring displacement and also with relatively wide frequency range. The loads to be measured are strictly proportional to the electrical charges generated by the platform and consequently converted by charge amplifier Kistler 5051 into output voltage, which was digitized and recorded by using a PC acquisition board and Labwiew 8.0 software.

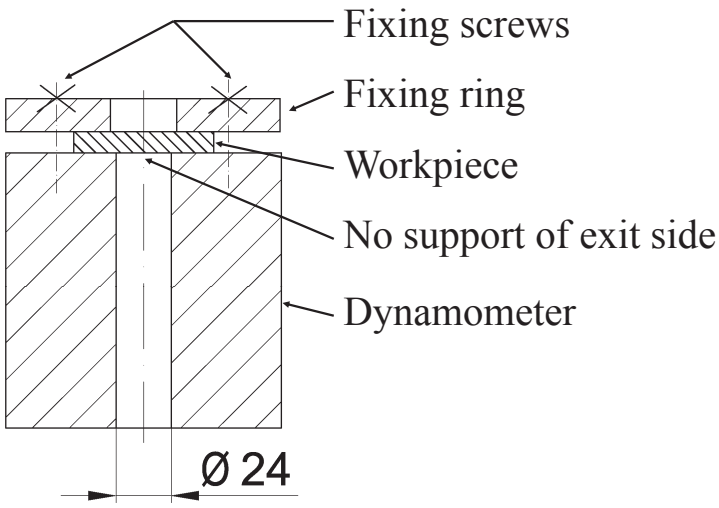

Figure 6.3: Schematic of clamping system used during the preliminary test.

6.1.7 Coolant

A 7 % oil emulsion MOTOREX SWISSCOOL 7755AERO was used during the tests. This emulsion is of the same kind as the one used in Bang & Olufsen workshop (HOCUT 795B — see Chapter 8.2.4). Both coolants are 7 % concentration of oil emulsion with water, resulting in milky-white, low foaming emulsion with good cooling and extremely high lubrication effect, especially suitable for machining aluminium and it's alloys.

6.1.8 Burr measuring devices

Infinite focus microscope

A non-contact, high resolution optical 3D measuring device the Alicona–Infinite focus was used for measuring of burr dimensions. As mentioned in chapter dealing with measurements of burrs (see Chapter 3.6), an optical system provides non-contact measurement which means that no surface damage is possible and the measurement results are much less error prone. The measuring system is based on Focus-Variation. Its operating principle combines the small depth of focus of an optical system with vertical scanning to provide topographical information from the variation of focus. The system provides the functionalities of an optical profiler and a micro coordinate measurement. Features several millimetres deep are robustly and traceably measured. Results are able to be reproduced with a vertical resolution of up to 10 nm even at scan heights up to several mm and a measurement field of up to 10 x 10 cm. On the other hand, optical systems encounter the difficulty of the burr edges with steep angles which may cause insufficient light intensity or reflection to the detector. Although the Infinite focus system allows dense and robust measurement exceeding 80°, the workpiece must be inclined in order to obtain the best measuring results. A detailed measuring procedure is described forth in Chapter 6.5.1. For detailed characteristic of the measuring device depending on used magnification see Table B.1, B.2 and Table B.3 enclosed as Appendix B.

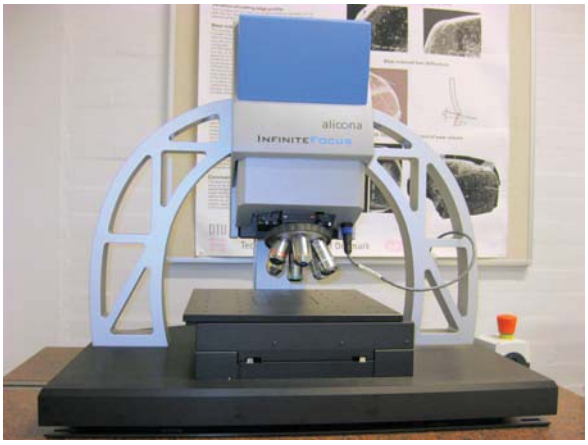

Figure 6.4: Infinite focus microscope.

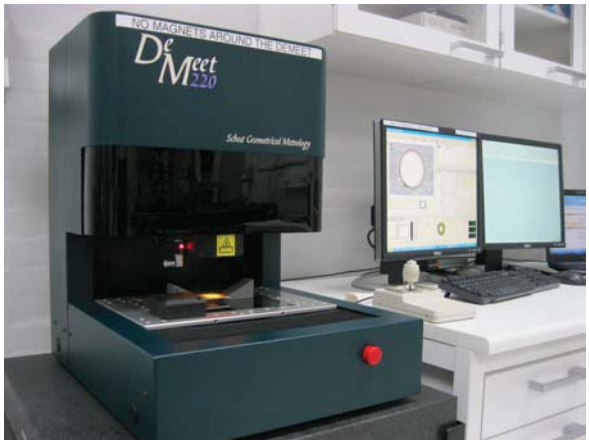

Figure 6.5: Optical CMM, DeMeet 220.

Optical CMM

An optical coordinate-measuring machine (CMM) DeMeet 220 from Shut Geometrical Metrology equipped with a X5 magnification lens providing a total screen magnification of X200 with a resolution of 0.1 μm was used for measuring of burr widths. The optical CMM working principle is based on measuring on the picture of the workpiece taken by a CCD-camera. The picture of the surface is digitized into an array containing information of the light intensity of each pixel. The picture processing computer detects edges based upon transition in the picture from dark to light and vice versa. This principle is used to determine the X and Y-coordinates of the measured object. The Z-coordinate is determinate by video focus. For detailed measuring procedure of burr widths see Chapter 6.5.2.

6.2 Experimental plan

The experimental plan of the preliminary test was based on DOE, testing one factor at the time (for details see introduction of DOE in Chapter 4, particularly in Section 4.3.2). Tested factors influencing burr formation were cutting speed and feed per revolution, more detailed in the corresponding sections.

6.2.1 Influence of cutting speed on burr formation

In the first setting, the fixed factor was drilling feed per revolution (uncut chip thickness) with various five levels of cutting speed in order to investigate cutting speed influence on burr formation. The values of tested levels of cutting speed were based on setting the basic level as an optimal magnitude proposed by the drill manufacturer. The basic level is usually set as the middle one, but since the interest was of reduction of producing time (speeding up the process) and moreover the literature survey indicated that higher cutting speed can have a positive influence on burr reduction, to test the field of higher speeds was desired. The value of fixed feed per revolution was kept as the value proposed by the drill manufacturer (see Table 6.5 for the test setting overview). In order to reduce variability and to obtain meaningful data for statistical evaluation, each setting order was repeated six times.

Table 6.5: Preliminary test setting, where influence of cutting speed on burr formation was investigated (fixed feed per revolution, varying cutting speed)

Order		1	2	3	4	5
Cutting speed (v_c)	[m · min^{-1}]	80.42	115.61	150.80	185.98	221.17
Feed per revolution (f)	[mm]			0.035		
Spindle revolutions (n)	[min^{-1}]	16000	23000	30000	37000	44000
Feed speed (v_f)	[mm · min^{-1}]	560	805	1050	1295	1540

6.2.2 Influence of feed per revolution on burr formation

In the second setting, the fixed factor was cutting speed of a magnitude proposed by the drill manufacturer. In order to investigate influence of various feeds per revolution on burr formation mechanism, five levels of feed per revolution were used. Again it was of the interest to investigate higher feeds in order to reduce producing time, therefore the magnitude of feed rate proposed by the drill manufacturer was set as the basic level. Each setting order was again repeated six times in order to reduce variability of the results. For the test setting overview see Table 6.6.

Table 6.6: Preliminary test setting, where influence of feed per revolution on burr formation was investigated (fixed cutting speed, varying feed per revolution)

Order		1	2	3	4	5
Feed per revolution (f)	[mm]	0.035	0.064	0.093	0.121	0.150
Cutting speed (v_c)	[m · min^{-1}]			80.42		
Spindle revolutions (n)	[min^{-1}]			16000		
Feed speed (v_f)	[mm · min^{-1}]	560	1020	1480	1940	2400

6.3 Experimental procedure

A preliminary drilling experiment was performed with equipment described above in Chapter 6.1. The dynamometer Kistler 9271A was mounted on the table of the milling machine Cincinnati Milacron Sabre 750 and connected with charge amplifiers Kistler 5051 and PC acquisition board equipped with Labview 8.0. The workpiece was clamped by the fixture directly on the dynamometer in sense of no support of drill exit side (see Section 6.1.5). The high speed spindle HES-BT 40 H was mounted to the main spindle of the milling machine and connected with control unit, air regulation and air compressor to provide cooling.

Drilling procedure was performed in the following order:

- Run-in with the new drill (15 holes, setting of an adequate measuring range of the dynamometer) $n = 16000\,\text{min}^{-1}$, $f = 0.035\,\text{mm}$.
- Drilling of the first setting — fixed feed with 6 replications for each level of cutting speed with applied coolant (resulted in 2 workpieces drilled, since 3

replications of each cutting speed level were used on one workpiece, see Figure 6.6).

Note: Coolant was applied manually via hand sprayer since insufficient sealing of cables connecting dynamometer with amplifiers was experienced in past when flooding of delivered coolant applied directly via machine pump.

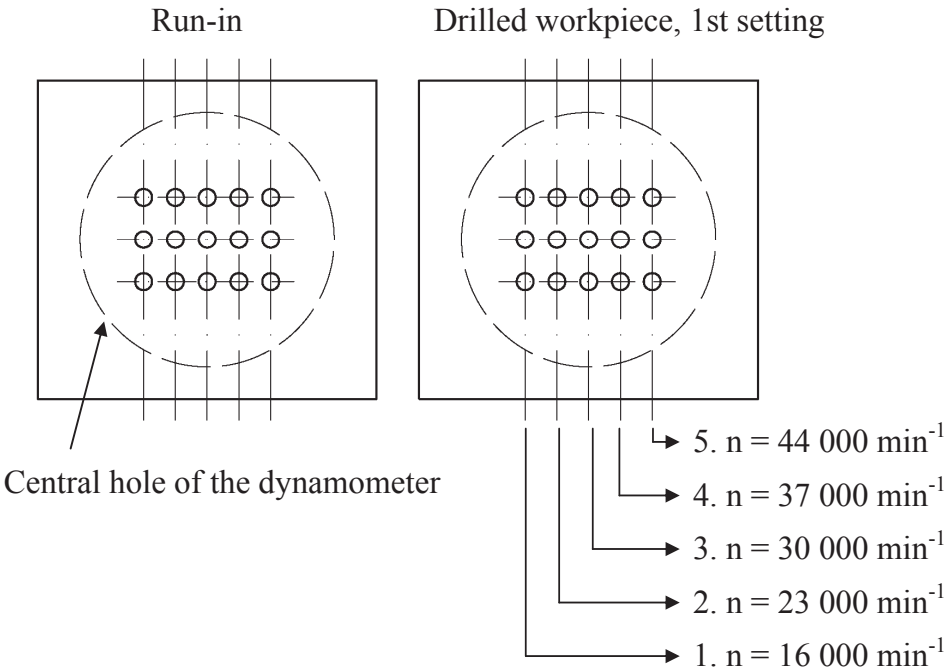

Figure 6.6: Schematic of the 1st drilling order setting on workpiece with 3 replications for each level of cutting speed (an investigation of influence of cutting speed on burr formation — Preliminary test).

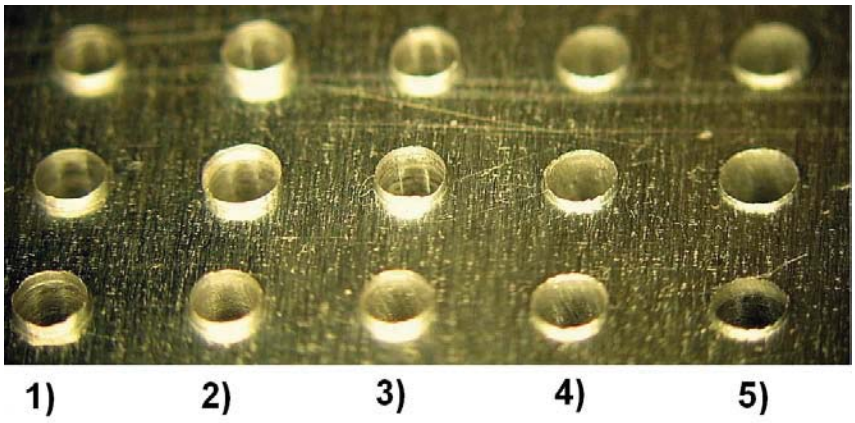

Figure 6.7: Photograph of exit burrs resulting from the 1st preliminary test setting (see Figure 6.6) with indication of used conditions (an investigation of influence of cutting speed on burr formation).

- Comparison of measured forces (thrust and torque) with theoretically calculated ones in order to check capability of the high speed spindle power requirements for the 2nd setting of the test with varying feed.

Note: Since the measured data of the torque were oscillating in a wide range during the drilling process, it was not possible to directly decide whether the theoretical calculations of the torque required matched with measured ones. No deceleration of the high speed spindle, which would indicate insufficient power of the electric motor, was noticed. Seeing that overreaching the torque requirement would result in stopping the spindle while the drill would still be fed into the material, which may result in breakage of the tool or even the ceramic bearings in the electrical high speed spindle to be damaged, it was decided not to use the high speed spindle for the 2nd test with varying feed. The requirements for necessary torque were expected to may be on the border of the capability of the high speed spindle for highest intended feeds to be used. Thus the second test with various feeds for investigation of feed influence on burr formation was decided to perform with using the main machine tool spindle, which is much more powerful than the electrical high speed spindle attached, but providing lower maximum rotational speed than was intended. In this way, the experimental plan had to be adjusted in accordance with maximum rotational speed of the machine used. The final decision of capability to use high speed spindle for consequent tests could be evaluated based on the force measurements data from such a adjusted test.

Adjustment of the second test parameters for feed influence evaluation

Since the machine tool used was capable of maximal spindle rotations of 8000 min^{-1} (see Table 6.3 for machine tool overview) whereas 16 000 min^{-1} was originally intended, the drilling parameters of the test had to be accordingly adjusted. It is generally advised not to use machine tool at maximum possible rotational speed because of wear of machine parts, but rather of at about minimal 10 % lower range. Therefore, the cutting speed intended to use during the test was adjusted to a magnitude of 35 $\text{m} \cdot \text{min}^{-1}$ whereas initially intended 80.42 $\text{m} \cdot \text{min}^{-1}$, resulting in spindle rotations of 6 963 min^{-1} (see Table 6.7 for overview of adjusted test parameters).

Table 6.7: Adjusted 2nd preliminary test setting, where influence of feed per revolution on burr formation was investigated (fixed cutting speed, varying feed per revolution)

Order		1	2	3	4	5
Feed per revolution (f)	[mm]	0.035	0.064	0.093	0.121	0.150
Cutting speed (v_c)	[$\text{m} \cdot \text{min}^{-1}$]			35		
Spindle rotations (n)	[min^{-1}]			6 963		
Feed speed (v_f)	[$\text{mm} \cdot \text{min}^{-1}$]	244	444	644	844	1044

- Drilling of the second, adjusted setting — fixed speed with 6 replications for each level of feed per revolution with applied coolant (resulted in 2 workpieces drilled, since 3 replications of each feed were used on one workpiece, see Figure 6.8).

Repetition of the tests — Suspicion of external sources influencing measurements

Because of findings discussed and showed in Chapter 6.6.1, it was decided to repeat the test with randomized order. All process parameters to be tested with replications were

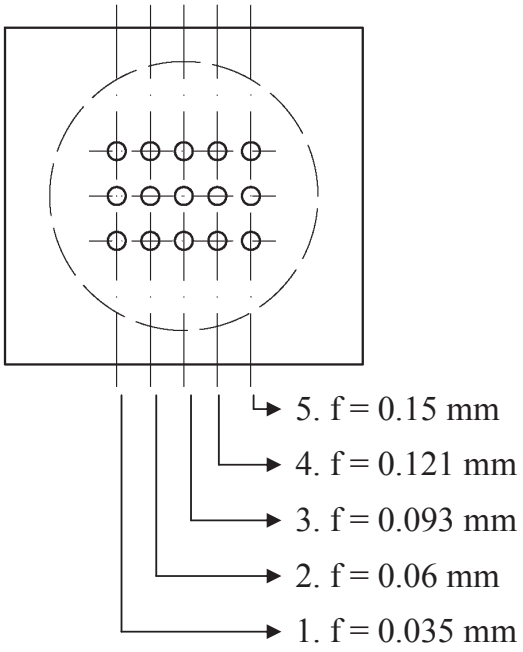

Figure 6.8: Schematic of the 2nd drilling order setting on workpiece with 3 replications of each level of feed per revolution (an investigation of feed per revolution on burr formation — Preliminary test).

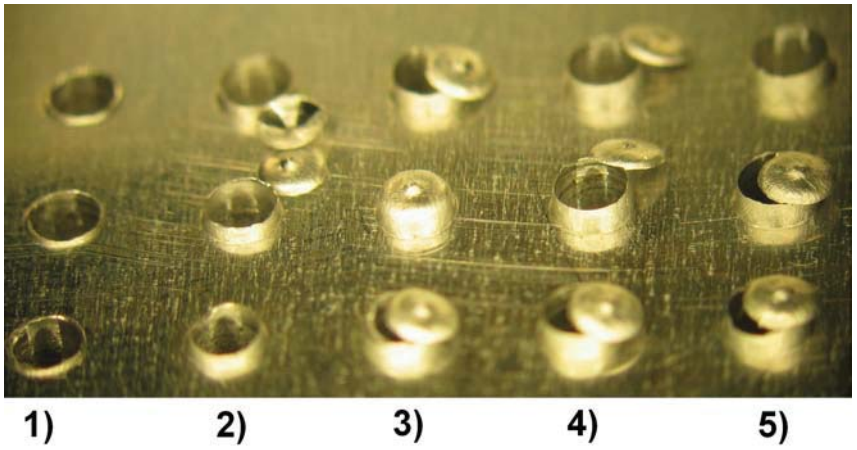

Figure 6.9: Photograph of exit burrs resulting from the 2nd preliminary test setting (see Figure 6.8) with indication of used setting (an investigation of feed per revolution on burr formation).

randomized as well as position of holes drilled on the workpiece. Such a setting makes difficulties with the test execution and consequent measurement of burr dimensions is more prone to be mistaken because of difficult order. However, with this setting it was possible to restrict any unwanted source influencing burr formation and to test only desired parameters. By comparison of initial non-randomized data with data gained from randomized test order, it was possible to evaluate signification of randomized setting for subsequent tests.

6.4 Force measurements

6.4.1 Setup

The feed force (thrust) and torque were recorded as a function of time for all holes drilled with using equipment described in Chapter 6.1.6. The measurements were performed by 2D piezo-electric transducer Kistler 9271A and 2 amplifiers Kistler 5015 (one for amplification of the thrust force output and second for the torque). Since the low amplitudes of measurands (thrust force and particularly drilling torque in a range of few Ncm) were of measuring interest, the measuring range of amplifiers had to be set as close to the expected maximal values as possible in order to gain precise measurement data. Therefore for the thrust force evaluation was the amplifier range set to 100 N over all tests and for drilling torque as 20 Ncm when testing different speeds and 50 Ncm when testing different feeds per revolution. The amplified output was then digitized and recorded by using PC acquisition board and LabVIEW 8.0 software at a sampling frequency of 10 kHz (see Table 6.8 for overview of measuring setting).

Table 6.8: Setting of force measurement equipment during preliminary test

Test / Equipment setting		1st setting (various cutting speeds)	2nd setting (various feeds)
Sampling frequency (f_s)	[Hz]	10000	10000
Thrust amplifier range	[N]	100	100
Torque amplifier range	[Ncm]	20	50

Minimal sampling frequency can be determined according to the spindle speed and number of cutting edges of the tool. In the present test, the highest spindle rotations of 44 000 min^{-1} and 2 flute drill was used, thus minimal measuring frequency is calculated forth in equation 6.1 and results in 1 467 Hz.

$$f_m = \frac{(2n)}{60} = \frac{(2 \cdot 44000)}{60} \cong 1467\,\text{Hz} \tag{6.1}$$

In order to prevent signal aliasing — a phenomenon that arises when a signal is undersampled (sampled too slowly) providing a poor representation of analog signal, the used sampling frequency was increased according to the Nyquist theorem. The Nyquist theorem (see [41] for more details) states that when you sample an analog signal, any signal components at frequencies greater than half the sampling frequency (f_s) appears in the sampled data as a lower frequency data. Generally speaking, a faster sampling frequency provides a better representation of the original signal. Therefore a 10 kHz sampling frequency was used securing no signal aliasing since a frequency at which cutting edges of the drill rotates (f_m) is lower than the Nyquist frequency (f_n), see Equation 6.2 [41].

$$f_m = 1467\,\text{Hz} < f_n = \frac{f_s}{2} = 5000\,\text{Hz} \tag{6.2}$$

6.4.2 calibration

Before initiation of the experiment, care had to taken about correct calibration of the measuring equipment. It is essential to be sure that voltage output, corresponding to forces applied, from the dynamometer is correctly conversed to forces output. Since the dynamometer was already calibrated and calibration list was present, calibration specifications were used for setting of the equipment and for validation of such setting, simple weight check was performed. The weights used were of range 0.2 to 2 kg calibrated by DANAK (see Table 6.9 for overview of weights used). The weight check showed very good agreement between forces resulting from weights applied with forces acquired by measuring system indicating no additional calibration to be required.
Moment calibration in a such a small range of at about 20 Ncm was rather more difficult. However, according to the dynamometer calibration sheet, it is enough to check only the axial force calibration, because of the moment sensitivity is virtually unaffected by the method of mounting or loading.

Table 6.9: Weights calibrated by DANAK used for calibration of force measuring equipment

Weight [kg]	Instrument number	Certificate number
0.2	1047376	C03570
0.5	1047377	C03599
1	1047318	C03500
2	1047379	C03601

6.4.3 Execution

For each hole drilled, during the test, thrust and torque measurements were taken. Gained data was properly designated and saved for later evaluation. Before subsequent hole to be drilled, the amplifiers were reset and new measurement of subsequent hole was taken.
Figures 6.10, 6.11 show first measurement data taken during the test with ordinary force measurement setting experienced from former force measurements at the workshop. From this figure it is apparent that measured signal was not very clean, making impossible to directly evaluate actual magnitude of the drilling torque and causing greater uncertainty of maximum feed force applied. Therefore more effort had to be put in revealing of the source of measurement data fluctuation.

6.4.4 Reduction of noise in force measurements data

In order to reveal source of the noise, spectral analysis based on a fast fourier transform (FFT) of the measured data was conducted via software Matlab, using FFT script accessible via Matlab help and modified according to particular needs. The theory behind FFT will not be detailed in present work, but it can be found via Matlab help or any other literature dealing with data processing and filtering (e.g. [41]).

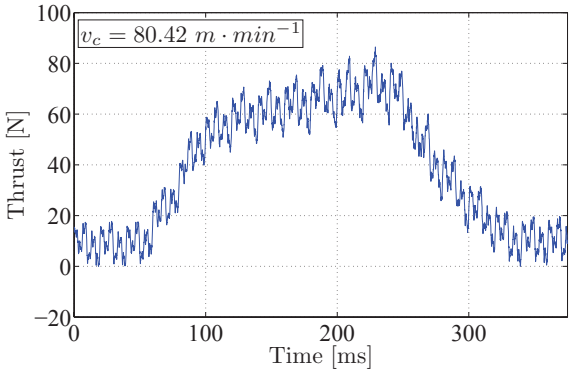

Figure 6.10: Thrust force measurement data influenced by electrical noise ($n = 16000\,\text{min}^{-1}$, $f = 0.035\,mm$).

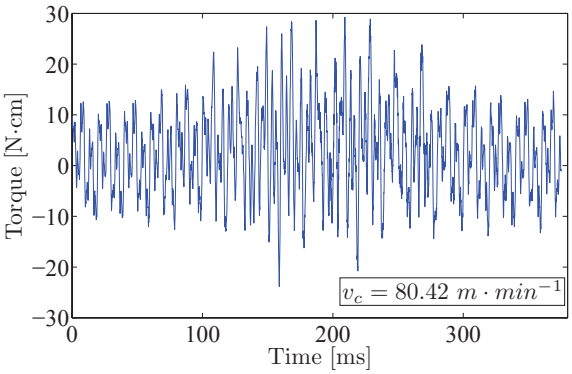

Figure 6.11: Torque measurement data influenced by electrical noise ($n = 16000\,\text{min}^{-1}$, $f = 0.035\,mm$).

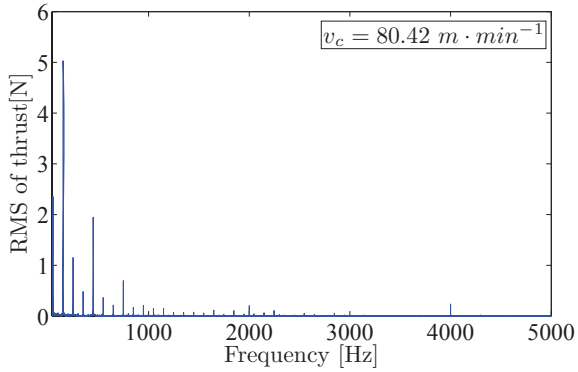

Figure 6.12: One sided spectral analysis using Fast Fourier Transform of thrust measurement data shown in Figure 6.10.

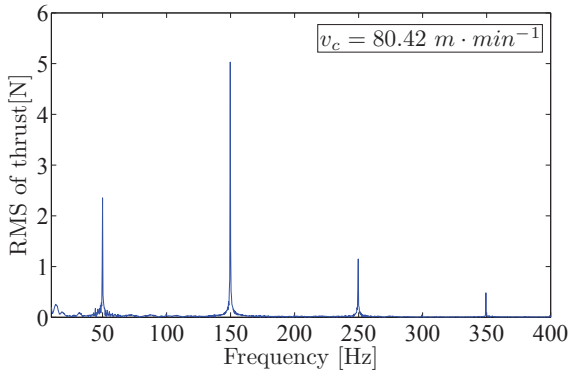

Figure 6.13: Zoomed spectral analysis on Figure 6.12.

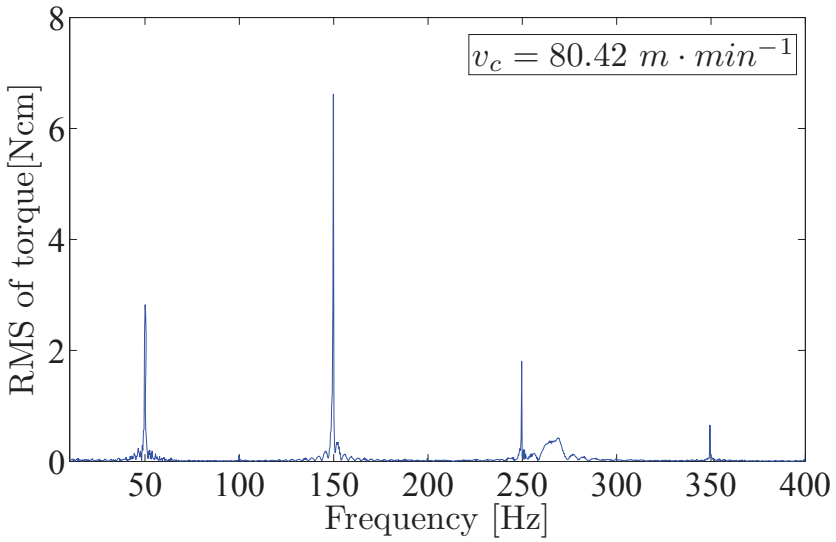

Figure 6.14: Zoomed spectral analysis of torque measurement data shown in Figure 6.11.

Performed spectral analysis, on thrust measurement data (depicted in Figure 6.10), is shown in Figure 6.12. The graph reveal significant frequencies present in lower range of frequencies from measurement. Hence, in order to reveal the source of present frequencies, the graph was zoomed only on low range of frequencies in range of 0 to 400 Hz and such s graph is shown in Figure 6.14. From this zoomed graph (Figure 6.14), it was possible to clearly reveal periodic frequencies of 50 Hz clearly indicating present electrical noise. This was caused because of the low amplitudes of measurands (thrust force and particularly drilling torque) were of measuring interest and it made the signal very susceptible to the effect of electrical noise. Almost all PC-based data acquisition applications are subjected to some degree of 50 or 60 Hz noise picked up from machinery or power lines and therefore investigation of proper grounding of the measuring system was necessary. In order to evaluate presence of the electric noise, all following spectral analysis plots are zoomed on the range of lower frequencies from measurement data.

The source of the electrical noise was found to be caused by difference in ground potentials of the tool machinery and measuring equipment, since the machine had its own grounding different from the one used for power lines to which was measuring equipment connected through an electrical socket in order to power the measuring equipment.

After elimination of the difference in ground potentials of the tool machinery and measuring equipment by using the same source of grounding, measured data shown in Figure 6.15 for thrust force and in Figure 6.16 for torque measurement were obtained, representing way much cleaner signal.

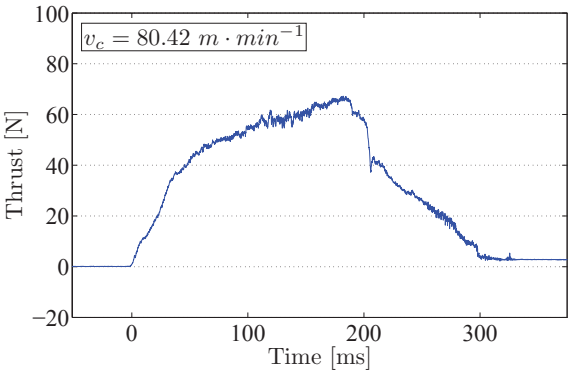

Figure 6.15: Thrust force measurement with proper grounding ($n = 16000\,\text{min}^{-1}$, $f = 0.035\,mm$).

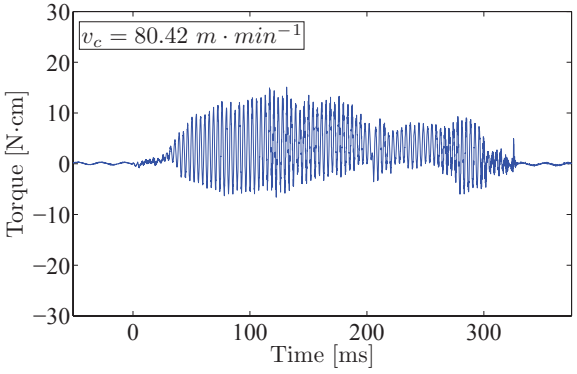

Figure 6.16: Torque measurement data with proper grounding ($n = 16000\,\text{min}^{-1}$, $f = 0.035\,mm$).

Spectral analysis performed on this measured data (see Figure 6.17 for thrust measurement data and Figure 6.18 for torque measurement data) showed that presence of the electrical noise was eliminated.

The remaining peak in zoomed spectral analysis of the torque measurement data in Figure 6.18 represents irregularities in geometry of cutting edges of the tool being not absolutely identical. This assumption can be proved by the known parameter, that the drill was rotating at 16000 revolutions per minute resulting in 266.7 rotations per second or expressed as rotational frequency of 266.7 Hz, which is exactly the value seen in Figure 6.18. Irregularities in drill geometry can contribute to drill wobbling

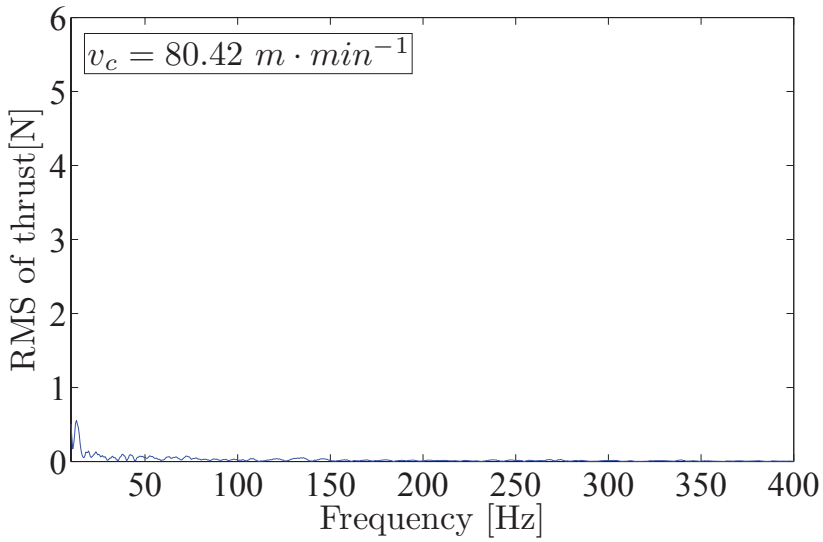

Figure 6.17: Zoomed spectral analysis of thrust measurement data with proper grounding shown in Figure 6.15.

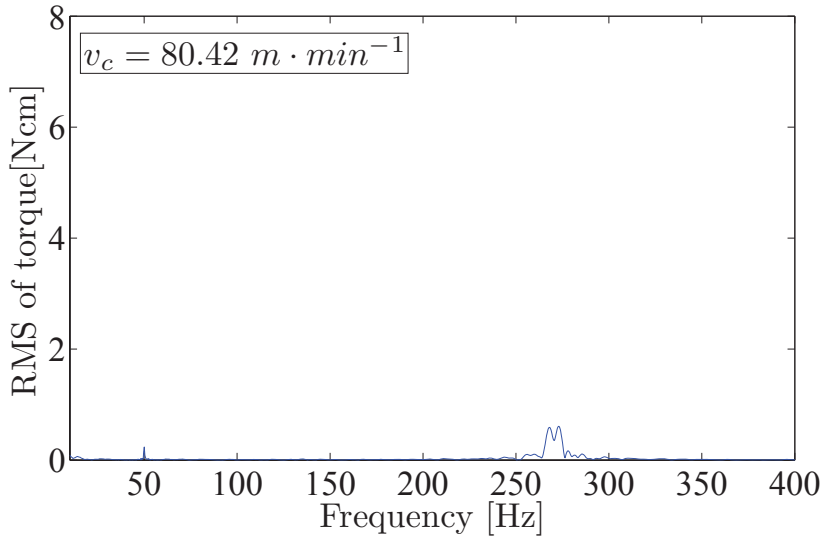

Figure 6.18: Zoomed spectral analysis of torque measurement data with proper grounding shown in Figure 6.16.

and drill wandering at the hole entry, which might result in defects at hole entry causing non-uniform appearance of the holes drilled. Hence, in spite of impossibility to manufacture drill with perfectly symmetrical edges, the symmetry of the drill must be kept as close as possible to avoid this.

6.4.5 Force data evaluation

Measurements taken with properly grounded measuring equipment were consequently treated, via created Matlab template, in order to plot the trend in thrust force and torque as a function of drilling time. By means of this template, the maximal thrust force and torque for each hole drilled were obtained.

Source of torque data fluctuation

For evaluation of drilling torque applied during drilling, the torque measurement data fluctuation had to be eliminated at first. It is apparent, that the maxim value of the torque in Figure 6.19 can not be considered as maxim torque applied during drilling operation, because the maxim torque output of the high speed spindle was only at about 6.5 Ncm while 16000 rev $\cdot$ min^{-1} used (see Figure 6.2 for high speed spindle power characteristics), whereas the data shows maximum value of at about 15 Ncm. Such a torque would result in stopping of the spindle. Any deceleration or even stopping of the spindle was not observed during the test. Therefore, the real magnitude of torque used was evaluated by filtering out the fluctuation. At first, the source of fluctuation, which was observed only in rage of the drilling process, was evaluated by zooming on small area of the data depicted in Figure 6.19 in order to reveal oscillation frequency. From zoomed area in Figure 6.20 it is possible to see, that the oscillation is repeating with constant frequency of bit lower magnitude than 4 ms^{-1}. This frequency is directly corresponding to the rotations of the spindle applied during drilling ($n = 16000\,\text{min}^{-1} = 266.6\,\text{s}^{-1}$or Hz $= 0.2666\,\text{ms}^{-1}$ resulting in 1 revolution of the drill in 3.75 ms $\Rightarrow$ observed oscillation frequency) and is seen in spectral analysis of the measurement data in Figure 6.18. As discussed in Chapter 6.4.4, it was caused by irregularities in geometry of cutting edges of the tool being not absolutely identical.

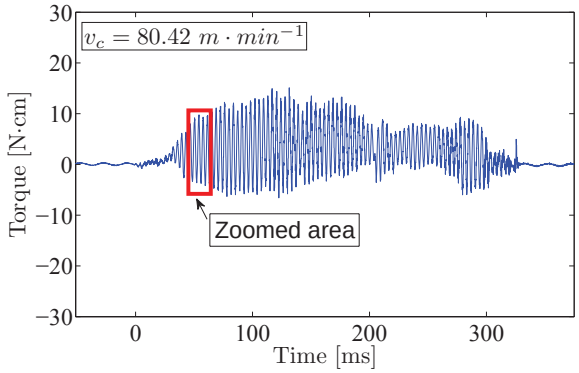

Figure 6.19: Torque measurement from Fig. 6.16 data with depicted zoomed area on fluctuation.

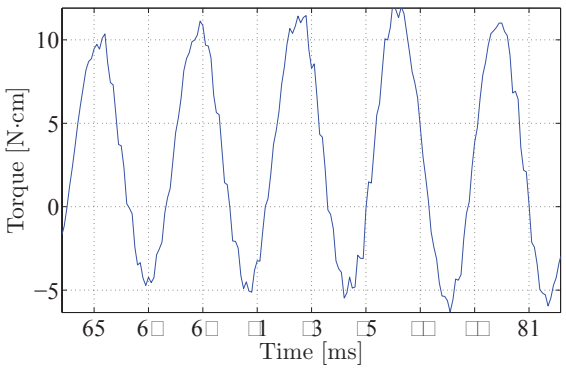

Figure 6.20: Zoomed area of torque data fluctuation depicted in Figure 6.19 for frequency evaluation.

Filtering of the torque fluctuation

In order to smooth out the torque measurement data, it was decided to use digital filter via Matlab software. The Savitzky-Golay smoothing filter — sgolayfilt — was used. Savitzky-Golay filter (also called digital smoothing polynomial filter or least-square smoothing filter) is typically used to "smooth out" a noisy signal whose frequency span (without noise) is large. In this type of application, Savitzky-Golay smoothing filters perform much better than standard averaging FIR filters, which tend to filter out a significant portion of the signal's high frequency content along with the noise. The major advantage of using this filter is that it tends to preserve features of the distribution such as relative maxima, minima and width, which are usually "flattened" by other adjacent averaging techniques (like moving averages, for example) [41],

[Matlab help]. The used value of length for signal processing used was 131 with using 3rd-order filter. Figure 6.21 shows the comparison of raw torque measuring data with data smoothed out with using digital Savitzky-Golay smoothing filter. From the shape of the filtered curve it is more distinctly possible to see behaviour of the torque with drilling time and to evaluate actual torque applied during drilling operation.

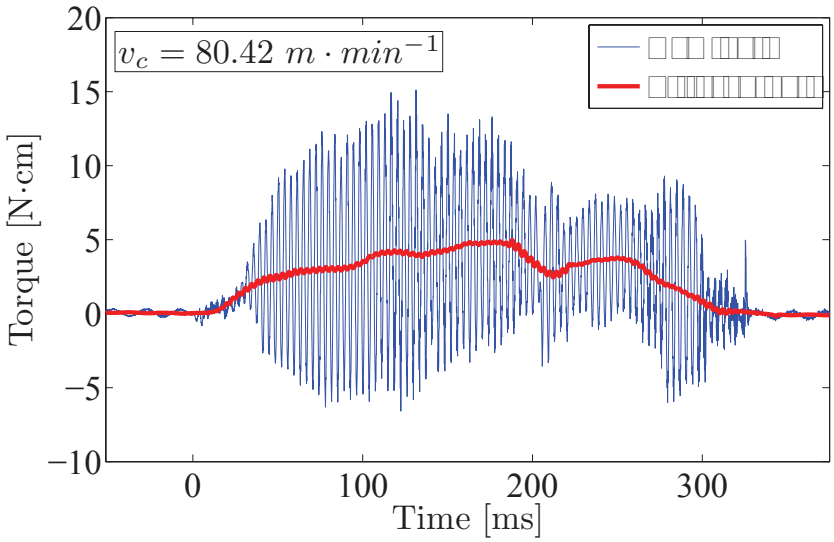

Figure 6.21: Comparison of raw torque measuring data with data smoothed out with using digital Savitzky-Golay smoothing filter on Fig. 6.16 data.

Drilling forces evaluation

In order to clearly show behaviour of drilling thrust and torque depending on drill position when drilling, the measuring data were plotted with dashed lines indicating the drill position. In the interest of graphs lucidity, only filtered curve representing the drilling torque is shown for all plotted graphs in connection with drilling thrust. The graphical description is shown in Figure 6.22. First dashed line marked as t0 represents the point when the drill touches the top layer of the workpiece, subsequently the second line labelled as t1 represents the position when full drill diameter got involved in cutting. The third line designated as t3 indicates the position when drill tip touches the bottom surface of the workpiece. The last line t4 shows the position when drilling is complete and the drill overrun follows. All drill positions were calculated according to drilling length and feed speed used for each setting indicated by label in each graph. The maximal thrust force and torque for each hole drilled was evaluated and the results are presented forth in Chapter **??**. The force measurement plots were produced for all holes drilled during the test and are enclosed in Appendix C.

6.5 Burr measurements

Since the ISO 13715 defines burr size only by one value as previously discussed in the literature survey (see Chapter 3), the measurement values used in present work were in accordance with Schäfer (see Chapter 3.5 for details). The reasons for measuring burr heights as well as thicknesses are presented in mentioned section of literature

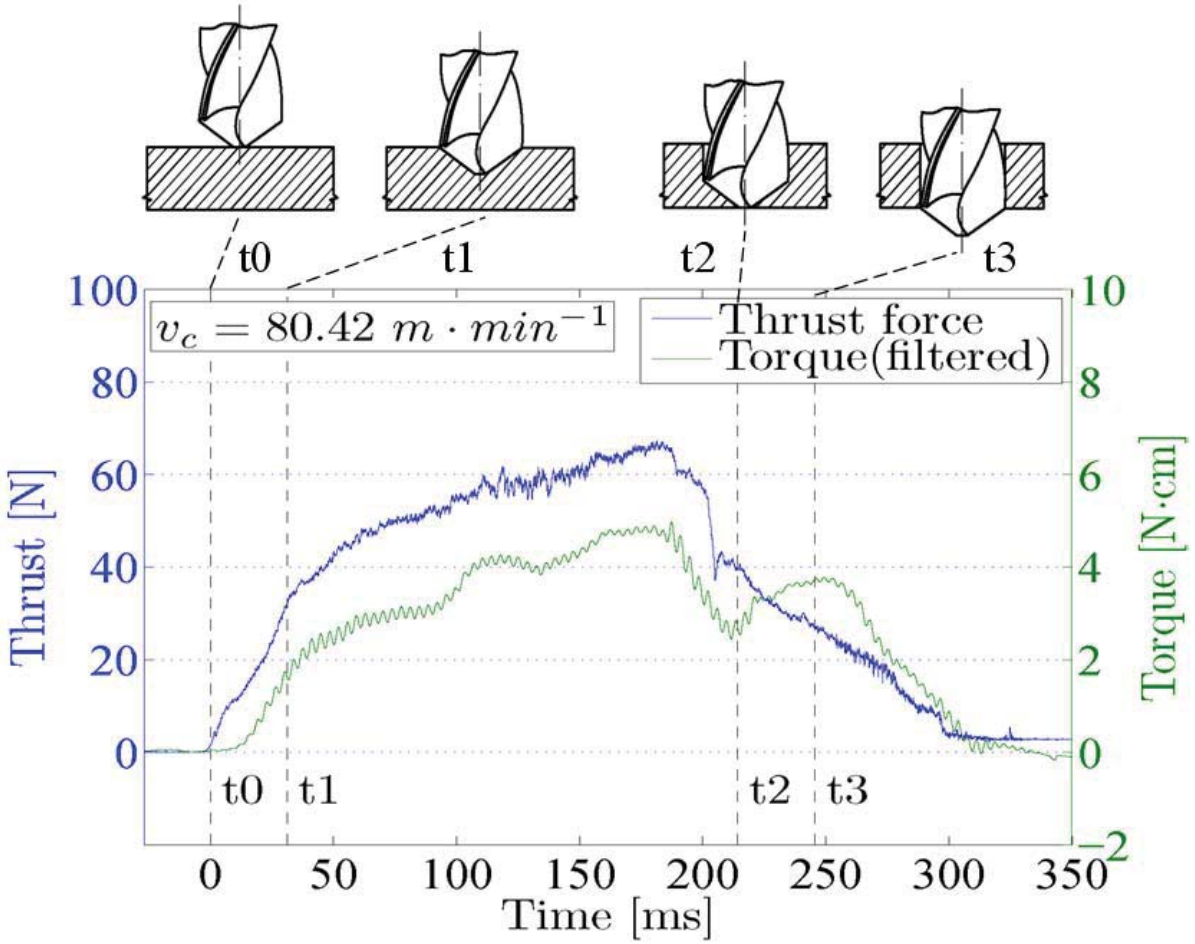

Figure 6.22: Description of force measurement plots with drill positions indicated.

survey. In present work was desired to reduce burr sizes to that size, which can be easily removed by consequent anodizing process in order to reach scratch protective surface of the workpieces. From gained experience in the company it was known that burr width plays very important role and it can not be neglected. The reason is that high thin burr can be removed much easily by consequent anodizing process than short, but thick burr which is made of work hardened basic material. The burr root width measured represents the distance from drilled hole circumference where the curvature of plastically deformed base material into the bur begins.

In contrast with Schäfer's measuring proposals, it was decided to neglect burr root radius value for present evaluation, because of the time restriction and great magnitude variation of the circle fitted to the burr root around the burr perimeter, making this measurements insufficient. In case of small proportion of an excessive burr height present (see Figure 6.24, right picture), caused by separation of drilling cap, it's height and angular proportion was measured in addition to the representative burr height. For overview of burr measured geometry evaluated in present work see Figure 6.23.

The sizes of burrs formed at the drill exit and entry side were measured for each hole drilled during the test according to burr geometry description characterized in Figure 6.23. Total of 120 burr measurements, 10 combinations of process parameters

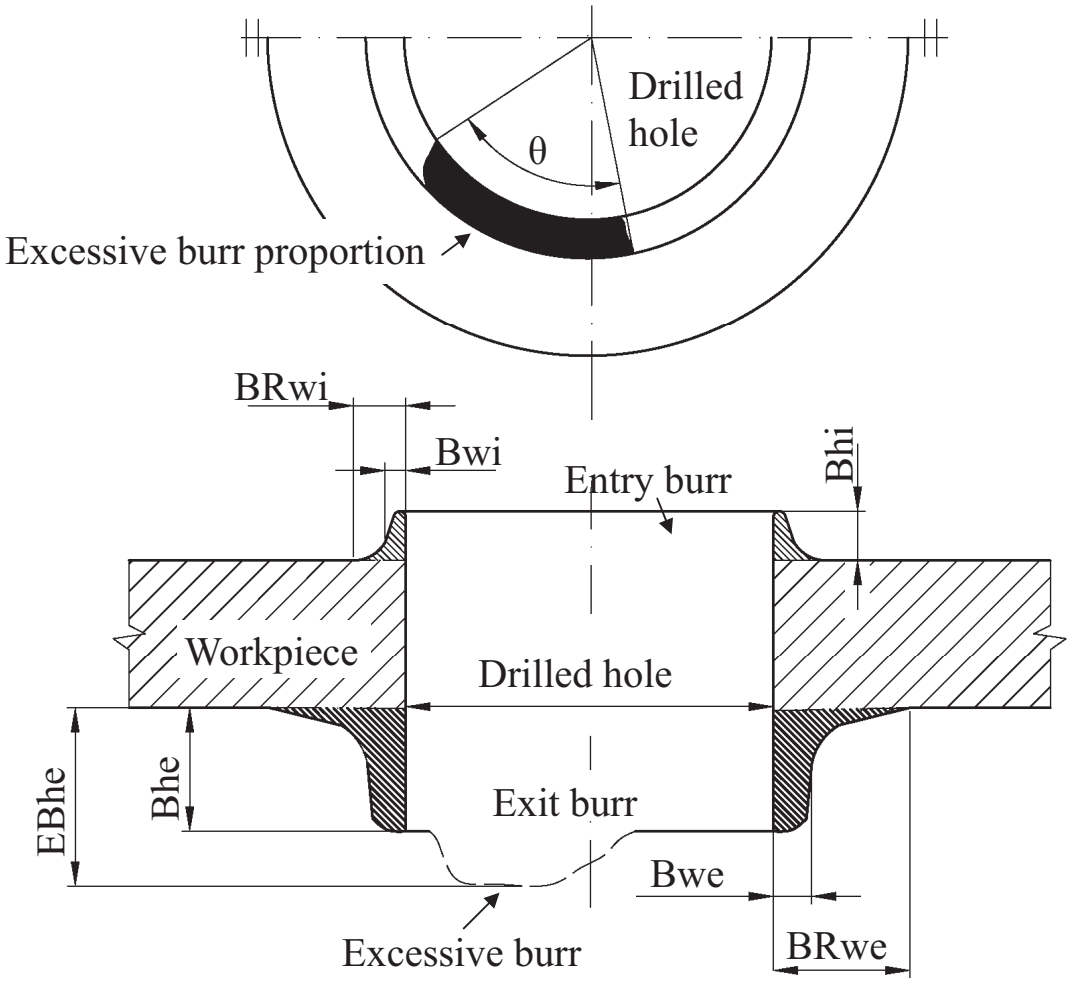

Figure 6.23: Description of measured burr geometry, where: Bhe — exit burr height, Bhi — entry burr height, $BRwe$ — exit burr root width, $BRwi$ — entry burr root width, Bwe — exit burr width, Bwi — entry burr width, $EBhe$ — Excessive burr height, θ — an angular proportion of an excessive burr.

with 6 replications for entry and exit burr were performed. For each entry and exit burr, the height(s) and widths (thicknesses) were evaluated and results are presented in Chapter 6.6.

6.5.1 Burr height

Burr heights were measured by using an optical measuring device Alicona Infinite-focus (for description see Chapter 6.1.8). In spite of the burrs were found to be uniform under the microscope (see Figures 6.7, 6.9), their height is somewhat varying around the circumference. Therefore whole burr perimeter was involved in measurements (see Figure 6.25). All holes drilled were measured, resulting in 6 measuring replications for each tested setting in order to reduce variability of the results.

Since the burr edges have steep angles making difficulties with light reflection, the measured workpiece was placed on stair-step fixture and placed on the table of the Alicona (Figure 6.24). This provided an inclination angle of 22 ° for scanning procedure in order to obtain the best measuring results. Magnification of 5X with measuring

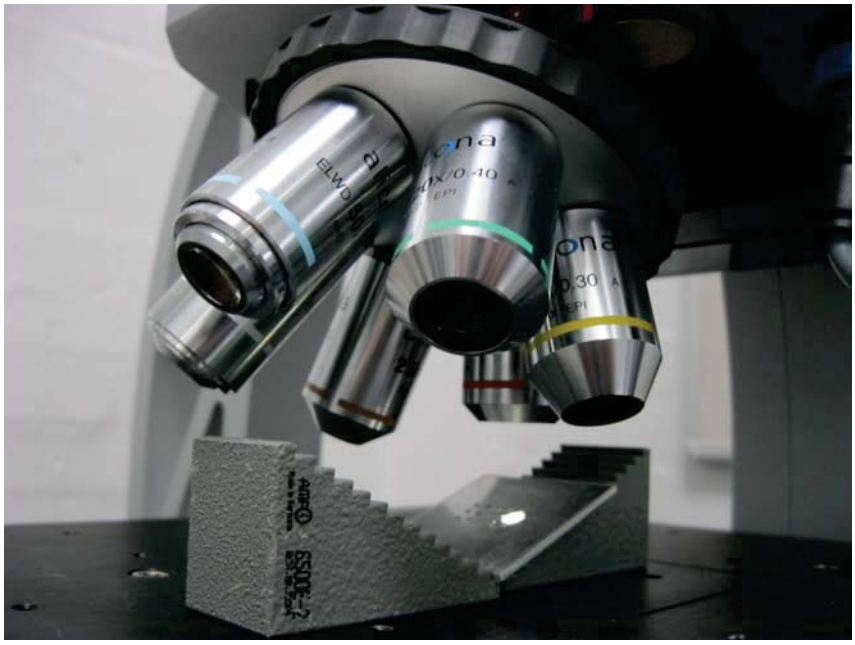

Figure 6.24: Workpiece clamping by means of stair-step fixture on Alicona Infinite-focus working table.

range of 2.8392 x 2.1538 mm was used and 3D reconstruction of whole burr formed was made by scanning of 2D vertical layers with vertical resolution of 5 μm in between 2 focused levels (lower = drilled sheet surface and upper one bit above the top of the burr height in Z–direction). Range of the scanned area in Z–direction was dependent on actual measured dimension of the burr and with the highest measured burr having magnitude of 3 mm. In order to avoid unintentional peaks in the 3D reconstruction, the polarized light was used. Without polarization filter was an image with a huge brightness range obtained which was caused by steep slopes of the sample. In that case some image parts may be too dark for 3D measurement which may result in unintentional peaks in the 3D reconstruction. For each measurement was created specific file containing the 3D burr model with an extension *.al3d. Such a file was properly designated and saved on a computer connected with Alicona measuring device for later evaluation.

Figure 6.25: 3D reconstruction of burr measured via Alicona Infinite-focus.

The files containing 3D burr models from Alicona were transferred to the portable PC and evaluated in MeX 5.1 software with using profile analysis tool. Coordinate system of the model was originally inclined under 22 ° from the measuring procedure and for measurement of the burr height was adjusted to 90 ° — side view of the

burr. Consequently, line having width 20 points corresponding to 35 μm , determining measuring range, was placed on the 2D side viewed burr profile. The averaged burr profile (Figure 6.27) in range of measured area (red in Figure 6.26) was consequently generated and the burr height could be measured. The 1st measuring point (reference measuring position) was placed on top of the burr and the 2nd measuring point was placed on the drilled sheet plane — root of the burr (see Figure 6.26). The distance in between those 2 points was evaluated as burr height.

Figure 6.26: Evaluation of the exit burr height in MeX 5.1 software.

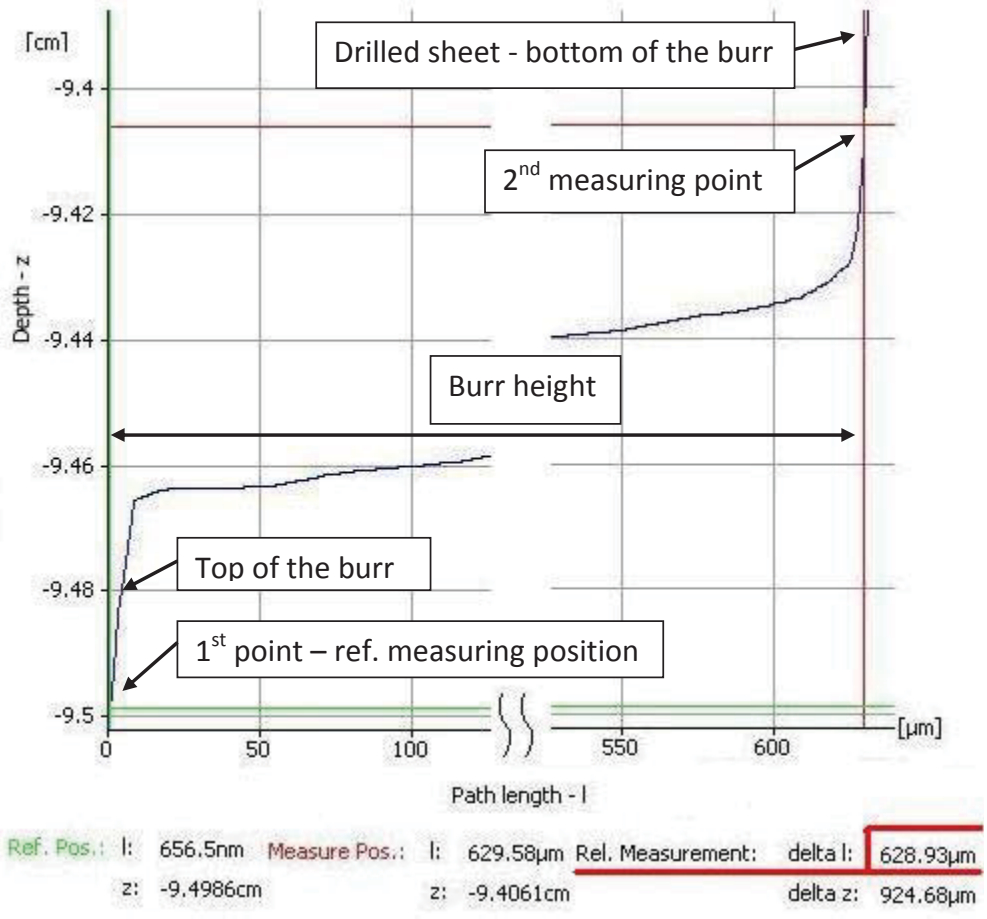

Figure 6.27: Profile measurement of the exit burr height in the MeX 5.1 software.

6.5.2 Burr widths

Burr widths and burr root widths were measured for all holes drilled on exit as well as entry side, again providing 6 replications of each tested drilling condition in order to reduce variability of the results. Measurements were performed in means of an optical coordinate-measuring machine (CMM) DeMeet 220 (see Chapter 6.1.8 for details). Workpiece was placed in horizontal position via fixture shown in Figure 6.28, light setting was adjusted to the magnitude of ring light of 8.5 %, bottom light of 25.2 % and top light source of 43.3 %. The circle for fitting was placed on a burr edge intended to measure (see Figure 6.29), measuring range and dark to light side orientation was adjusted and the picture processing computer automatically detects edge based upon transition in the picture from dark to light and vice versa. In order to extract burr widths from measurements of burr edges diameter, the drilled hole diameter was measured from entry side and an it's value was subtracted from diameter of burr edges. This value was consequently halved, resulting in desired burr widths dimension.

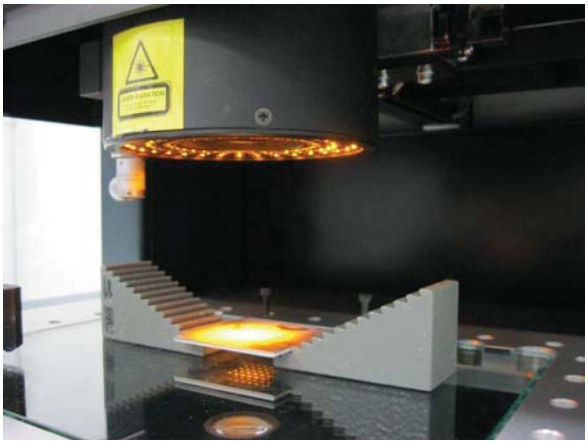

Figure 6.28: Workpiece placement when burr widths measured via the optical CMM.

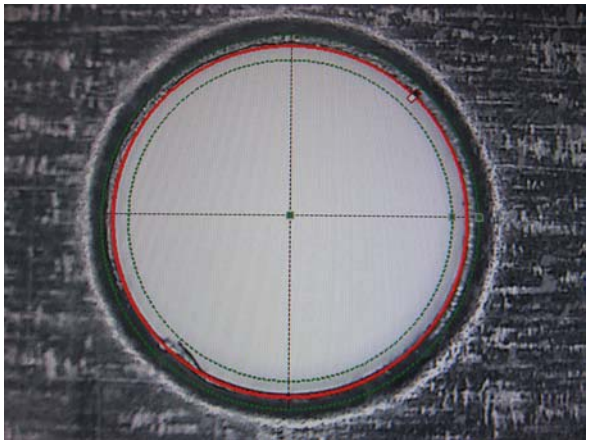

Figure 6.29: Measuring principle of burr widths based on circle fitting to the edges on the CMM.

6.6 Results

6.6.1 Influence of cutting speed on drilling forces and burr formation

In this section, dealing with influence of cutting speed on burr formation, measured results are present. All plots showing correlations of different cutting speeds on investigated burr dimensions include error bars representing experimental standard deviation (STD) of measured burr dimension resulting from 6 replications for each level of tested cutting speed. For complete overview of measured data with calculated STD and coefficient of variation (COV) see Appendix D.1. For force measurement data with calculated average values, STD, and COV see Appendix C.1.

Drilling forces

Force measurements data for all holes drilled during the preliminary test, where influence of cutting speed on burr formation was investigated, are enclosed as Appendix C.1. In this appendix, there are tables including drilling conditions used during investigation with corresponding maximal thrust and torque measured. From 6 replications of each level of tested cutting speed (6 holes drilled), average thrust, average torque, standard deviation (STD), and coefficient of variation (COV) were calculated and included in the tables.

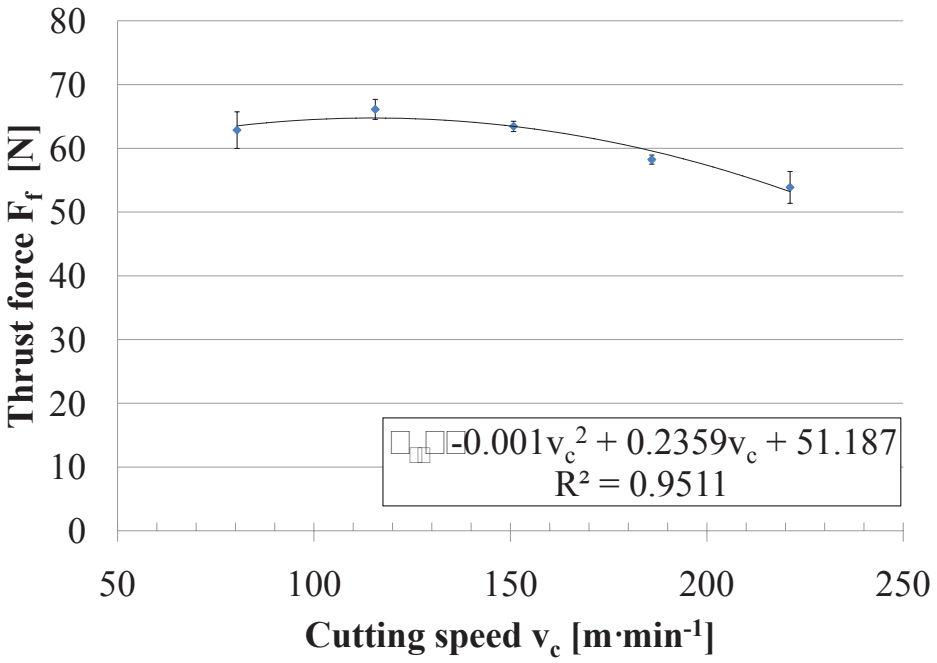

Figure 6.30: Influence of cutting speed on drilling thrust force.

The graph of averaged thrust force as a function of each level of cutting speed tested, with error bars representing standard deviations calculated, is seen in Figure 6.30. From the graph, increasing trend in thrust force when increasing cutting speed up to certain level was experienced. From this certain level of cutting speed, the thrust force began to decrease while cutting speed was increased. This behaviour is generally

explained by material strength increase due to work hardening associated with high strain rates at the shear plane, proportional to cutting speed. When the higher range of cutting speed used, the greater heat generation at the shear plane and the tool-workpiece interface occur, resulting in thermal softening of the material. This thermal softening causes material flow stress to drop, material strength to decrease, and thus resulting in lower cutting forces required. Moreover, as cutting speed increases, the metal flow around the tool edge become more uniform and material build-up is reduced, resulting in freer cutting. The behaviour is well described by polynomial function of the second order, shown in the graph in Figure 6.30.

For the same reasons above discussed, the same trend can be seen for drilling torque applied (see Figure 6.31). For more detailed explanation of this behaviour see Chapter 3.7.3, in the literature survey.

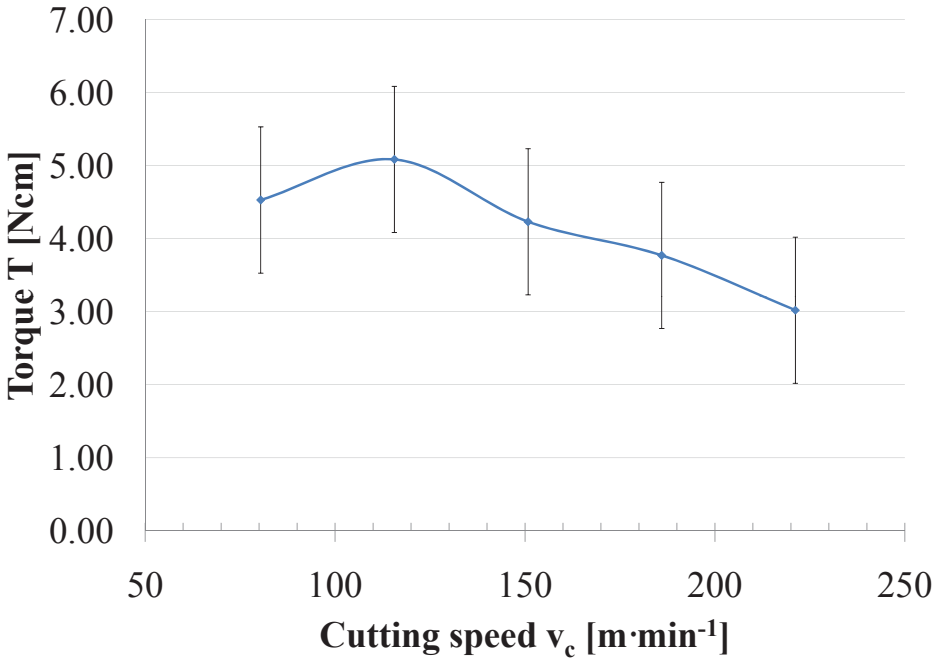

Figure 6.31: Influence of cutting speed on drilling torque.

The graphs of thrust force and filtered drilling torque as a function of drilling time for each hole drilled are depicted in Appendix C.1. The graphs clearly show the behaviour of drilling thrust and torque against drilling time. As previously described in Chapter 6.4.5 and in Figure 6.22, the dashed lines in the graphs indicate the drill position during drilling process.

From drilling initiation, when the drill firstly touched the top layer of the workpiece (dashed line — t0), the drilling thrust linearly increased, as bigger proportion of the drill diameter got involved in cutting. This steep increase lasted up to the time designated by dashed line — t1, indicating the position when entire drill diameter got involved in cutting. Steady-state cutting follows from (t1) to (t2), where increased thrust represents increasing friction from increasing proportion of drill margins in contact with the surface of drilled hole. When the drill tip approached the exit of the hole, in the end of this zone (dashed line — t2), the plastic deformation at the drill tip occurred. The thin layer of deformed material, in front of the drill tip, was rather

formed by the thrust force than to be cut, because there was not enough support to be entirely cut by the drill. This is represented by drop in drilling thrust close to (t2). The initial plastic zone formed near the drill tip in the center of the drill expanded to the edges of the drill with drill continuously being fed (t3). This thin layer of deformed material pushed out without being cut was later turned to a drilling cup or a burr. With further drill movement in feed direction, the remaining plastically deformed material could not sustain the deformation and the crack at the corner of drill edges was initiated. The crack expanded at the edge of the drill circumference and drilling cap was separated from remaining exit burr (no additional thrust force afterwards).

The drop in drilling forces can be seen from the graphs when high cutting speeds used ($n = 37000$ and $44000\,\text{min}^{-1}$). This drop is seen to occur more often with the highest speed used, and represents the above discussed thermal softening of the workpiece material.

Exit burr heights

In Appendix D.1, measured exit burr heights (Bhe) are present. In case of an excessive proportion of burr height present, it's height and angular proportion was measured in addition (EBhe).

- Initial measurements

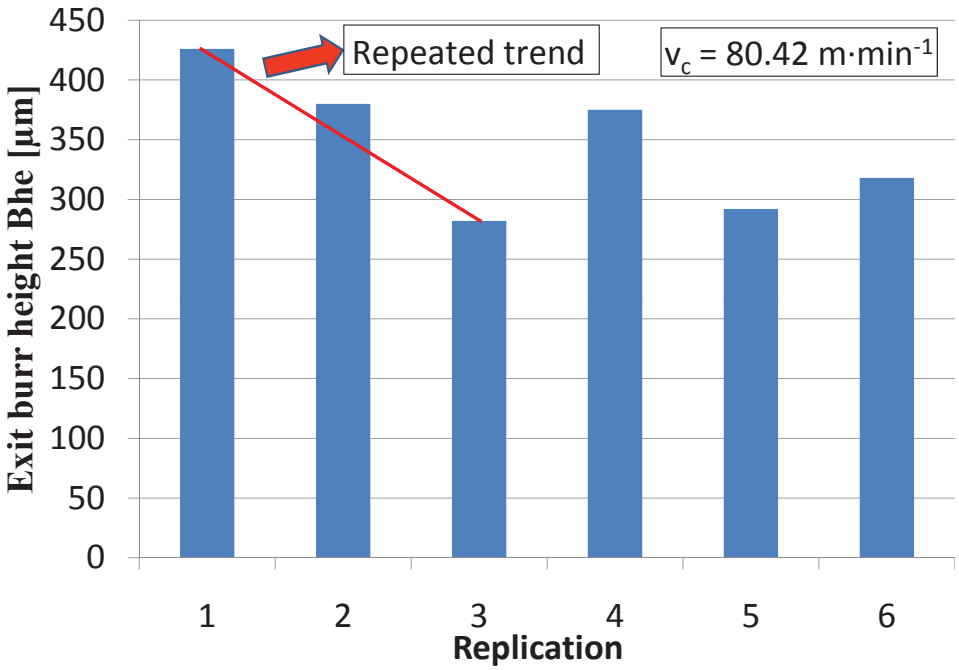

Figure 6.32: Burr heights variation when 6 replications of single drilling condition performed (n = 16000m · min^{-1}, f = 0.035 mm).

The first measurements performed (see Figure 6.32) shown clean trend in variation of burr heights of repeated single drilling condition for first 3 holes representing one workpiece. In order to evaluate whether it was random error caused by process variation or if it was error with repeated trend for other settings, which would indicate

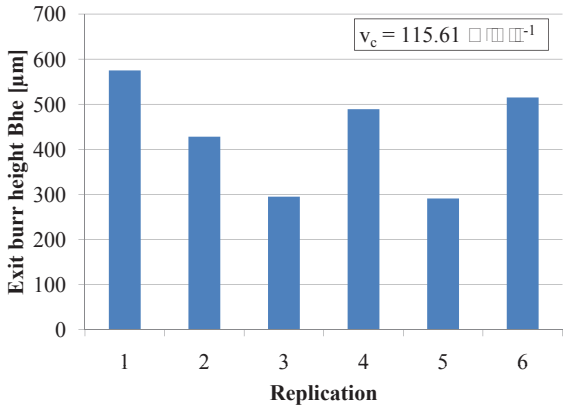

Figure 6.33: Burr heights variation when 6 replications of single drilling condition performed (n = 23000 m · min^{-1}, f = 0.035 mm).

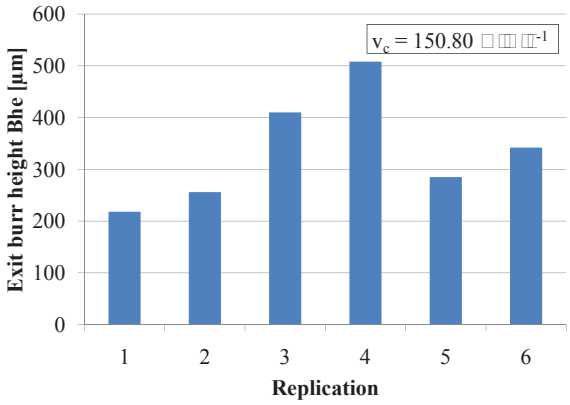

Figure 6.34: Burr heights variation when 6 replications of single drilling condition performed (n = 30000 m · min^{-1}, f = 0.035 mm).

presence of other external source such as clamping system influence affecting the process, measurements were performed for other 2 settings (see Figures 6.33 and 6.34).

From Figures 6.32, 6.33 and 6.34 it is possible to see an apparent repeating trend for first 3 holes drilled, representing first workpiece. This trend in height variation could not be caused by increased temperature when subsequent holes drilled since there was a break in between replications in order to save acquired force measurement data and to reset the amplifiers. As likeliest reason causing this variation was considered to be positioning of the holes with regard to the clamping system. In order to restrict any unwanted source influencing burr formation, it was decided to repeat the test with randomized setting of hole positions and process parameters (see Chapter 6.3).

- Measurements of randomized setting

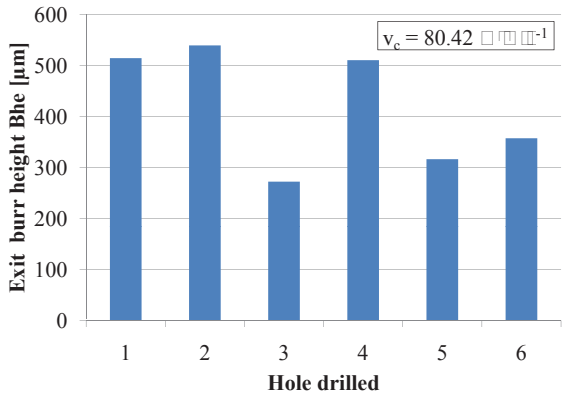

Figure 6.35: Burr heights variation when randomized 6 replications of single drilling condition performed (n = 16000 m · min^{-1}, f = 0.035 mm).

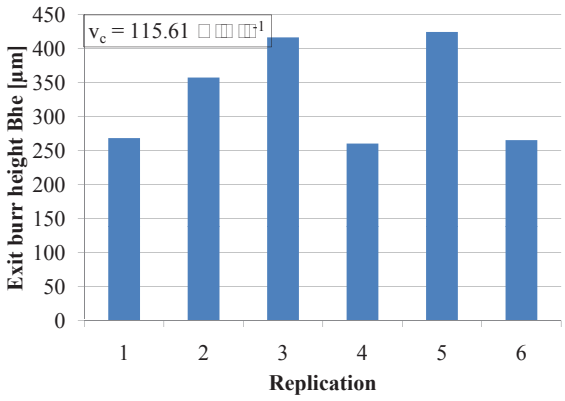

Figure 6.36: Burr heights variation when randomized 6 replications of single drilling condition performed (n = 23000 m · min^{-1}, f = 0.035 mm).

The graphs in Figure 6.35 and 6.36 show burr heights variations with randomized order. There is still an apparent trend in 6.35 even with randomized setting. After

evaluation of all data, it appeared to be random behaviour caused by big variation in burr heights when lower speeds used, which is caused by the process itself.

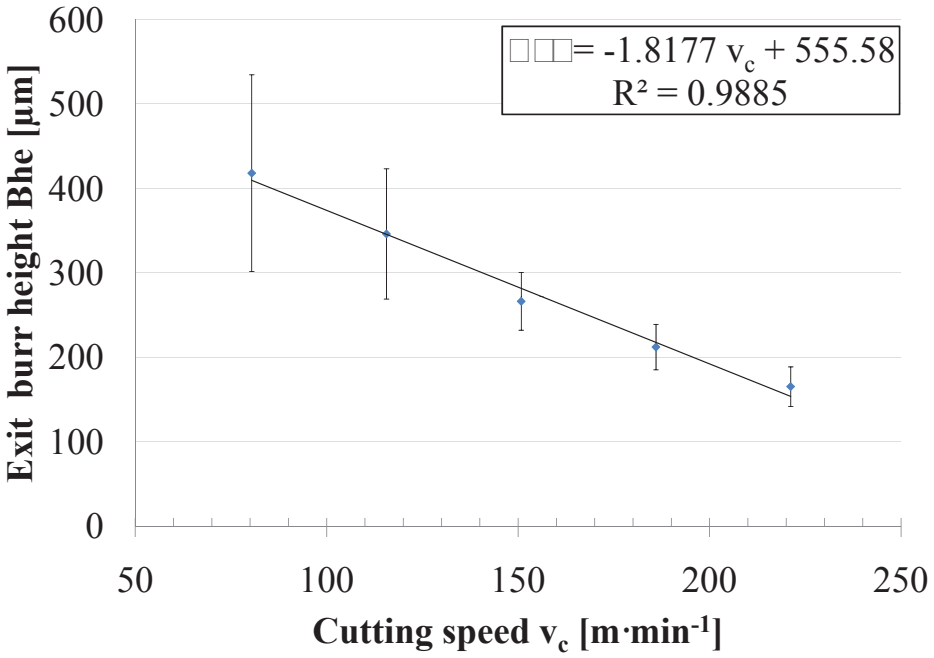

Figure 6.37: Influence of cutting speed on exit burr height.

The graph in Figure 6.37 clearly shows the influence of cutting speed on exit burr formation for present material used during the test. A decreasing behaviour of exit burr heights with increasing cutting speeds is well defined by linear relation. The bars represent experimental standard deviation of exit burr heights resulting from 6 replications for each level of tested cutting speed. For complete overview of measured data with calculated standard deviation and coefficient of variation (COV) see Appendix D.1. Either from calculated data enclosed in previously mentioned appendix or directly seen from the graph in Figure 6.37, it is apparent that the variation in exit burr heights significantly decreases with increased cutting speed. The calculated coefficient of variation shows the range of height variation to be halved and stabilized for higher speeds. For speed higher than 150 m · min^{-1} having magnitude about 13 % instead of 28 – 22 % when lower speeds used. The reasons, why the red marked burr measurements (see Appendix D.1 were excluded from calculations are present in mentioned appendix as table notes and entry hole problem causing so called "star effect at entry hole" is more detailed forth in section **??**. This problem at the hole entry might cause the drill to be wobbling through its drilling length, resulting in bigger diameter of hole drilled and extraordinary exit burr formed.

Exit burr widths

The exit burr width is also seen to decrease when cutting speed increases (see graphs in Figures 6.38 and 6.39). The exit burr root width, representing the distance from drilled hole circumference where the curvature of plastically deformed base material into the burr started, shown to be well defined by decreasing linear function while

cutting speed increased. Red marked measurements, present in Appendix D.1, were excluded from calculations for the reasons explained in previous section with exit burr heights results and shortly mentioned as the table notes in the Appendix D.1.

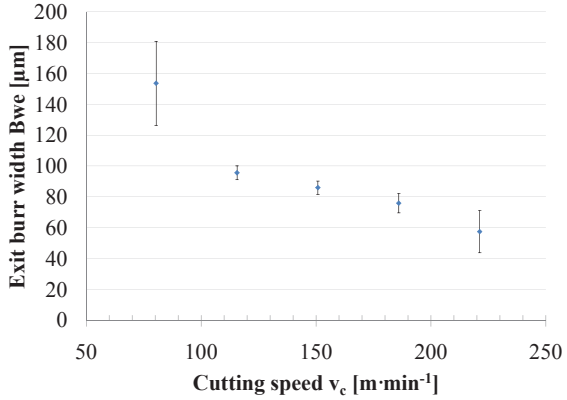

Figure 6.38: Influence of cutting speed on exit burr width.

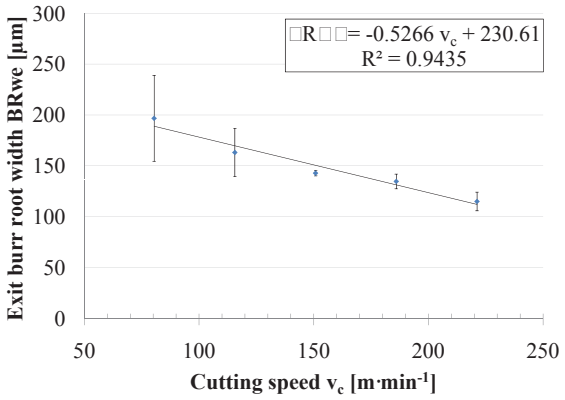

Figure 6.39: Influence of cutting speed on exit burr root width.

Entry burr heights

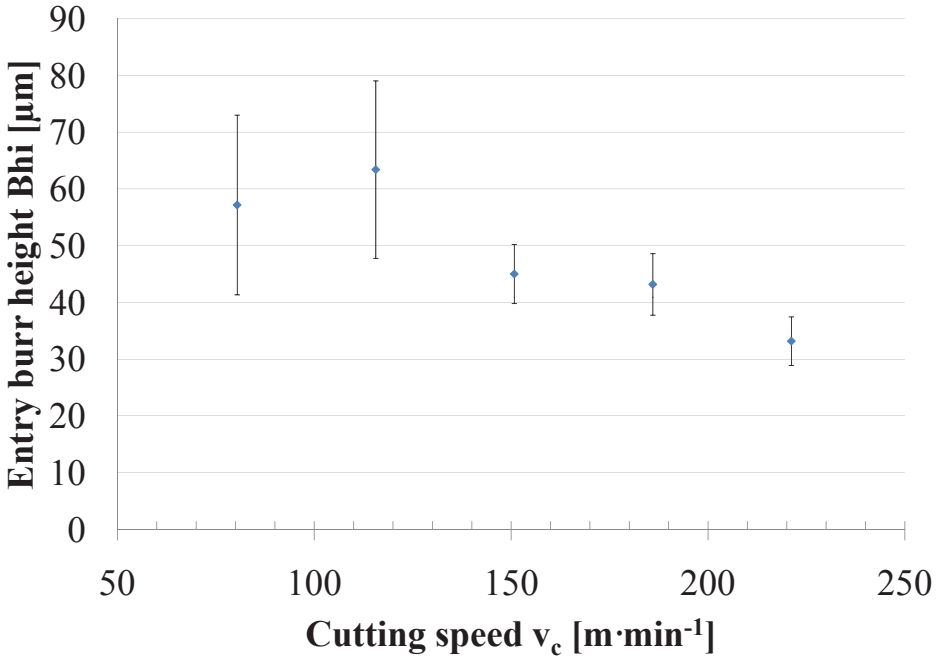

Figure 6.40: Influence of cutting speed on entry burr heights.

Entry burr heights, as seen from the graph in Figure 6.40, have also decreasing tendency while cutting speed is increased. The range of entry burr height variation was seen to be notably reduced while greater cutting speed used. From all measured data enclosed as Appendix D.1 it is clearly possible to see, that the variation in entry burr heights was reduced in the same range as the exit burr heights with increasing cutting speed (COV of the same ranges). The cause of internally so called "star effect

at hole entry", at the company Bang & Olufsen, was experienced during the test and marked by red color in measurement data in Appendix D.1. This measurement was excluded from calculations and this phenomenon is detailed forth in the Section 6.6.3.

Entry burr widths

Entry burr width as well as entry burr root width was seen to be linearly decreasing with increasing cutting speed as can be clearly seen from the graphs in Figures 6.41 and 6.41. The range in width variation was seen to have decreasing trend as when cutting speed increased as well.

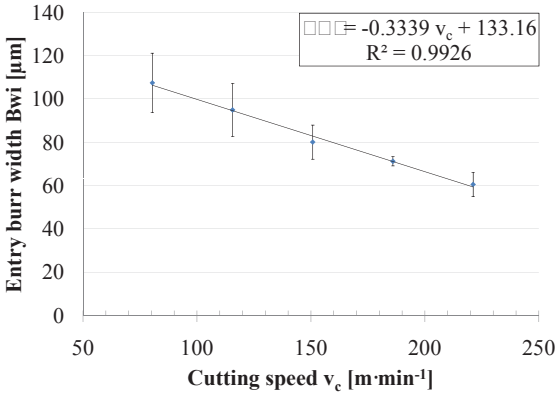

Figure 6.41: Influence of cutting speed on entry burr width.

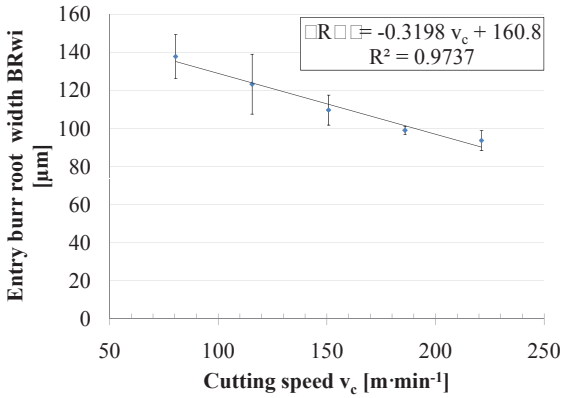

Figure 6.42: Influence of cutting speed on entry burr root width.

6.6.2 Influence of feed per revolution on drilling forces and burr formation

In this section, results from investigation where influence of feed per revolution on burr formation was evaluated are present. All plots showing correlations of different feeds per revolution on investigated burr dimensions include error bars representing experimental standard deviation (STD) of measured burr dimension resulting from 6 replications for each level of tested feed per revolution. For complete overview of burr dimensions measured data with calculated STD and coefficient of variation (COV) see Appendix D.2. For force measurement data with calculated average values, STD, and COV see Appendix C.2.

Drilling forces

As shown in Figures 6.43 and 6.44, the drilling forces linearly increase with increased feed, which is in line with that the force is directly proportional to area of uncut chip (being roughly the product of the feed per tooth and the drill diameter (see Chapter 2, dealing with drilling characteristics, for details).

Exit burr heights

The graph in Figure 6.45 shows the influence of feed per revolution on exit burr height. From the graph, it can be seen that the exit burr height steeply increases with increasing

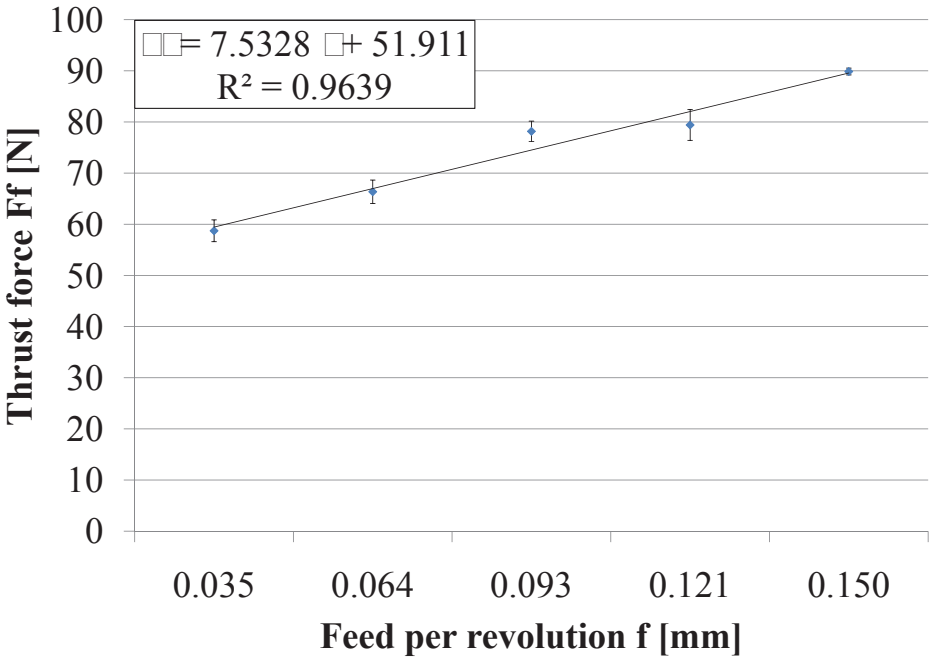

Figure 6.43: Influence of feed per revolution on drilling thrust force.

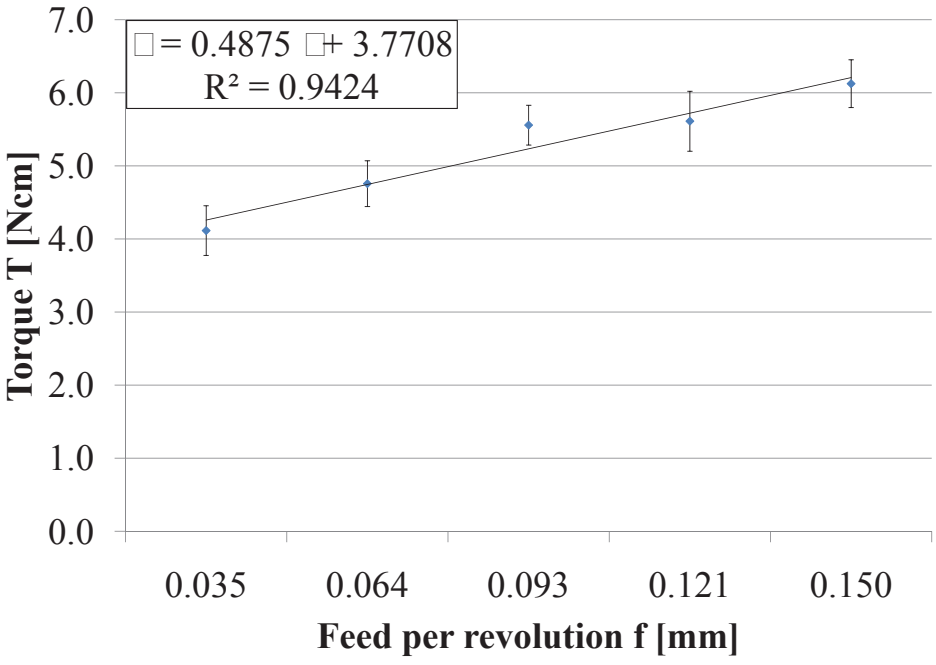

Figure 6.44: Influence of feed per revolution on drilling torque.

magnitude of feed per revolution, in range of lower feeds. Following increase in higher feed causes moderate increase in exit burr height, well described by polynomial function of the second order, up to certain maximum value when the height stabilizes and it is not further increasing, while the feed rate is increased.

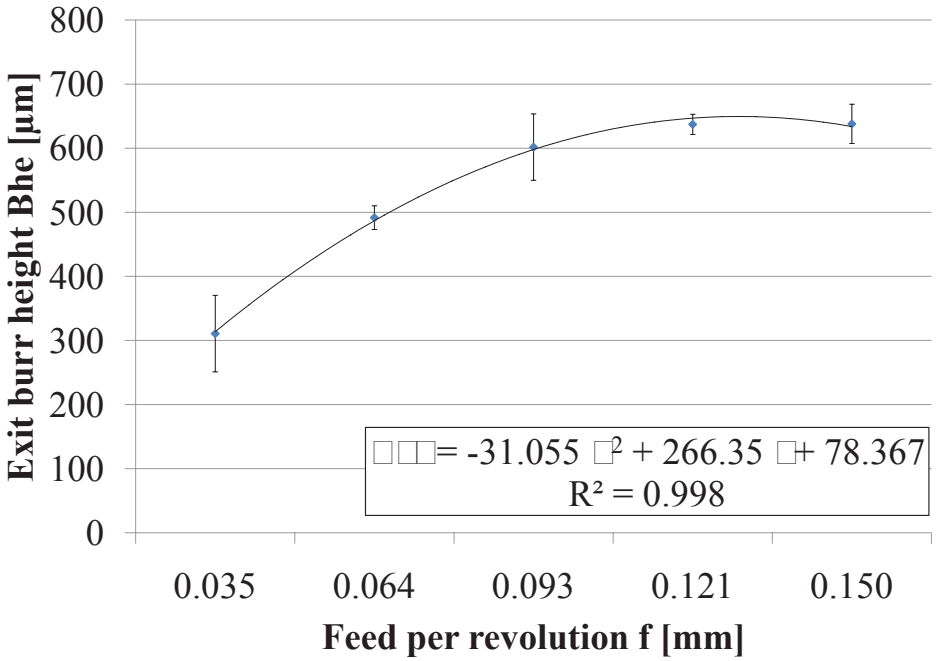

Figure 6.45: Influence of feed per revolution on exit burr heights.

Exit burr widths

Exit burr widths, as shown in the graphs in Figures 6.46 and 6.47, increases while the feed per revolution is increased, very well described by logarithmic regression. In range of lower feed rates, the burr widths increases more rapidly than in range of high feed rates used. The range of variation in exit burr heights, represented by error bars in the graphs, is seen to be proportionally reduced with increased feed rates (see Appendix D.2 for all measurement data with calculated STD and COV representing the variation range).

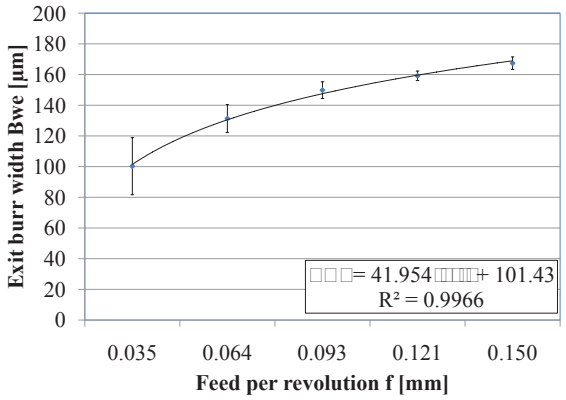

Figure 6.46: Influence of feed per revolution on exit burr width.

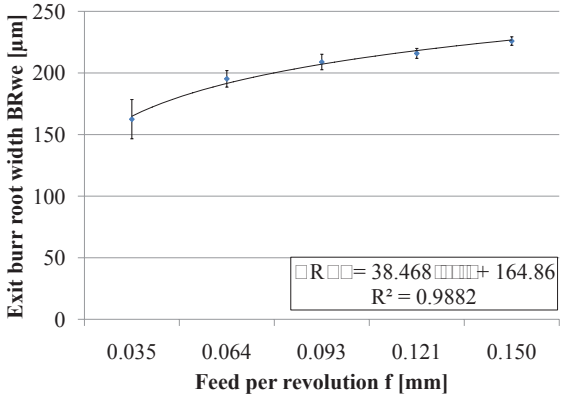

Figure 6.47: Influence of feed per revolution on exit burr root width.

Entry burr height

From the graph in Figure 6.48, burr entry height is seen to be rather stabilized for different lower feeds used and might be minimally decreased when higher feed rates used.

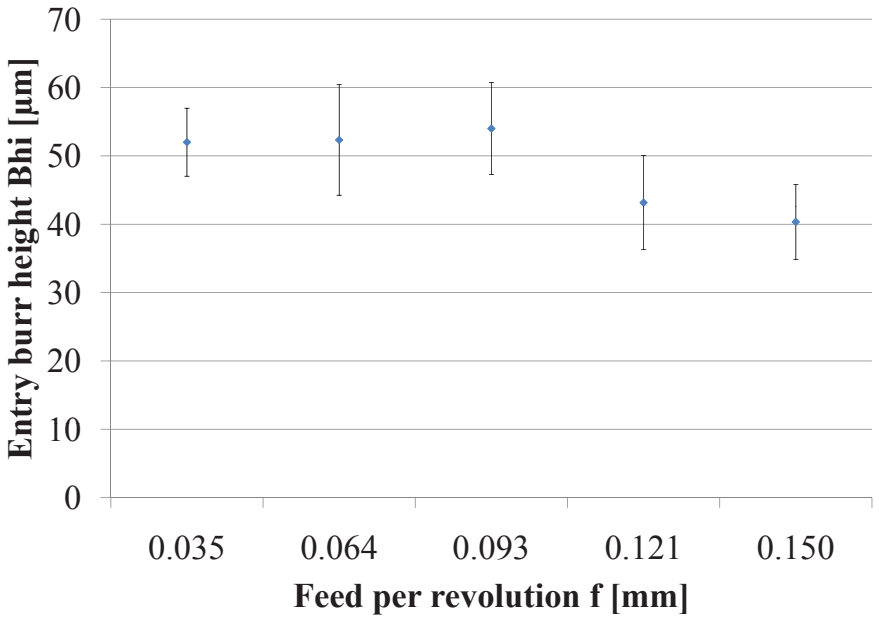

Figure 6.48: Influence of feed per revolution on entry burr height.

Entry burr widths

The entry burr widths as a function of different feed per revolution can be seen in Figures 6.49 and 6.50. From the graphs, it is apparent that entry burr widths increase with increased feed rate used, until reaches certain value where stabilize. This behaviour is well described by polynomial regression of the second order, shown in the graphs.

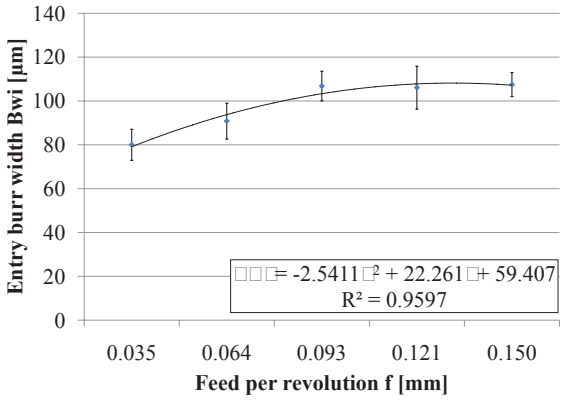

Figure 6.49: Influence of feed per revolution on entry burr width.

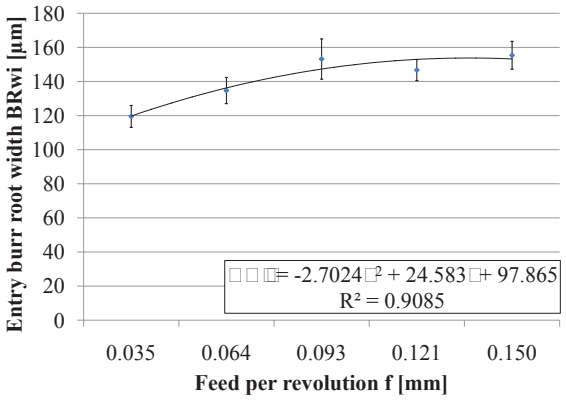

Figure 6.50: Influence of feed per revolution on entry burr root width.

6.6.3 Hole entry problem

During the first phase of the preliminary test — influence of cutting speed test execution, hole entry problem causing so called "star effect at hole entry" was experienced. This problem causing non-uniform hole pattern appearance, resulting in faulty workpiece, was discussed in Chapter 1 — introduction as one of the main goals of this work.

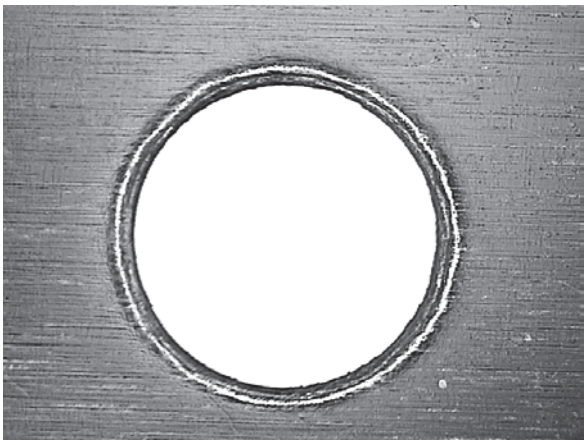

Figure 6.51: Ordinary hole entry with burr formed.

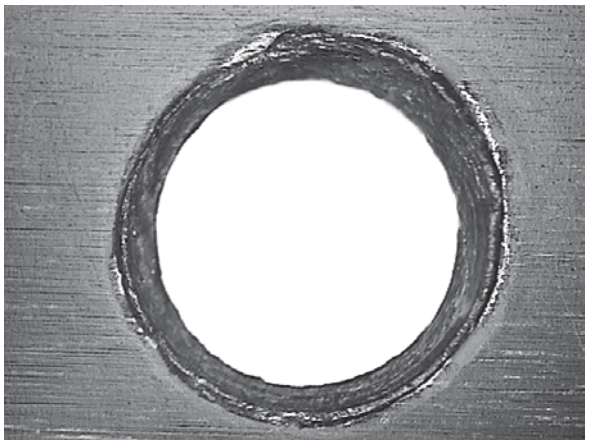

Figure 6.52: Hole entry defect with burr formed.

For photographs of this phenomenon see Figures 6.52 and 6.53 and Figure 6.51 for comparison with an ordinary hole entry with entry burr formed. From those pictures it can be seen that there is a conical defect at the hole entry causing non-uniform appearance in holes drilled. When such a defect appears among the great number of hole drilled, it causes light reflection in different way than all other holes drilled with proper hole entry. Such a defect results in faulty piece which can not be repaired. This conically shaped defect at the hole entry was caused by drill point wandering on the workpiece surface when drilling was initiated. This phenomenon is from literature survey seen to be possibly eliminate either by higher feed rate used, by using drill point geometry with better centering capability, or with using bushing to avoid drill wobbling.

In the following section, where influence of feed per revolution on burr formation was investigated, the assumption with using higher feed rates to avoid this phenomenon was under examination and results are discussed forth in Chapter 6.7 (Summary of the preliminary test). Different drill geometries were tested forth in the last phase test (see Chapter 8 — tool geometry investigation), where results are present. Overall findings and recommendation in order to restrict this phenomenon are present in Chapter 9 — conclusions.

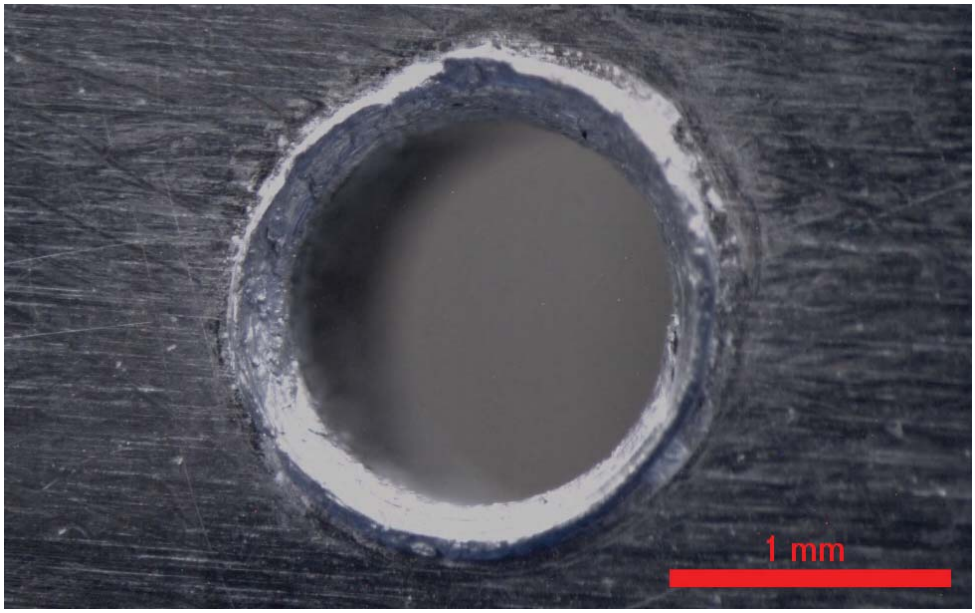

Figure 6.53: Problem at the hole entry caused by drill wandering on the workpiece surface when drilling began.

6.7 Summary

Feed per revolution and cutting speed, according to previous researches pertinent to the project goals, were found to be the most influencing drilling parameters on burr formation. In order to evaluate the influence of these drilling parameters, find burr formation mechanism for the wrought aluminium Al99.7Mg0.5Cu–H24 used in this project, and verify capability of experimental equipment for subsequent tests, this preliminary test was performed.

First, the influence of cutting speed was evaluated by varying five levels of cutting speed, while fixed value of feed per revolution was used, and measuring of the resulting burr size. Next, the effect of feed per revolution was revealed by varying five levels of feed, while fixed value of cutting speed, and consequent measuring of burr formed. HSS drill 1.6 mm in diameter, a 7 % oil emulsion applied by hand sprayer, high speed spindle attached in a tapper of vertical milling tool, and no support of drill exit side by means of clamping system were used. An uniform appearance of drilled holes was visually checked and occurrence of any design errors ,while different cutting parameters tested, was evaluated.

Since burr size defined by single value according to ISO 13715 was found to be insufficient, because a burr thickness contributes more to deburring costs than a burr height, measurements of burr height, width, and root width at entry and exit side of the drilled holes were performed in accordance with Schäfer's recommendations. The burr measurement strategies utilized proved to be advantageous and traceable. Measurement of burr height by autofocus optical instrument was fast (approximately 30 seconds per measurement of whole burr on the microscope and later evaluation on PC), allowing precise evaluation due to entire burr perimeter involved in measurement. In comparison with standard measuring method, where maximum burr hight is measured by profilometer, measurement was not misrepresented, if small excessive burr proportion caused by drilling cap separation was present. In such case,

representative burr heigh was evaluated with excessive burr height and it's angular proportion noted. Burr width and burr root width measurements, by optical CMM, also involved whole burr circumference, resulting in traceable measurement.

The type of burrs formed, for present material used, was seen to be uniform with drilling cap. The burr measurement data showed that all entry as well as exit burr dimensions were reduced with increased cutting speed. The exit burr height, exit burr root width, and entry burr widths shown to be linearly decreasing with higher cutting speed used. Variation in all burr dimensions was seen to be reduced with higher cutting speed utilized, representing stabilization of the process.

With greater feed rates, it was found that burr height and widths increase, with moderating trend, up to certain value where stabilizes and it is not further increasing, while the feed rate is increased. This was seen only with exception of height of burrs an the entry side, which may be minimally decreased with increasing feed.

The drilling forces were seen to be slightly increasing up to certain value when lower cutting speeds used. This behaviour is seen to be caused by material strength increase due to work hardening, associated with high strain rates at the shear plane, proportional to cutting speed. Subsequent increase in cutting speed of high range caused greater heat generation, resulting in thermal softening of the material, causing material flow stress to drop, material strength to decrease, and thus resulting in lower cutting forces required.

The maximal power and torque output of the high speed spindle was found to be insufficient for consequent tests, where it was of interest to test cutting conditions providing the highest productivity, of which was capable the new two spindle machine tool purchased by the company. This new machine tool was capable, for long term production, of at about $n = 40\ 000\,\text{min}^{-1}$ and $v_f = 7\ 000\,\text{mm} \cdot \text{min}^{-1}$, resulting in $f = 0.175$ mm in order to fast up the production. It was of interest to test such conditions and find optimal setting intended for production, meanwhile the new machine tool will be delivered and installed at the company workshop. Such optimization had to ensure reproducibility of the results at the company workshop. From the Figure 6.2, it can be seen that the maximal torque output of high speed spindle when $n = 40\,000\,\text{min}^{-1}$ used is of 4 Ncm, whereas the measured torque applied during the preliminary test for $f = 0.150$ mm was 6.1 $\pm$ 0.3 Ncm. Therefore, the high speed spindle can not be used for subsequent tests and another solution mus be found.

Hole entry problem causing so called "star effect at hole entry" (shiny ring around the hole periphery) was seen to be caused by the conical defect at hole entry, reflecting light in different directions than other, properly drilled holes. This defect was caused by drill wandering on workpiece surface when drilling was initiated with low feed rate. With high feed rate utilized, this phenomenon was seen to be restricted.

Chapter 7

Clamping system investigation

Whereas the previous chapter was concerned with identifying the influence of process parameters on burr formation, this chapter describes the work done in the interest of investigation the other predominant factor in burr formation, namely clamping conditions. As discussed in the literature survey dealing with burr formation, if there is any room restriction or force opposing to the workpiece material to be formed into burr at the drill exit, the burr formation can be significantly reduced.

The initial step taken was to construct such a fixture, which ensure reproducibility of the results at Bang & Olufsen workshop and meets good conditions for the investigation (force measurements). The construction procedure and drawing of the clamping system constructed are present in this chapter. Next, the same tool and drilling conditions as used during the preliminary test were tested, allowing the influence of the clamping system on burr formation to be evaluated. The results with respect to cutting forces (thrust and torque), burr formed and uniformity of the holes drilled are present forth in this chapter together with conclusions.

7.1 Construction of the clamping system

It was desired to keep the clamping conditions as close as possible to those used in the company because of reproducibility of the test results in Bang & Olufsen's workshop. In this respect, the vacuum clamping fixture was constructed. Such a fixture provides uniform multipoint clamping particularly good for clamping workpieces in the form of thin plates. In this case, the clamping entails no bulging of the plate workpieces, allows machining of the outer shape of the part and restrict the room for burr formation at the hole exit side. In an ideal case, there would be no room for burr formation around the hole exit circumference, if the workpiece bottom surface would rest by entire area on fixture surface without any gap in between. In this interest, planar surface on the top of the fixture which would act as support of worpiece bottom side is firstly aligned. On this surface, grooves for even distribution and sealing of the vacuum pressure providing multipoint clamping are milled. Consequently, the plate workpiece is clamped by vacuum and the hole pattern is drilled with 1 mm drill overrun into the fixture surface. Drilled workpiece is subsequently unclamped and another plate workpiece with the same hole pattern can be fixed and drilled. In case of different hole pattern, the 1 mm surface with hole pattern resulting from drill overrun can be removed and previous steps are repeated with hole pattern desired.

The overall fixture geometry was constructed in a way to be mounted on the load cell measuring device with dimensions and less material volume in respect to measuring accuracy (e.g. eccentric load, measuring frequency). For 3D model of an assembly of the vacuum fixture constructed and fixed on the dynanometer see Figure 7.1. In this figure, there is shown an explode view of the assembly in the interest of lucidity of all important parts used. There are two rubber O-rings serving as vacuum seal fitted into the sealing grooves assuring air tightness when vacuum applied. In between those sealing grooves, there is a vacuum groove providing even pressure distribution at the entire bottom workpiece surface. The plate workpiece of 50 x 50 – 2 mm is directly placed on the sealing and positioned into the corner provided by two indent surfaces. This provides fast positioning of the workpiece and restricts it's movement in two linear dimensions and rotation. The fixture is firmly tightened on the dynamometer via four screws and the housing providing vacuum for clamping is connected to the fixture.

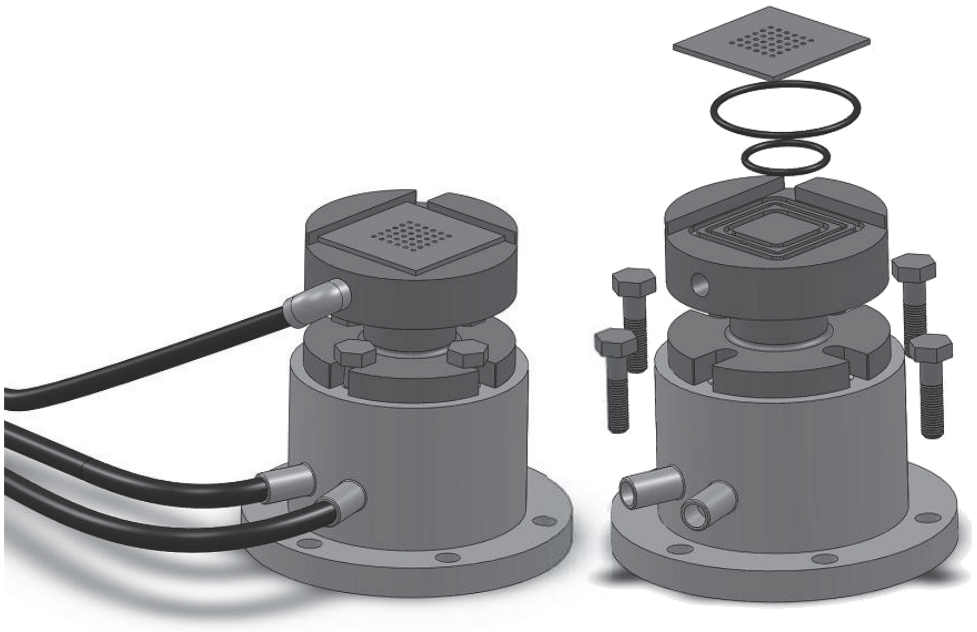

Figure 7.1: 3D model of the vacuum fixture constructed placed on the dynamometer.

7.1.1 Vacuum sealing

As vacuum seal, two NBR (Nitrile butadiene rubber) O-rings of size 29.6 x 2.4 mm and 51.6 x 2.4 mm, were used and fitted into the sealing grooves. This material is the most commonly used for vacuum seal. It has the lowest permeability rate for gases, with good physical properties for a seal and a useful temperature range of - 40 to 100°C [42, 43]. It was originally intended to use O-rings having hardness of 40 Shore but since the retailer had run out of samples for the desired dimensions, the O-rings having 70 Shore hardness were used instead.

7.1.2 Geometry of sealing grooves

The geometry of sealing grooves and size of the sealing cord (O-ring) are important for the normal operation of the fixture. The groove geometry and size of the sealing were chosen in accordance with recommendation of sealing producer detailed in [42] and handbook dealing with 0-rings and their application in [43]. The vacuum groove is placed in between the sealing grooves in order to provide even pressure distribution at the workpiece clamping surface. The seals surround the vacuum groove, placed in vacuum grooves, and the workpiece rest directly on it. In Figure 7.2, there is a cross sectional sketch of the vacuum fixture detailing the vacuum groove and the sealing grooves in which the sealing O-rings are placed in unloaded state. The area in between grooves serves as a plain supporting the drill exit side of the workpiece. There are six shallow holes depicted in this area, which represent drill overrun of 1 mm through the workpiece into the fixture.
When vacuum is applied, the O-rings fills in the grooves ideally leaving no freeboard between the fixture and bottom surface of the workpiece (see Figure 7.3 for the sketch). For detailed dimensions of the grooves see drawing of the whole fixture enclosed as an appendix J.

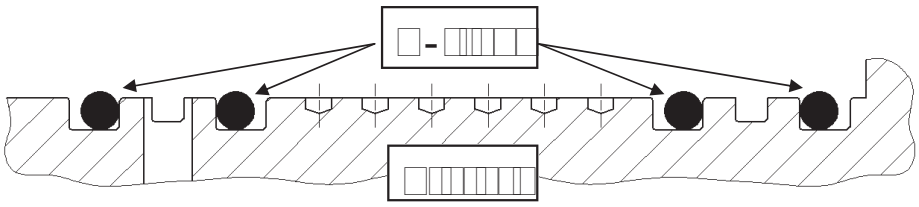

Figure 7.2: Geometry of fixture sealing grooves with fitted sealing.

7.1.3 Clamping force calculation

The vacuum clamping device operates using the atmospheric pressure for clamping the workpiece. The atmospheric pressure acts upon each surfaces of every body by even pressure of approximately 1 bar. By means of vacuum pump, the air under the clamped workpiece is sucked out while the ambient pressure pushes the workpiece on the fixture according to the vacuum pressure. Such a force must be great enough to firmly hold the worpiece and to compress the sealing into the sealing grooves in the interest of gaining full contact of bottom workpiece surface with fixture without any gap in between, which would ideally provide no room for burr formation at the hole exit side. The bigger the clamping area upon the vacuum is applied on, the bigger the resulting clamping force is.

Calculation:

$$Force = Pressure \cdot Area \tag{7.1}$$

$$[\mathrm{N}] = [\mathrm{MPa}] \cdot [\mathrm{mm}^2]$$

Where:

- Pressure (p) = pressure-difference (the atmospheric pressure of 1 bar = 0.1 Mpa– output pressure from the vacuum pump used (0.2 bar = 0.02 MPa of the absolute pressure)

  Note: The output absolute pressure of the high vacuum pump used is according to the manufacturer specifications of this pump $1 \cdot 10^{-5}$ bar (see Table 7.1). Since some pressure losses are expected because of housing connections, the output pressure value was adjusted for calculation of the clamping force to the magnitude of 0.2 bar, taking into account pressure losses.

- Area (A) = clamping area upon the vacuum is applied on (colored area in Figure 7.3, equal to 1 070 mm^2)

  Thus resulting in:

$$F_{clamp} = p \cdot A = (0.1 - 0.02) \cdot (1070) = 85.6\,\mathrm{N}$$

Since the drilling torque expected was only up to 6 Ncm when drilling with 1.6 mm drill in diameter in soft aluminium and moreover the drill presses the workpiece down onto the fixture by axial component of the force in feed direction (thrust) during drilling, such a clamping force ensure firm clamping. In addition, in order to restrict workpiece movement in two dimensions and rotation, stepping is provided on the fixture (see Figure 7.1 for 3D model of the fixture).

7.2 Experimental setup

Except of the clamping system, the same setup including the same toll as used during the preliminary test and previously described in chapter 6.1 was used in this test. In order to investigate influence of the clamping system on burr formation, the vacuum clamping system constructed and above detailed in chapter 7.1 was used during the test. The basis setup of the clamping investigation drilling test is depicted in Figure 7.4. Force measurements were performed with the same equipment as detailed in Chapter 6.1.6. Burr measurements were also performed on the same measuring equipment as during the preliminary test, detailed in Chapter 6.1.8.

7.2.1 Vacuum pump

Table 7.1: High vacuum pump Speedyvac ES100 characteristics

Characteristic	Unit	Magnitude
Ultimate vacuum	[mbar]	$1 \cdot 10^{-2}$
Pumping capacity	[m$^3 \cdot$ hod^{-1}]	6
Pump type		Single rotary stage — oil sealed

In order to ensure vacuum for clamping, high vacuum pump Speedyvac ES100 from manufacturer Edwards Vacuum, Inc. was used and connected to the vacuum fixture through vacuum regulation.

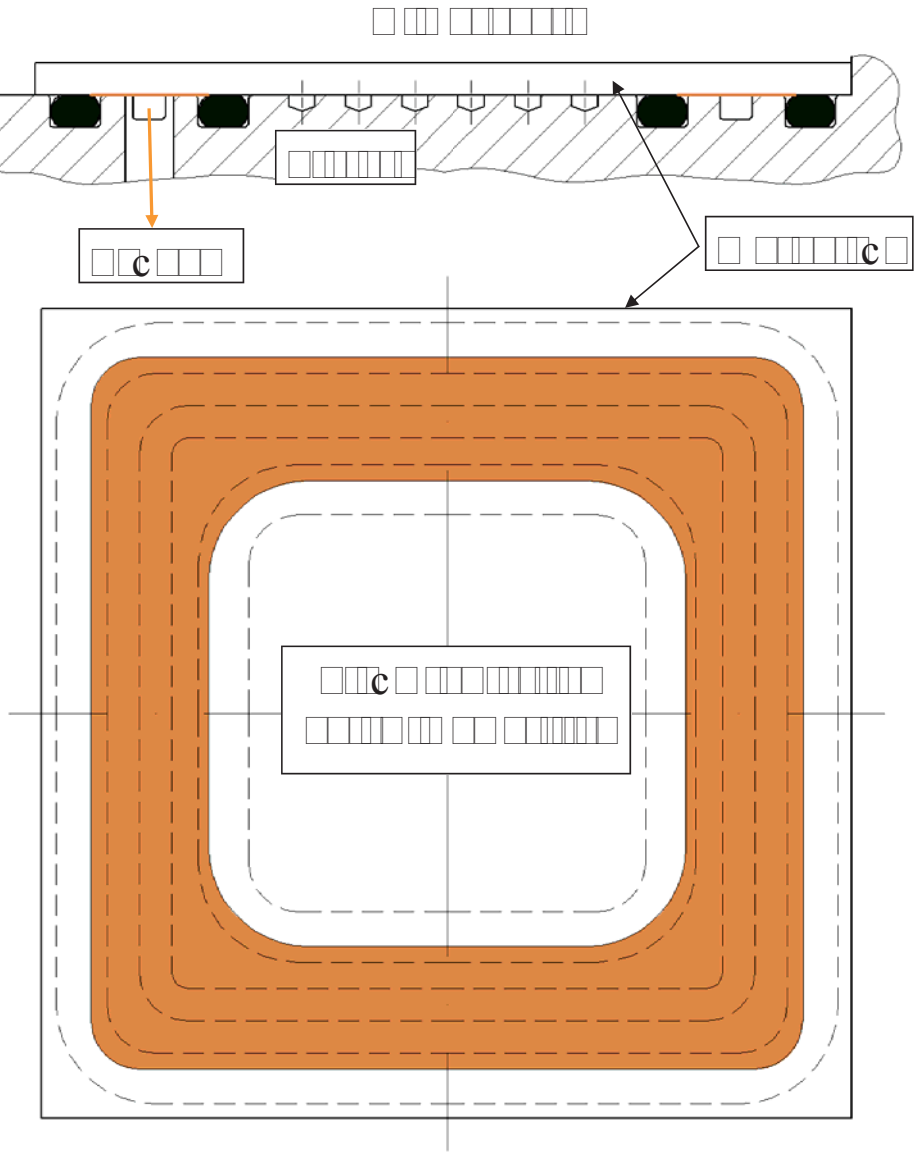

Figure 7.3: Sketch of the testing workpiece 50 × 50–2 mm fixed by applied vacuum (an area on which the vacuum is applied, resulting in clamping force, is marked by orange color).

7.2.2 Vacuum regulation

In the interest of measuring real vacuum pressure used for clamping, easy end quick regulation of the pressure to clamp and release the workpiece and to avoid any debris to be sucked by the high vacuum pump, the vacuum regulation was constructed. This regulation is shown in the Figure 7.4 and consists of a vacuum gauge, shut-off valves, a vacuum filter, push-in fittings and connectors for easy and fast manipulation.

7.3 Experimental plan

As previously mentioned, the same drilling conditions and tool geometry as during the preliminary test (see Chapter 6.2) were tested, allowing the influence of the clamping

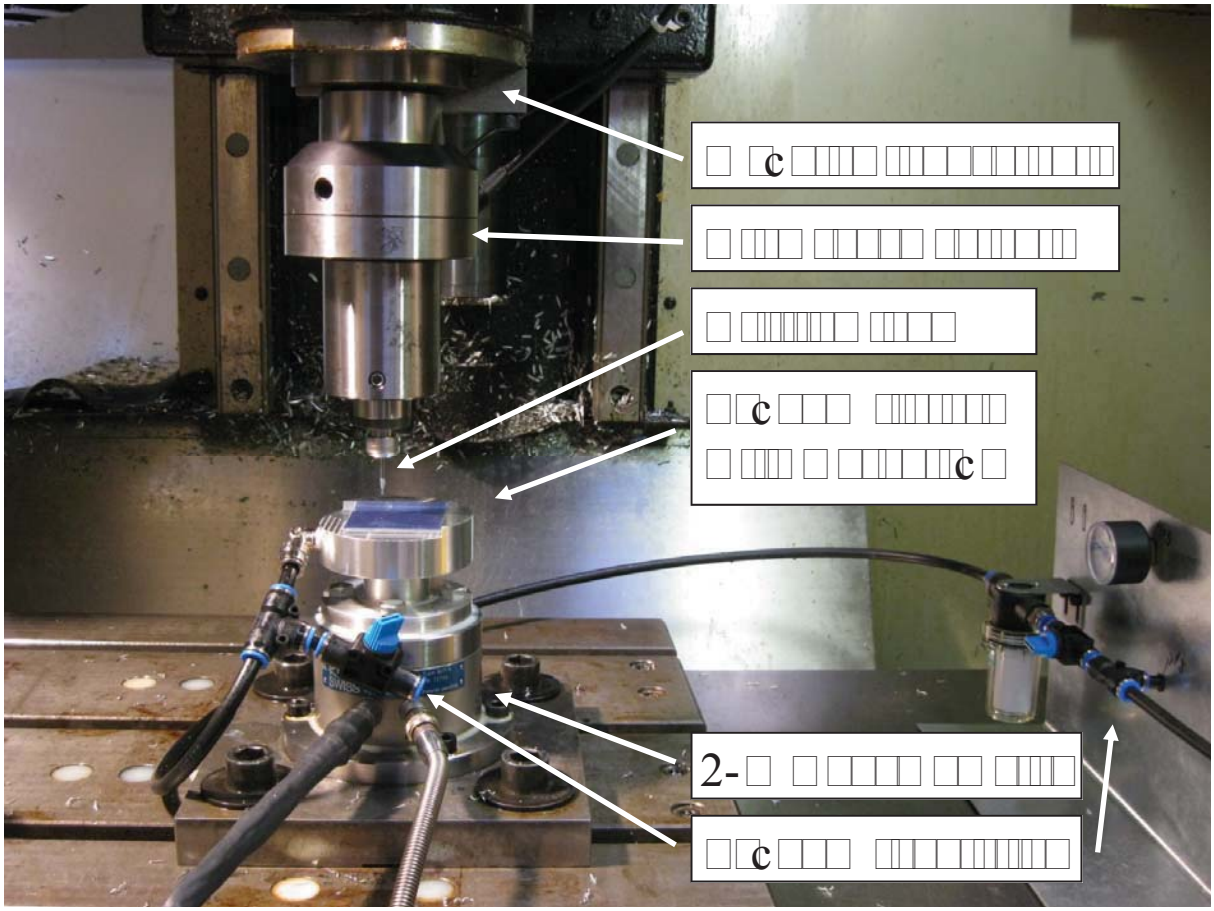

Figure 7.4: Experimental setup of the clamping system investigation test.

system on burr formation to be evaluated. Based on the results of the preliminary test investigation shown in Chapter 6.6, it was decided to use non randomized setting. The reason is that the drilling process itself causes major variation in burr size formed and contribution from non-randomized hole positions would rather play insignificant role. In this way, the measurements were more lucid and the risk of mistaken the results was reduced.

7.4 Experimental procedure

With the equipment discussed above, the test was performed. The dynamometer was mounted on the table of the milling machine and connected with charge amplifiers and PC acquisition board equipped with Labview 8.0. The vacuum fixture constructed was then placed on the dynamometer and fixed by four screws. The vacuum regulation was placed on the table of the milling machine, close to the fixture, in the interest of easy and quick manipulation. Afterwards, housing from vacuum pump to the vacuum regulation and vacuum fixture was connected via fast push-in connectors in order to provide vacuum for clamping. The plate workpiece was consequently placed on the fixture and vacuum pressure was applied, resulting in firm clamping in sense of supported bottom side of the workpiece (hole exit).

Drilling procedure was performed in the following order:

- Run-in with the new drill (30 holes drilled through the workpiece with 1 mm drill overrun into the fixture, resulting in hole pattern at the fixture surface produced), $n = 16000\,\text{min}^{-1}$, $f = 0.035\,\text{mm}$.
- Drilling of the first setting (see Table 6.5 for setting overview and Figure 7.5 for sketch of the drilling order positioned on workpiece) — fixed feed with 6 replications for each level of cutting speed with applied coolant by hand sprayer (for reason of coolant applied in this way see Chapter 6.3).

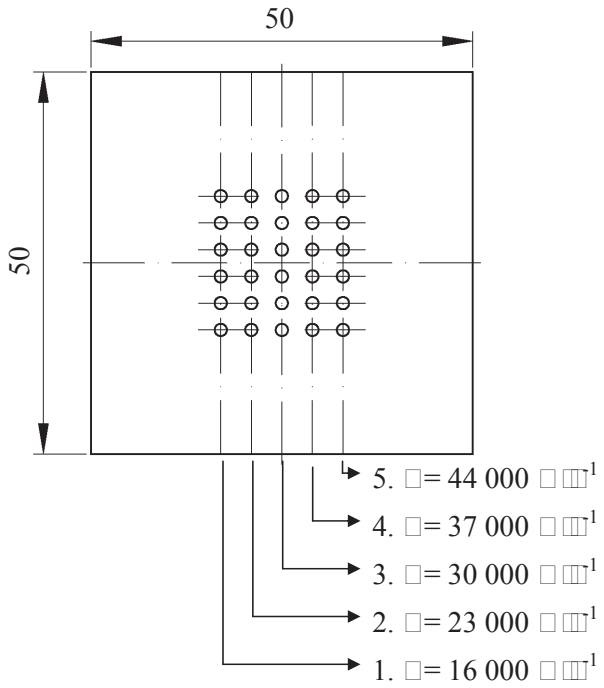

Figure 7.5: Schematic of the 1st drilling order setting on workpiece with 6 replications of each level of cutting speed (an investigation of influence of cutting speed on burr formation — Clamping system investigation).

- Removing of the high speed spindle and using the main machine tool spindle for subsequent test.
- Drilling of the second setting (see Table 6.7 for setting overview and Figure 7.7 for sketch of the drilling order positioned on workpiece) — fixed speed with 6 replications for each level of feed per revolution with applied coolant by hand sprayer.

7.5 Force measurements

The same force measuring equipment and setup as during preliminary test, previously described in Chapter 6.4, was used during this clamping system investigation. As

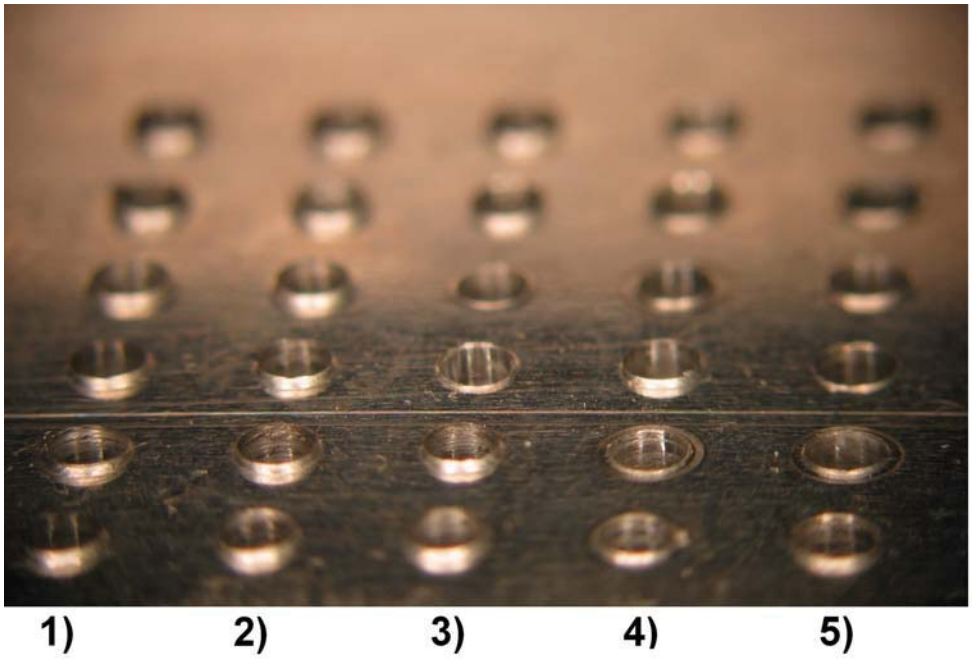

Figure 7.6: Photograph of exit burrs resulting from the 1st clamping investigation setting (see Figure 7.5) with indication of used conditions (an investigation of influence of cutting speed on burr formation).

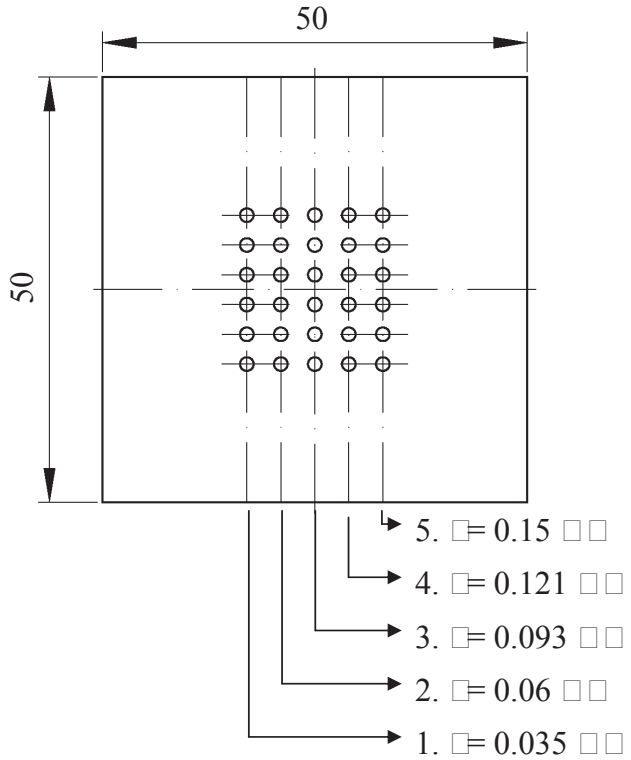

Figure 7.7: Schematic of the 2nd drilling order setting on workpiece with 6 replications of each level of feed per revolution (an investigation of feed per revolution on burr formation — Clamping system investigation).

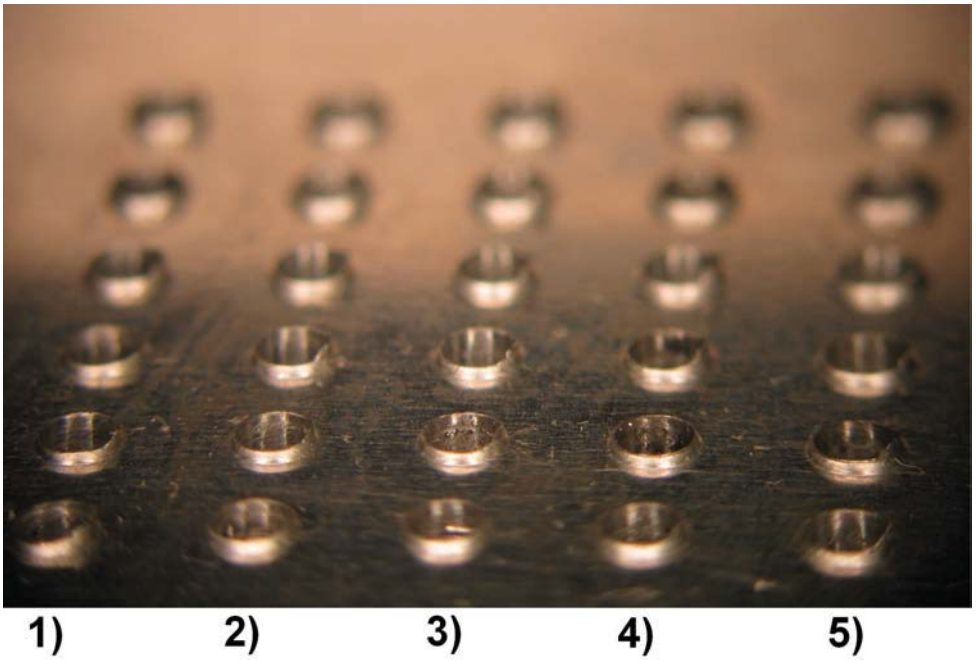

Figure 7.8: Photograph of exit burrs resulting from the 2nd clamping investigation setting (see Figure 7.7) with indication of used setting (an investigation of feed per revolution on burr formation).

first, the equipment was properly grounded, calibrated (see Chapter 6.4.2) and setting shown in Table 6.8 was used for measurements. Subsequently, the drilling feed force (thrust) and torque were recorded as a function of drilling time for all holes drilled .

Measured data were subsequently treated, as described in Chapter 6.4.5, and the graphs showing the trend of drilling thrust and torque as function of drilling time are enclosed in Appendix E. The dashed lines, in the graphs, represent drill positions during the drilling process. For description see Chapter 6.4.5 and Figure 6.22.

7.6 Burr measurements

Since the clamping fixture provided restricted room for burr formation at the drill breakthrough (hole exit), without influence on hole entry side, measurements were performed only for exit burrs. Burr heights were measured on Alicona measuring instrument (see Chapter 6.1.8 for details) in the same way as previously detailed in the preliminary test investigation (see Chapter 6.5.1). Burr widths were measured via the optical CMM machine used in the preliminary test and for detailed measuring procedure see Chapter 6.5.2. All measured data is enclosed as Appendix F.

7.7 Results

The present results reveal the effectiveness of the constructed clamping fixture to reduce burr formation at the drill exit. Results of the exit burr measurements for both parameters tested (various cutting speeds and various feeds) are presented and consequently compared with volume of burr formed from the preliminary test, where

no room restriction for burr formation was provided. In this way, the influence of clamping fixture on burr formation could be evaluated.

7.7.1 Influence of cutting speed on burr formation

All plots showing correlations of different cutting speeds on investigated burr dimensions include error bars representing experimental standard deviation (STD) of measured burr dimension resulting from 6 replications for each level of tested cutting speed. For complete overview of measured data with calculated STD and coefficient of variation (COV) see Appendix F.1. For force measurement data with calculated average values, STD, and COV see Appendix E.1.

Exit burr heights

The graph in Figure 7.9 shows comparison of exit burr heights resulting from various cutting speed tested during preliminary test and clamping system investigation, representing two different clamping conditions. Vacuum clamping fixture used during clamping system investigation was seen to reduce the size of exit burr height by 35 % in compare with preliminary test. In contrast to preliminary test results, the variation of exit burr heights, represented by error bars in Figure 7.9, was increasing with greater cutting speed. From the photograph of exit burrs in Figure 7.6, scratched rings around the exit holes periphery can be noticed when higher cutting speed was used. Such scratches causes design defect, resulting in faulty piece produced. See Chapter 7.7.3 and Figure 7.19 for details of this defect. The bigger variation in burr heights was caused by this defect and its occurrence observed during measurement is present in the tables, Appendix F.1, marked by yellow color with footnote (a).

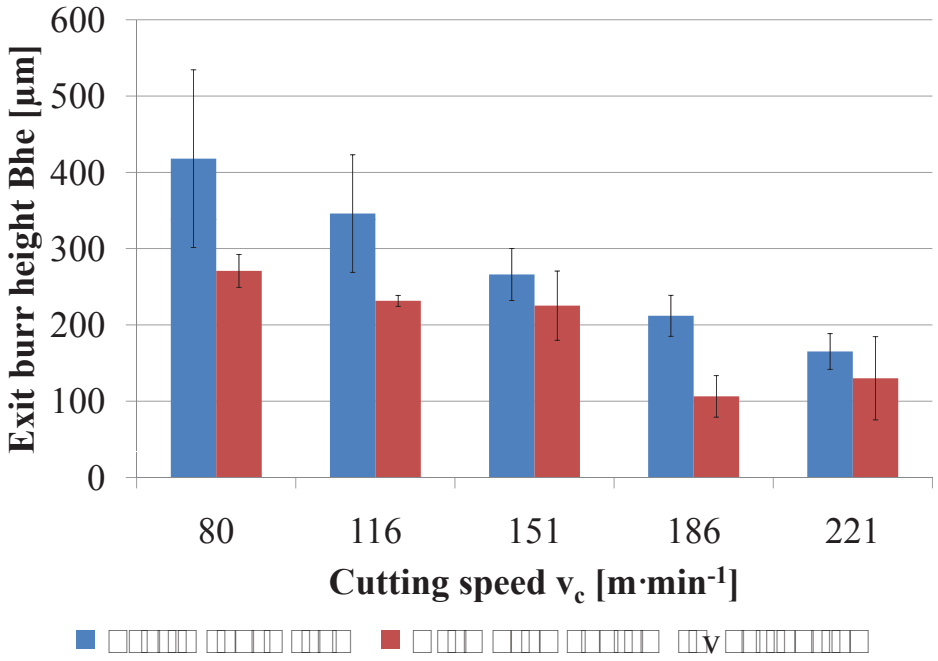

Figure 7.9: Exit burr heights resulting from various cutting speeds used when different clamping conditions tested.

Exit burr widths

Exit burr widths, as seen from the graphs in Figure 7.10 and Figure 7.11, were seen to be decreased by 14 % in burr width and by 16 % in burr root width. However, looking at the burr size variation caused by the process and represented by STD error bars, precise assessment can not be made and influence of clamp used on burr width reduction is seen to play rather insignificant role.

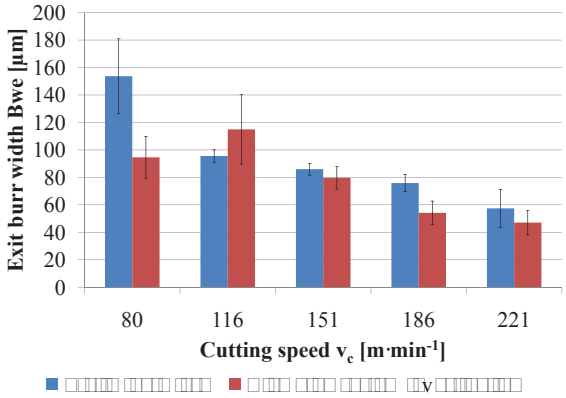

Figure 7.10: Exit burr root width resulting from various cutting speeds used when different clamping conditions tested.

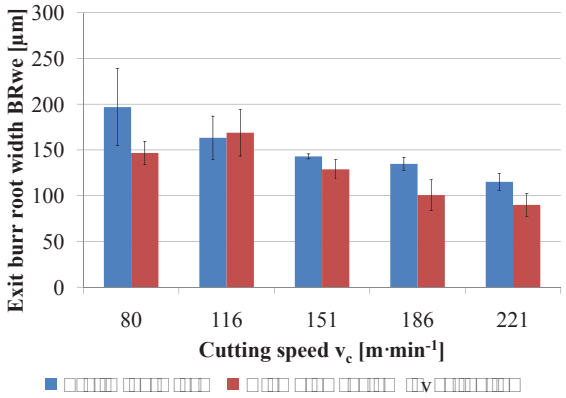

Figure 7.11: Exit burr root width resulting from various cutting speeds used when different clamping conditions tested.

Drilling forces

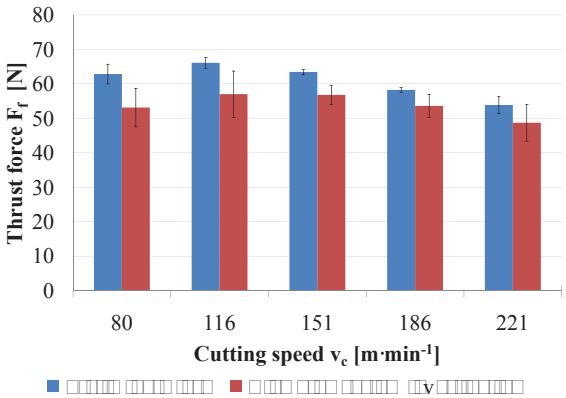

Figure 7.12: Thrust force resulting from various cutting speeds used when different clamping conditions tested.

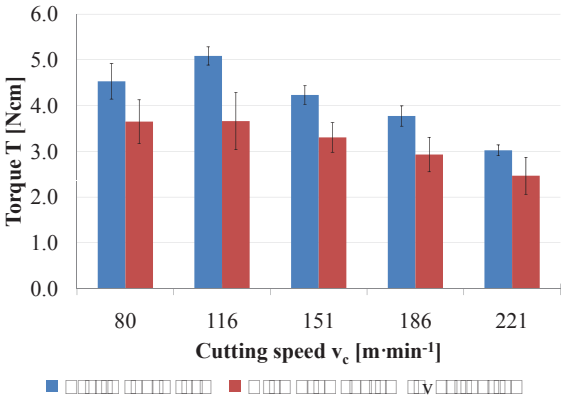

Figure 7.13: Torque resulting from various cutting speeds used when different clamping conditions tested.

Since the drilling parameters during both tests were the same, drilling forces were assumed to be the same. The variation of magnitude shown in Figure 7.12 and Figure 7.13 was caused by process itself (error bars showing STD), evaluation method (maximum force measured) and because of dulling of the drill. While force measurement data of preliminary test represent the drill already used for repeated tests, due to reasons already discussed in Chapter 6 dealing with the preliminary test,

the drill used in vacuum clamping investigation might still have an initial sharpness from manufacturing process even after 30 holes drilled as run-in before measurement initiation.

7.7.2 Influence of feed per revolution on burr formation

All following plots in this section include error bars representing STD of measured burr dimension resulting from 6 replications for each level of tested feed per revolution. For complete overview of measured data with calculated STD and COV see Appendix F.2. For force measurement data with calculated average values, STD, and COV see Appendix E.2.

Exit burr heights

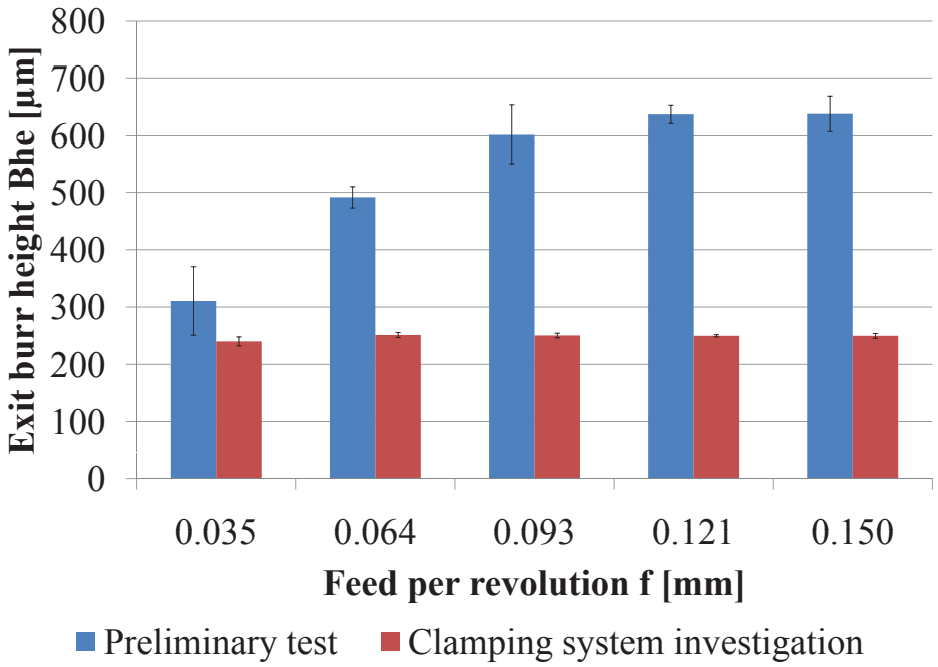

Figure 7.14: Exit burr heights resulting from various feed rates used when different clamping conditions tested.

The comparison of exit burr heights formed when different clamping conditions used, plotted as function of various feed rates used , is shown in Figure 7.14. From the graph it is clear that maximum burr height was restricted at certain value of about 250 μm with vacuum clamping used. Seeing again the results form previous test in Figure 7.9, where various cutting speeds were tested, the maximum heights were also of magnitude about 250 μm. This finding clearly reveals the fact that vacuum sealing was not pressed enough to fill in the groove leaving no freeboard between the fixture and bottom surface of the workpiece. Such setting reduced the size of exit burr height by 50 % in compare with preliminary test, where no support of the workpiece exit side was provided.

From the Table including burr height measurements, in Appendix F, significant occurrence of excessive burrs can be noticed. Location of these excessive burrs was

seen to be repeating, at one side of exit hole periphery of majority holes drilled. An angular proportion of these burrs was also seen to be greater in compare with those experienced from preliminary test, where excessive burr proportions represent separation of drilling cap from rest of the burr. The reason of repeated location of excessive burrs was seen to be caused by machine tool positioning error, because the CNC machine was turned off between the tests and during consequent switching-on, the machine coordinate origin was found with small difference than last setting.

Exit burr widths

As seen from the graph in Figure 7.15 and Figure 7.16, the burr widths were not influenced by used clamp because of the gap between plate workpiece and vacuum clamp. From the graph it can be seen that the burr formation was well reproduced in both tests with different clamping systems used.

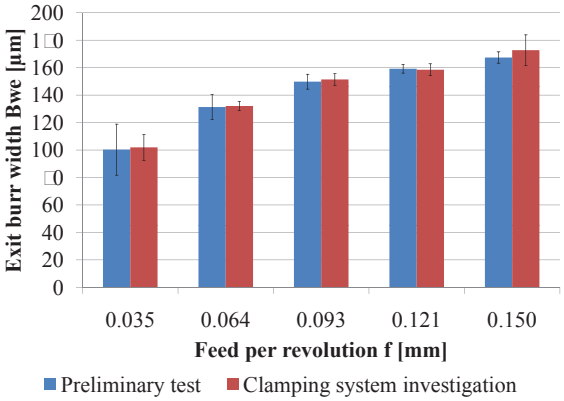

Figure 7.15: Exit burr root width resulting from various feed rates used when different clamping conditions tested.

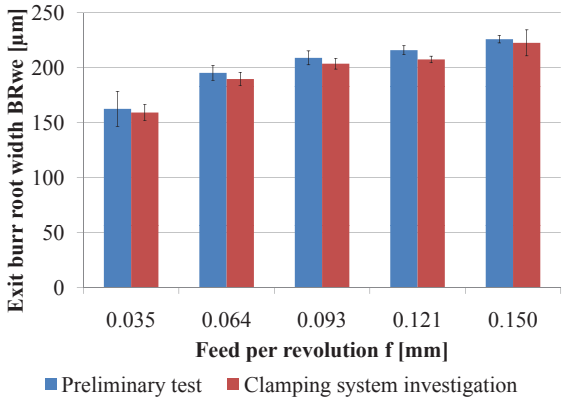

Figure 7.16: Exit burr root width resulting from various feed rates used when different clamping conditions tested.

Drilling forces

As already discussed in previous section, where various cutting speeds were tested, drilling parameters used during both test were the same, resulting in the same magnitude of drilling forces with small variations (see Figures 7.17 and 7.18). The variations were caused by process itself, evaluation method and dulling of the drill (see previous section for details).

7.7.3 Visual uniformity of the holes drilled

During clamping system investigation tests, visual defect at hole exit was experienced. For photograph of this defect see Figure 7.19. This shiny ring around the exit holes periphery occurred only when higher cutting speeds were used (influence of cutting speed on burr formation, Chapter 7.7.1) and resulted in unrepairable design defect and consequently in faulty workpiece. The scratches were caused by chip jammed between the plate workpiece and vacuum clamp with given rotation from rotating drill. This rotated chip caused the scratches of circular (ring) shape and exit burrs to be torn,

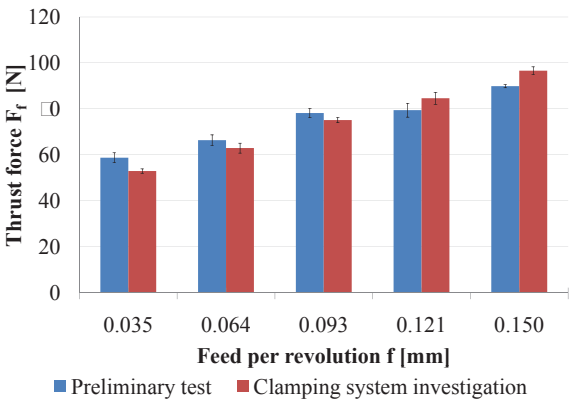

Figure 7.17: Thrust force resulting from various feed rates used when different clamping conditions tested.

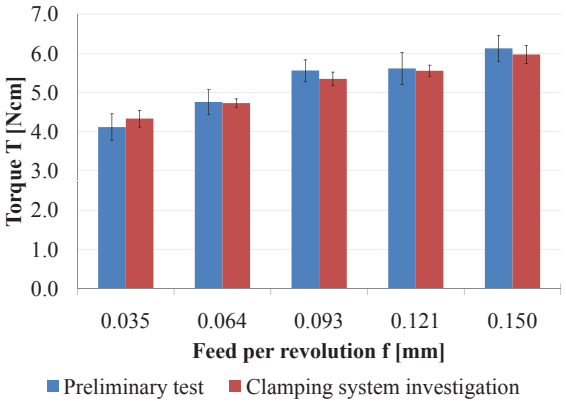

Figure 7.18: Torque resulting from various feed rates used when different clamping conditions tested.

thus resulting in big variation of resulting burr sizes measured (see Appendix F.1 for measurement data and Chapter 7.7.1 for data evaluation).

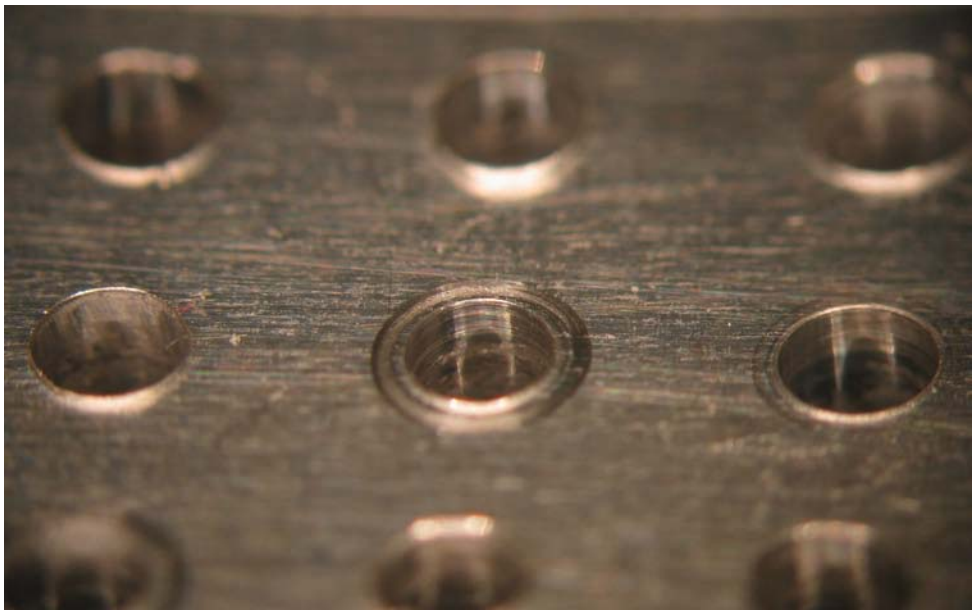

Figure 7.19: Scratched ring around the exit holes periphery.

This design defect may be eliminated with a properly designed clamp, providing restriction of the freeboard in between the workpiece and vacuum clamp leaving no room for jammed chips in between.

7.8 Summary

The present chapter deals with the investigation of clamping conditions affecting the exit burr formation. The first step taken was to construct such a clamp fixture, which provided room restriction for burr formation, ensured reproducibility of the results at the Bang & Olufsen workshop, and made investigation possible (force measurements). Since vacuum clamping system was already in use at the company, the same principle providing uniform multipoint clamping, particularly good for clamping workpieces in the form of thin plates, was used. The vacuum seal and geometry of vacuum grooves, in which the sealing must fill, was chosen according to the literature and recommendations of the seal retailer. In order to evaluate influence of clamping system constructed, the same drilling conditions and tool as during the preliminary test were used, allowing comparison of exit burr formed.

The results from various cutting speed used shown an average reduction of 35 % in exit burr height compare to those resulting from the preliminary test. Burr widths were rather seen to be unaffected by different clamping conditions.

Various feed rates used resulted in stabilized exit burr heights of about 250 μm, providing reduction of 50 % in comparison with burr heights resulting from the preliminary test. Seeing again the results from previous test where various cutting speeds were tested, the maximum heights were also of magnitude about 250 μm. This finding clearly reveals the fact that vacuum sealing (NBR O-rings having 70 Shore hardness) were not pressed enough to fill in the groove leaving no freeboard between the fixture and bottom surface of the workpiece. However, it was proved that with a properly designed clamp fixture and seal used (softer sealing required), it is possible to significantly reduce exit burr formation.

Defect in visual uniformity of drilled holes occurred at hole exits when higher cutting speed used. Scratches forming shiny rings around the periphery of the exit holes were caused by chip jammed between the sheet workpiece and clamp fixture with given rotation from the rotating drill. This rotated chip caused the scratches of circular shape and exit burrs to be torn. This defect can be eliminated with a properly designed clamp, providing restriction of the freeboard in between the workpiece and vacuum clamp leaving no room for jammed chip in between.

Chapter 8

Tool geometry investigation

This chapter details the experimental work undertaken to find a drill geometry suitable for minimizing burrs at both entry as well as exit side of drilled holes, reaching high production productivity, and ensuring uniform appearance of drilled holes. Such optimized process had to be applicable for production at the company workshop. Therefore, and due to insufficient power output of high speed spindle tested during preliminary test for this test, the test was performed at Bang & Olufsen workshop, using machine tool and clamping system intended to use for production.

First, tool geometries for investigation had to be selected based on previous researches pertinent to the goals named above. Next, experimental parameters had to be selected based on recommendations of tool manufacturers and company requirements for high productivity.

Measurements were carried out with respect to drilling thrust (feed force), final burr dimensions for hole entry as well as exit side (height and widths) and visual uniformity of drilled holes was evaluated. Description of the test setup, conditions, data analyses and conclusions are presented in the following.

8.1 Drill geometries selection

Selection of drill geometries to be tested was based on previous researches listed in literature survey on burrs (Chapter 3), survey on drilling process (Chapter 2), and brief overview of research findings and recommendations is presented in Chapter 3.8. Fixed parameters for all drills tested were chosen to be diameter of 2 mm, helix angle 30°, and point angle 140°. Different drill point geometries were of interest to be tested.

Step drill geometry was from previous researches found to reduce burrs at drill exit side. But since such geometry requires longer drilling length, because of step in diameter (small diameter precedent to final hole diameter, see Figure 2.22 for sketch) resulting in longer drilling time and thus lower productivity, it was decided not to use this geometry for the test. It is of interest to reach high productivity and speed up the production process, where great amount of holes are drilled in single workpiece, therefore drilling time must be kept as low as possible.

A multifacet drill specially designed for drilling thin sheets (see Figure 2.4 was already tested at the company and proved unsatisfactory toll life since the sharp edges at the drill corners got worn too early. Multifacet drills designed for drilling in aluminium (see Figure 2.20) are expensive to grind because of complicated geometry. Hence, MFD drill geometry was not used during the test.

The first drill point geometry tested was of double cone (or chamfered) point (see Figure 8.1). This geometry was according to literature and previous researches seen to provide burr free edge at the drill exit for cast iron worpiece material. The drill was tailor-made type 180841-1 by Danish drill manufacturer TN Slib A/S with increased body clearance of 0.5 deg (normally 0.1 deg according to the standard DIN 338 for standard drill geometries). Also margin width was reduce to 60 μm instead of size of 130 to 300 μm according to the standard DIN 338. Both adjustments were made in order to reduce friction between the drill and the surface of drilled hole and thus resulting in lower heat generation. Surface of the drill flutes was polished in order to prevent chip packing and material build-up. The tool is throughout the present chapter designated as Drill A and for summary of the drill geometry, description and photograph of the drill point (tip) geometry see Table G.1.

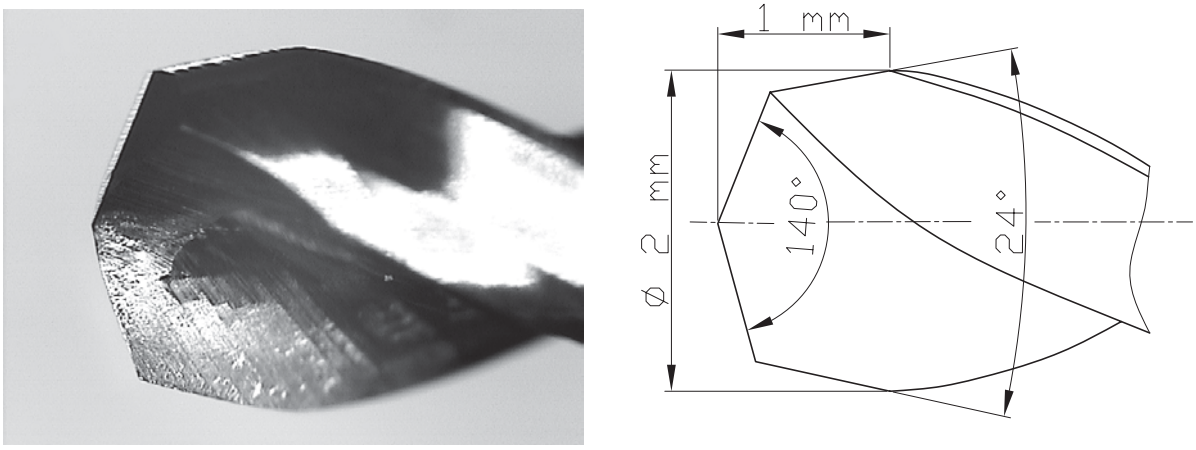

Figure 8.1: Profile of double cone point Drill A.

The second drill tested (Drill B) was of single cone point with six-facet geometry. This modified geometry entirely removes the chisel edge, provides better self-centring, requires less power ant thrust and permits increased feed rates to the drill. This geometry is widely available on the market and thus cheaper in compare with tailor made tools with complicated geometries. The drill was of type WX-MX-GDS from Japanese drill manufacturer OSG, made of sintered carbide with surface coating. For summary of the drill geometry and photograph of the drill point (tip) geometry see Table G.1.

The third drill tested and designated as Drill C during the test was single cone drill with helical point. This modification produces an S-shaped chisel edge providing continuous cutting across the drill web. Advantages of this geometry are according to literature seen in better selfcentering capability and some reduction of thrust. The drill was also produced as tailor-made type (180841) by Danish drill manufacturer TN Slib A/S with increased body clearance of 0.5 deg, reduced margin width to 60 μm, and having polished flutes for the same reasons as explained above for double cone Drill A. For summary of the drill geometry and photograph of the drill point (tip) geometry see Table G.1.

The last drill tested and designated as Drill D, throughout the test, was 3 flute coated sintered carbide drill from Swiss drill manufacturer Mikron Holding AG of CrazyDrill^{TM} Alu type. The thrust force was expected to decrease compared to when using 2 fluted drills, since the chip load will be evenly divided among the 3 cutting

edges provided, instead of 2 when 2 fluted drills used. Such feed force (thrust) reduction may result in less material volume to be formed into the burr and at the same time higher feed rates could be used, resulting in higher productivity and limiting the potential occurrence of entry hole error ("Star effect at hole entry") caused by drill wandering. On the other hand, the 3 flute geometry for such small drill diameter will result in smaller stiffness and the tool will be more prone to breakage. For summary of the drill geometry and photograph of the drill point (tip) geometry see Table G.1.

Table 8.1: Summary of drills studied in tool geometry investigation

Drill point	Tool desig-nation	No. flutes [-]	Material/ Coating	Point angle [deg]	Helix angle [deg]	Flute length [mm]	Price [DKK]
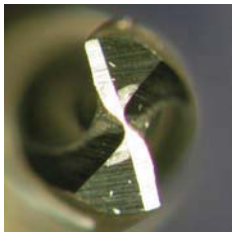	Drill A	2	Tungsten carbide HM /none	140/24	30	6	325
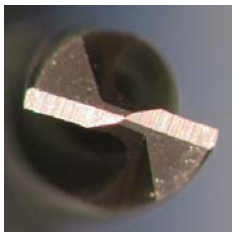	Drill B	2	Sintered carbide/ WX — Multi layered composite TiAlN	140	30	12	70
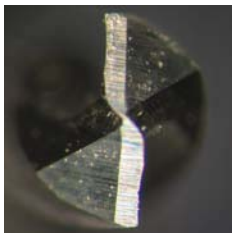	Drill C	2	Tungsten carbide HM /none	140	30	6	325
	Drill D	3	Carbide alloy /coated	140	30	10	375

8.2 Experimental setup

A vertical double spindle CNC machining centre Chiron DZ 12K W high speed plus was used during tool geometry investigation. The four drill geometries were tested (see previous section for drill geometeries selection and for overview of the drills investigated see Table G.1). Sheet aluminium workpiece was firmly held by special vacuum clamp fixture and vacuum for clamping was provided by high vacuum pump. The vacuum clamp was directly placed on 3D-dynamometer Kistler 9257BA with buil-in charge amplifiers for measuring forces during drilling process. The data from force measurements were processed and recorded by PC equipped with software DynoWare from Kistler. Burr height measurements were performed on Alicona optical auto-focus measuring instrument and and processed in software Mex 5.1 from Alicona Imaging GmbH. Burr widths were measured on the optical CMM machine DeMeet 220. All equipment used is described forth in this chapter. The basis setup of the experiment is depicted in Figure 8.2.

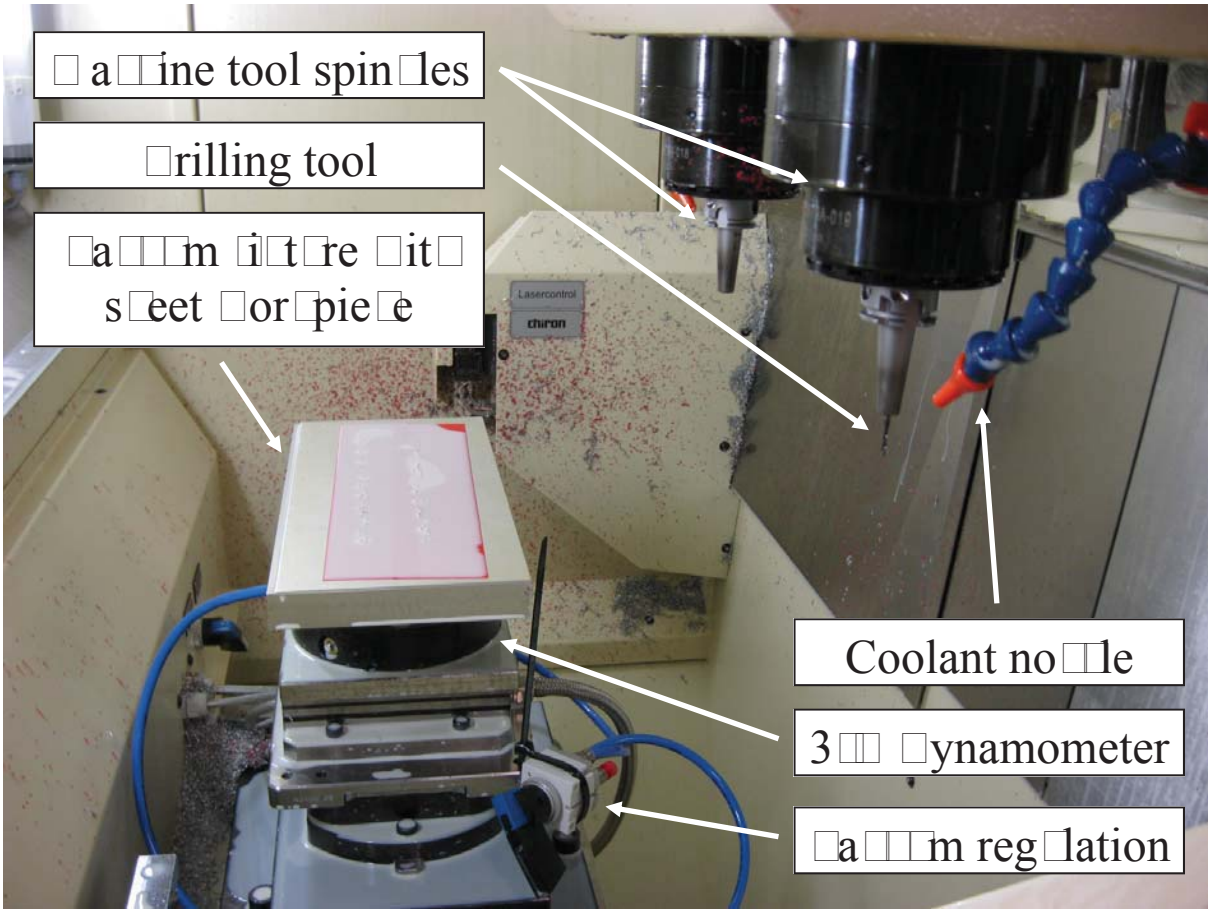

Figure 8.2: Experimental setup of tool geometry investigation test.

8.2.1 Machine tool

The machine tool used for the test was vertical double spindle CNC machining centre Chiron DZ 12K W high speed plus, from German manufacturer CHIRON-WERKE GmbH, with 3 motion axes provided by spindles. The machine was equipped with

table swiveling from 0 to 180° providing quick workpiece exchange. For summary of the main characteristics of the machine tool see Table 8.3.

Table 8.3: Chiron DZ 12K W high speed plus characteristic

Characteristic	Unit	Magnitude
X/Y/Z axis travel	[mm]	550/320/360
Spindle revolutions	[min^{-1}]	up to 40,000
Rapid traverse speed	[$m \cdot min^{-1}$]	up to 90
No. of tools		max. 2×32
Tool taper		HSK-A-50
Tool change time	[s]	approx. 0.9
Motor power	[kW]	up to 14
Machine type		Vertical

Note: K = machine with chain magazine
W = machine with workpiece changer

8.2.2 Workpiece clamping system

Special vacuum clamping system, constructed at the company, was used during the test. For photograph of the system see Figure 8.3. With vacuum provided by high vacuum pump, a soft sealing material completely filled in sealing grooves, leaving no gap between the sheet workpiece and clamp fixture. In this way, room restriction for exit burr formation was provided.

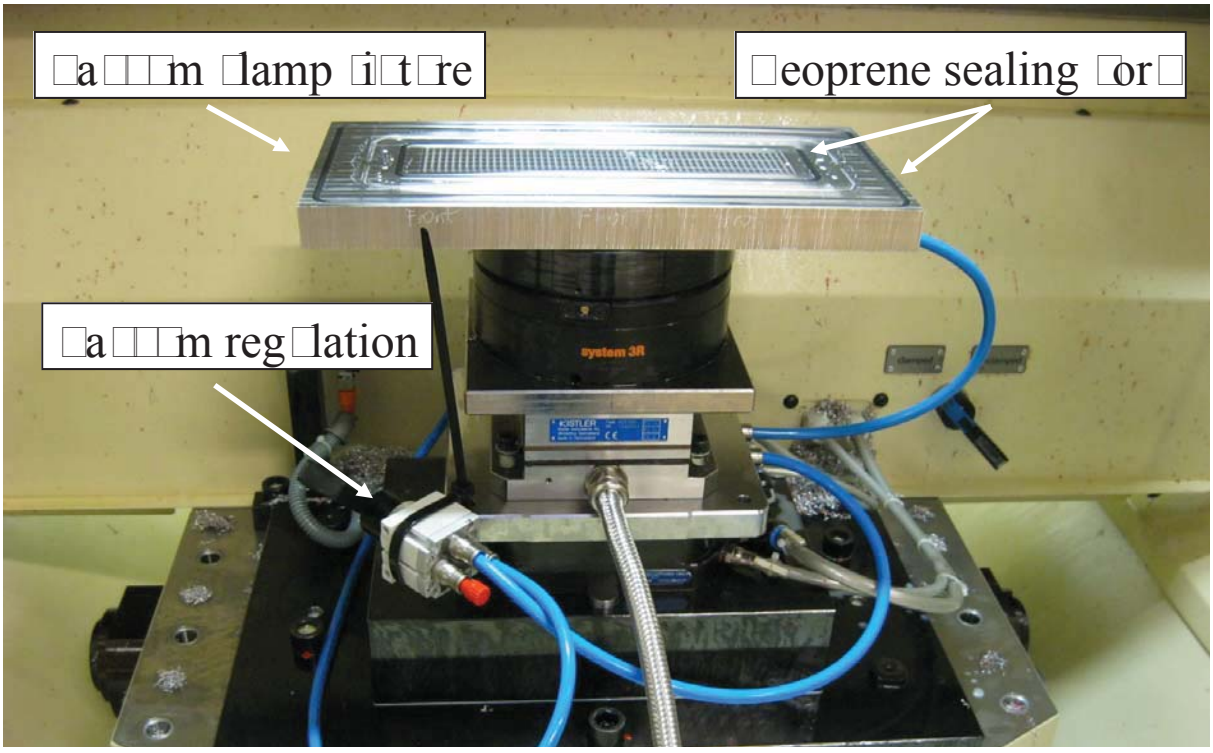

Figure 8.3: Vacuum clamping system used during tool geometry investigation.

Vacuum sealing

Compared to vacuum clamping system used during the second test, dealing with influence of clamping system on burr formation (Chapter 7), soft neoprene rubber was used as vacuum sealing. This soft sealing material ensures that there is not any freeboard between the workpiece and clamp fixture when vacuum applied, ideally resulting in no room for exit burr formation.

Geometry of sealing grooves

In order to avoid any swarf or debris from drilling process falling into the sealing grooves and to keep the sealing cord in place during the process of repeated clamping and unclamping of the workpieces, the dovetail groves were provided as sealing grooves. For sketch detailing cross-section of the vacuum clamp fixture used see Figure 8.4.

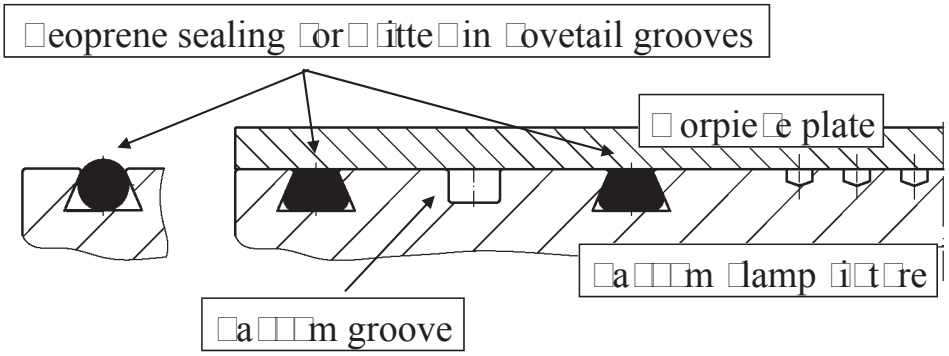

Figure 8.4: Cross-sectional sketch of vacuum clamp fixture with fitted neoprene sealing cord (left — unloaded state, right — clamped state).

Clamping force

The clamping force applied is calculated in the same way as for the vacuum clamping system constructed in Chapter 7.1.3 dealing with clamping system investigation. The working principle of vacuum clamping is also detailed in mentioned Chapter 7.1.3. For present clamp fixture used , the clamping area upon the vacuum was applied on was 28 100 mm^2. With pressure provided by high vacuum pump used during the test (0.02 MPa of absolute pressure) is the clamping force calculated according to Equation 7.1 and resulting in:

$$F_{clamp} = p \cdot A = (0.1 - 0.02) \cdot (28\ 100) = 2\ 248\,\mathrm{N}$$

8.2.3 Force measuring device

The three-component measuring piezo-electric transducer Kistler 9257BA, S. No. 1492351 was used for thrust measurements during drilling process. The dynamometer was of low impedance because of charge amplifiers were directly buil-in the dynamometer. The thrust measurement data was consequently digitized and recorded by using PC equipped with software DynoWare from Kistler.

8.2.4 Coolant

A 7% oil emulsion HOCUT 795B was used during the test. The fluid is concentration of oil emulsion with water, resulting in milky-white, low foaming emulsion with good cooling and extremely high lubrication effect, especially suitable for machining aluminium and it's alloys.

8.3 Experimental plan

It was of interest to test the four previously discussed different drill geometries and at the same time to reach high drilling productivity. Therefore the lowest value of cutting speed and feed used was in accordance with drill manufacturers recommendations and the highest values were limited by machine tool capabilities (see Table 8.4 for overview of drilling conditions used during the test). Despite the machine tool is according to characteristics shown in Table 8.3 capable of maximum 40 000 rev $\cdot$ min^{-1}, it is generally advisable to decrease maximum rotational speed used for continuous production. Thus the maximal cutting speed tested was 226 m $\cdot$ min^{-1}resulting in 35 969 rev $\cdot$ min^{-1}. Maximum feed speed was also accordingly chosen with machine tool capabilities for long-term production and resulted in 6 834 mm $\cdot$ min^{-1}, providing maximum production when both maximum drilling condition utilized.

Table 8.4: Drilling conditions utilized in tool geometry investigation

Order		1	2	3	4	5
Cutting speed (v_c)	[m $\cdot$ min^{-1}]	50	94	138	182	226
Feed per revolution (f)	[mm]	0.05	0.085	0.12	0.155	0.19
Spindle revolutions (n)	[min^{-1}]	7 958	14 961	21 963	28 966	35 969
Feed speed (v_f)	[mm $\cdot$ min^{-1}]	398	1 272	2 636	4 490	6 834

In order to investigate the burr formation process and the occurrence of errors in visual uniformity of drilled holes, while restriction of exit burr formation was provided by means of clamp fixture used, wide ranges of process conditions were used. For each drill geometry, all combinations of five levels of cutting speed and feed speed previously discussed were of interest to observe. Resultant feed per revolution of some of 25 combinations resulted in too big or too small chip load. Such conditions would provide inconvenient drilling process, possibly resulting in tool breakage. On this account, colour marked settings in the Table G.1 included in Appendix G were excluded from the test order (see corresponding notes below the table explaining the reasons for exclusion). This resulted in 22 settings intended to use during the test.

An observation of errors in uniform appearance of drilled holes was of vital importance, hence great amount of holes drilled for each setting was required. Since used workpiece material has only very small silicon content and thus does not evoke substantial wear and experienced and for production required tool life was at about 700 000 drilled holes per one drill, it was decided to drill 200 holes for each setting with all drills tested. The drilled samples were subsequently halved. First half of the sample with 100 drilled holes was used for internal investigation at the company and the second one for measurements performed at the university (DTU). This result,

in overall, 4 400 holes to be drilled with each tested drill geometry. In order to avoid possible drill wear influencing measurements, order of drilling setting tested was randomized with keeping the most important setting for the highest productivity as first setting for all tested drills. For summary of randomized test setting order of all conditions used during tool geometry investigation see Table G.1 included in Appendix G.

8.4 Experimental procedure

The test investigating different tool geometries was performed with the equipment discussed above and depicted in Figure 8.2. The dynamometer with special vacuum clamping system was mounted on the table of the machining centre and connected with PC for force data processing. Vacuum for clamping was provided by the high vacuum pump and controlled by vacuum regulation connected to the clamp fixture. In this way, the sheet workpiece was firmly clamped. The drill tool to be tested was chucked into the spindle (only one spindle used during the test) and measuring equipment was set. Force measurement was initiated after first 20 holes drilled (serving as run-in with the new drill — only for the first test of each drill geometry) with flooding coolant applied and directed to the tip of the drill. Drilling order was kept randomized and for summary of test order used with drilling conditions utilized see Table G.1 included in Appendix G. This test order was repeated for all four drills tested. Every drilled sample was accordingly designated (according to sample code in Table G.1)

During the test with tool geometry (drill B), swarf clogged in drill flutes were very often (see Figure 8.5). Ten times out of 22 settings tested clogged with swarfs had to be manually removed from drill flutes before another setting was run. This had to be done in order to avoid tool breakage caused by insufficient chip flow or hole entry defects caused by drilling cap stuck on a drill tip.

When the last drill geometry was tested (drill D), tool breakage occurred at 5th setting (see Table G.1 in Appendix G). This was caused because of insufficient chip load per cutting edge when using 3 fluted drill. The small feed used in the 4th drilling setting resulted in too small chip load on single cutting edge of the drill, providing unfavourable cutting process, creation of BOE, excessive tool wear and swarft clogging in flutes. This resulted in excessive forces required for cutting and consequent tool breakage due to overload. In order to avoid repeated breakage, test plan for the last drill geometry tested was adjusted and settings resulting in too small feeds were executed from the test plan. See the Table G.1 for the adjusted test plan.

8.4.1 Force measurements

Before test initiation, force measuring equipment was set to a low range of measured forces (1 000 N in vertical direction — Fz and 500 N in horizontal directions — Fx, Fy) and sampling frequency of 10 000 Hz due to high spindle rotations used. Before initiation of each drilling setting, equipment was reset. After drilling process initiation, forces in all three orthogonal directions were recorded as a function of time for 10 seconds of the drilling process, and visualized on PC equipped with software DynoWare from Kistler (see Figure 8.6). The measured data was accordingly

Figure 8.5: Swarf clogged in drill flutes (drill B).

designated and saved on PC for later evaluation. This procedure was repeated for each drilling setting.

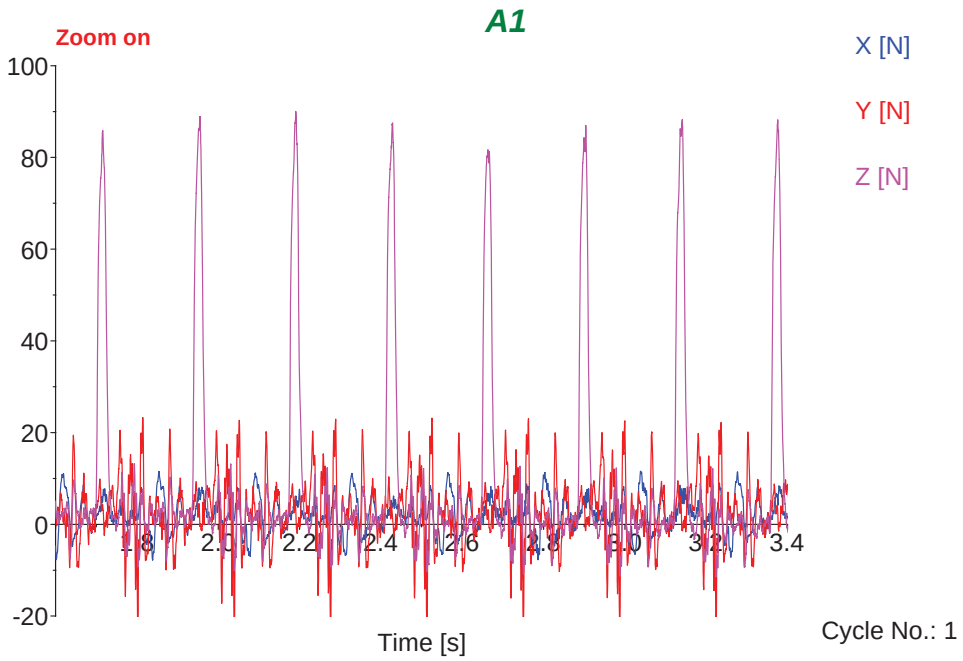

Figure 8.6: Forces measurement for the 1st test setting — A1 (Drill A, 1st setting). Measured forces in all 3 directions, zoomed on 1.8 second measuring period, where peaks in Z direction of the forces represent drilling of the holes, displayed in software DynoWare.

Drilling forces evaluation

As already recognized, trust force is of vital influence on burr formation. Therefore it was of interest to compare thrust force required during drilling for each drill geometry while the same cutting conditions used. For the reason discussed, force data evaluations were reduced to thrust force evaluation only. The forces measured data were processed via software DynoWare from Kistler. In some measurements, drift in measured data over measured time was apparent and greatly misrepresenting the actual magnitude of thrust force applied (see Figure 8.7). In such case, the data were remedy by using drift compensation tool via the software (see Figure 8.8). This signal correction enabled evaluation of an actual magnitude of thrust force applied during the drilling process.

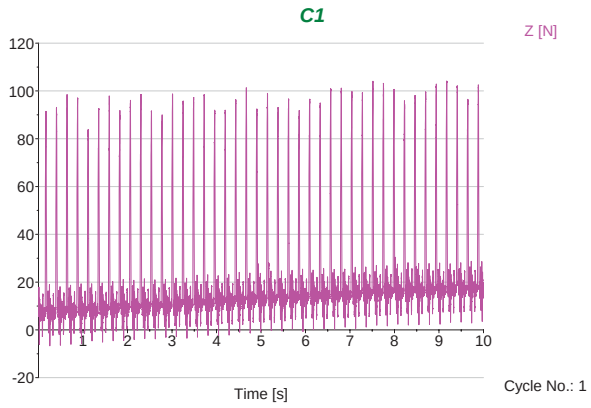

Figure 8.7: Thrust force measurement with signal drift (drill C, the first test setting).

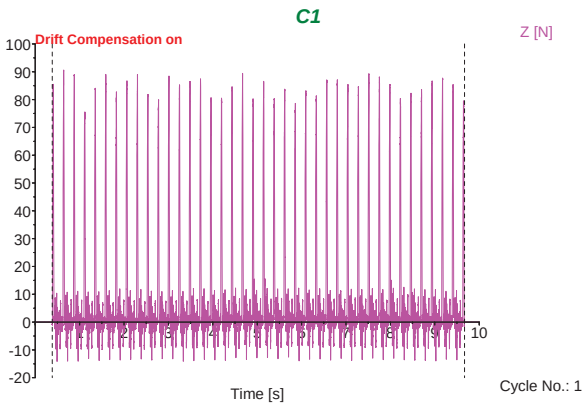

Figure 8.8: Thrust force measurement from Figure 8.7 with signal drift compensation applied.

With respect to project goals, burr reduction and high production productivity was required. Based on results from preliminary tests, where the highest cutting speed proved to be advantageous for both named requirements, it was of interest to investigate the highest cutting speed used for all drill geometries tested in detail. Since the error causing the so called "star effect at entry hole" was seen to be reduced with increasing feed and the burr volume tends to be greater with increasing feed rate, it was of interest to investigate different feed rates used and consequently find an optimal setting for the production. For discussed reasons, evaluation of the highest cutting speed used ($v_c = 226\,\mathrm{m \cdot min^{-1}}$) with four levels of different feed rates for all the four drill geometries tested was performed. For all measured data and plots showing trend in thrust force versus drilling time applied during drilling, for all drills tested, see Appendix H. Average values of thrust force (in Table H.1 and Table H.1) results from 20 drilled holes within 10 second force measuring range for each drilling setting utilized and drill tested.

8.4.2 Burr measurements

For the same reasons discussed above, the burr measurements were also limited to samples drilled with the highest cutting speed and different feed rates for all the four drill geometries tested. Measurements of burr heights, widths and root widths were performed for both hole entry and exit side of drilled sheets. For the most important

setting providing the highest productivity (highest cutting speed with the highest feed rate used), 6 measurements of each burr dimension were performed in order to reduce variability of the measurements. For other settings used, 3 measurements of each burr dimension were performed.

Burr heights were measured on Alicona, an optical measuring instrument (see Chapter 6.1.8 for details), in the same way as previously detailed in preliminary test investigation (see Chapter 6.5.1) with some small adjustments. Since bigger diameter was drilled during this test (diameter of 2 mm in compare with 1.6 mm during both previous tests), it was not possible to fit the whole burr formed within the measuring range of 2.8392 $\times$ 2.1538 mm resulting from 5X magnification used in both previous tests. Hence, stitching of the captured images was automatically performed during the measurements, keeping the same magnification of 5X with measuring range of 2.8392 $\times$ 4.3076 mm. This enabled to capture entire burr formed in single file, providing 3D reconstructed model of entire burr for subsequent measurement via MeX software.

Burr widths were measured via the optical CMM machine used in both previous tests and for detailed measuring procedure see Chapter 6.5.2.

All burr measurement data are enclosed in Appendix I in tables corresponding to drill geometry tested.

8.5 Results

8.5.1 Thrust force measurements

Thrust measurements data of 20 holes drilled with calculated average values, standard deviations and coefficient of variations for four levels of feed rate utilized and drill geometry tested are enclosed in Table H.1 and Table H.2 in Appendix H. Summary of the measurements is listed in Table 8.5 bellow.

Table 8.5: Averaged thrust force for each drill geometry tested ($v_c = 226\,\mathrm{m} \cdot \mathrm{min}^{-1}$)

Feed per revolution [mm]	0.035		0.073		0.125		0.190	
Measured thrust force [N]	AVG	STD	AVG	STD	AVG	STD	AVG	STD
Drill A	39	1.3	57	0.8	85	2.9	87	2.9
Drill B	37	0.8	53	1.7	77	2.4	80	3.2
Drill C	31	0.6	46	1.8	81	3.1	85	3.8
Drill D	12	0.5	13	0.7	22	0.6	41	1.0

Previously discussed problem with swarf clogging drill flutes of Drill B tested (see Chapter 8.4 and Figure8.5) was also seen in force measurements. In Figure 8.9, an excessive force can be seen. This force exerted during drill retraction movement was caused by swarf clogged in drill flutes with tendency to lift the workpiece and to which is vacuum clamping force opposing. Such excessive forces can result in drill overload and tool breakage (especially for fragile carbide drills). This clogging was caused by surface roughness of the drill flutes. As summarized in Chapter 3.8 — Summary and recommendations of literature survey, polished flute surface is recommended to prevent chip packing and material build-up when soft ductile materials drilled.

For sintered carbide drills without any surface treatment is the surface roughness determined by size of the carbide grains and in present case of the drill material, very fine micro grains are required to prevent this.

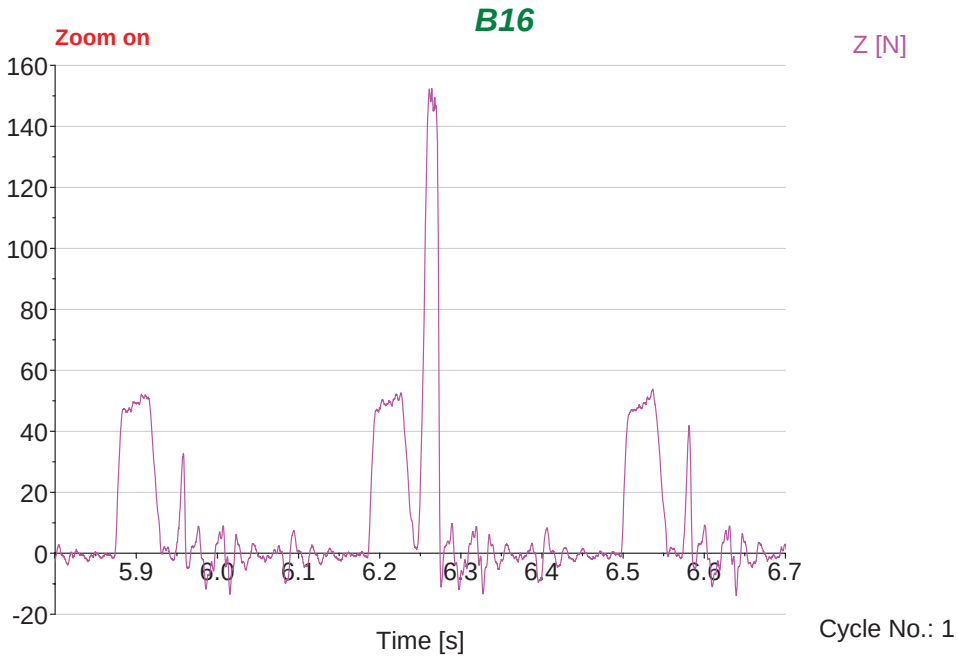

Figure 8.9: Peak in thrust force due to swarf clogged in drill flutes during drill retraction.

The graph in Figure 8.10 shows comparison of thrust force resulting from the four different drill geometries tested as a function of four different feed rates used. The graph include error bars representing experimental STD of thrust force measured over 20 drilled holes for each drill and feed used.

From the graph, it is apparent that Drill D requires only at about 25 to 50 % of thrust force compared to the other drill geometries tested for different feed rates used. Lower thrust force is favourable in the interest of less material volume which undergo plastic deformation and shearing out of the workpiece material at the drill exit. Other three drill geometries represent nearly the same values of thrust force exerted with some variations. These measured thrust forces represent maximum values exerted during the whole drilling process. For exit burr formation, the breakthrough thrust force is of vital importance though. Hence, closer look on trend in thrust force during drilling of single hole was made in order to evaluate the actual breakthrough thrust force responsible for exit burr formation (see Figure 8.11). Plots showing trend in thrust force versus drilling time of single hole drilled were made for 6 holes drilled when the first test setting (drilling parameters) utilized for all the four drills tested. Those plots are enclosed in Appendix H in corresponding sections. Dashed lines with designations t0 to t3 indicate drill positions during drilling and for detailed description see Chapter 6.4.5 and Figure 6.22.

From the graph in Figure 8.11 and Appendix H.0.1 it can be seen that for Drill A, the breakthrough force is of at about 50 % of the maximum thrust force measured. Breakthrough thrust force of Drill B, shown in Appendix H.0.3, is of at about 85 % , and about 75 % for Drill D (see Appendix H.0.4), of maximum thrust force measured. Whereas the maximum thrust force measured of Drill C represents the

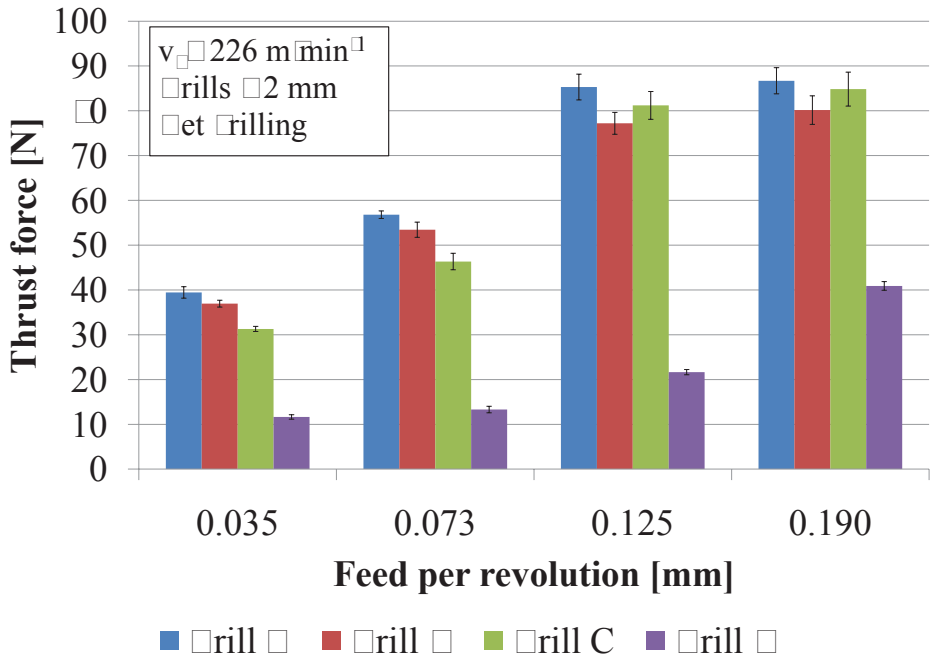

Figure 8.10: Comparison of drilling thrust force resulting from four different drill geometries tested.

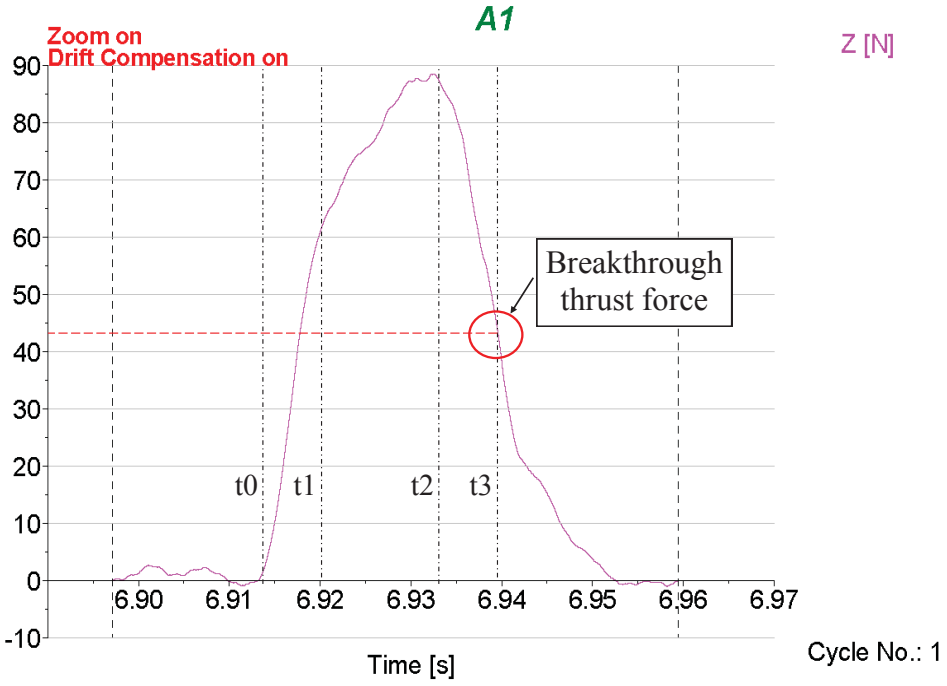

Figure 8.11: Measured breakthrough thrust force of Drill A, 1st test setting. Drill positions indicated by the dashed lines (see Chapter 6.4.5 and Figure 6.22).

actual breakthrough force (see Appendix H.0.4). From such thrust force distributed over drilling time can be concluded that Drill A and Drill D provide the lowest breakthrough thrust force, which in theory should result in less workpiece material formed into exit burr. Drill B also represents maximum thrust force exerted earlier in drilling process and favourable lower breakthrough force, but it is of greater

magnitude than resulting from Drill A and Drill D. On the contrary, Drill C is seen to exert maximum thrust force during drilling process at the drill breakthrough and thus should result in unfavourable greater exit burr volume formed.

8.5.2 Burr measurements

Burr measurement data resulting from measurements discussed in Chapter 8.4.2 are present in Tables corresponding to drill geometry used in Appendix I with calculated AVG, STD and COV.

All plots showing comparison of burr formed resulting form the four different drill geometries tested are present forth in this section. The graphs include error bars representing experimental standard deviation (STD) of measured burr dimension.

Entry burr heights

As seen from the graph in Figure 8.12, Drill A created entry burr heights of 2 to 3 times greater than resulting from other drill geometries. With the highest feed rate used, Drill D reduced burr height by 85 %, Drill B by 65 %, and Drill C by 55 % compared to burr height resulting from using Drill A. Whereas the the trend in burr height is increasing with increasing feed for Drill A, B and C, for Drill D is conversely decreasing with increasing feed used. This suggest favourable application of higher feed used, due to three cutting edges involved in cutting process, providing convenient chip load per single edge for Drill D.

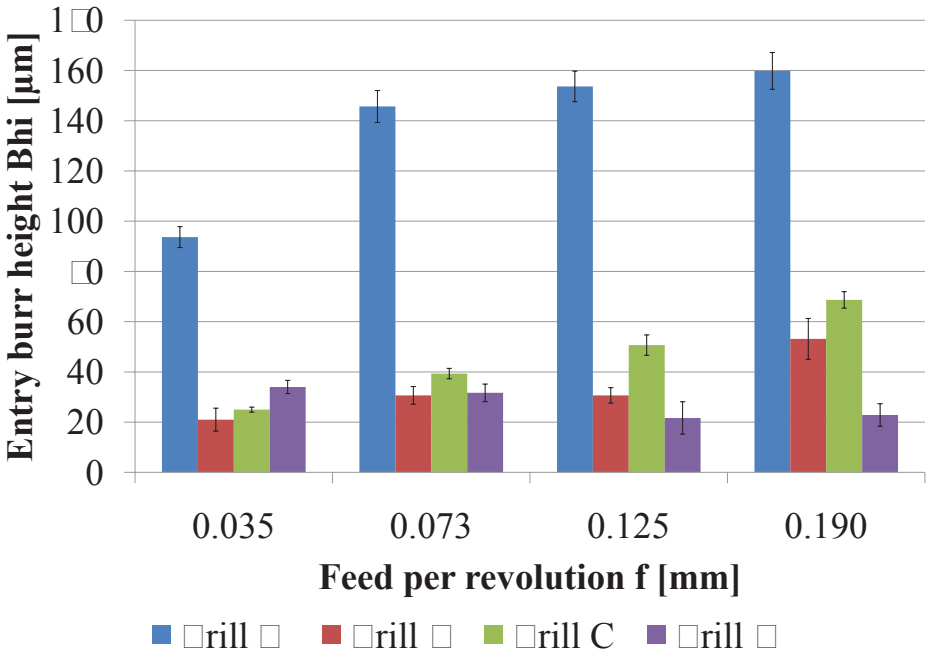

Figure 8.12: Comparison of entry burr heights resulting from four different drill geometries tested.

Entry burr widths

Drill D was again seen to overcome other drill geometries tested in creation of burr widths, as seen from Figure 8.13 and Figure 8.14, whereas Drill A created unfavourable great burr widths.

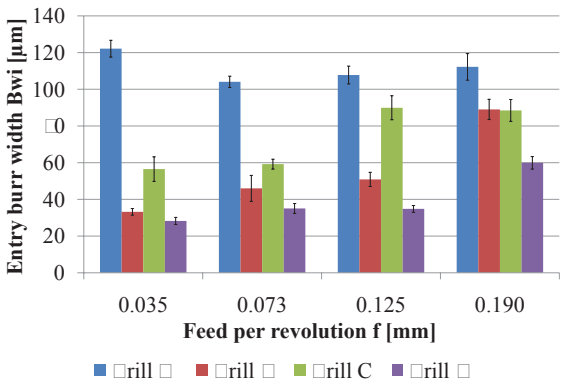

Figure 8.13: Comparison of entry burr widths resulting from four different drill geometries tested.

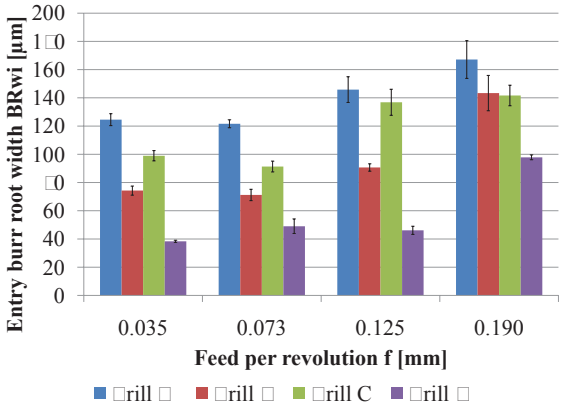

Figure 8.14: Comparison of entry burr root width resulting from four different drill geometries tested.

Figure 8.15: Photograph of hole entry burrs, Drill A, 1st setting ($v_c = 226\,\mathrm{m} \cdot \mathrm{min}^{-1}$, $f = 0.190\,\mathrm{mm}$).

Exit burrs

Exit burrs were not measured for drill A due to unfinished drilling at the hole exit because of insufficient drill overrun (see Figure 8.16 and Figure 8.17 for photographs). Drilling of full drill diameter with double cone drill geometry required longer drilling length (see Figure 8.1 for photograph of double cone drill A). The drill overrun used was 1.1 mm and full drill diameter of Drill A was distant 1 mm from the drill tip. It was decided not to repeat the test due to apparent unacceptable excessive entry burrs evaluated in previous section.

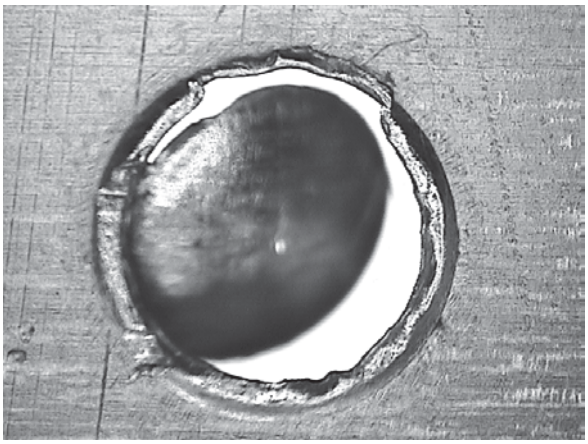

Figure 8.16: Photograph of hole exit burr, Drill A, 1st setting ($v_c = 226\,\mathrm{m \cdot min^{-1}}$, $f = 0.190\,\mathrm{mm}$).

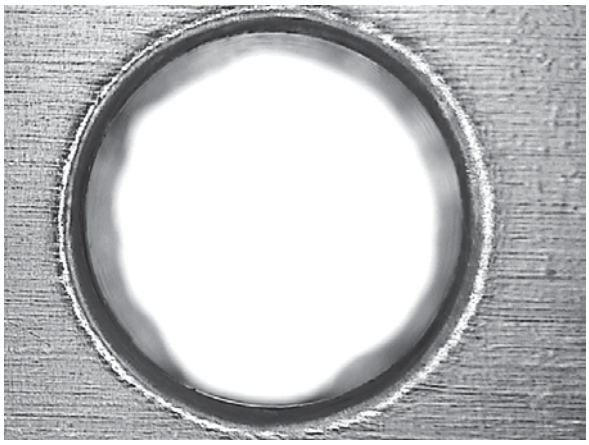

Figure 8.17: Photograph from hole entry side of Figure 8.16. Unfinished full drill diameter at the hole exit.

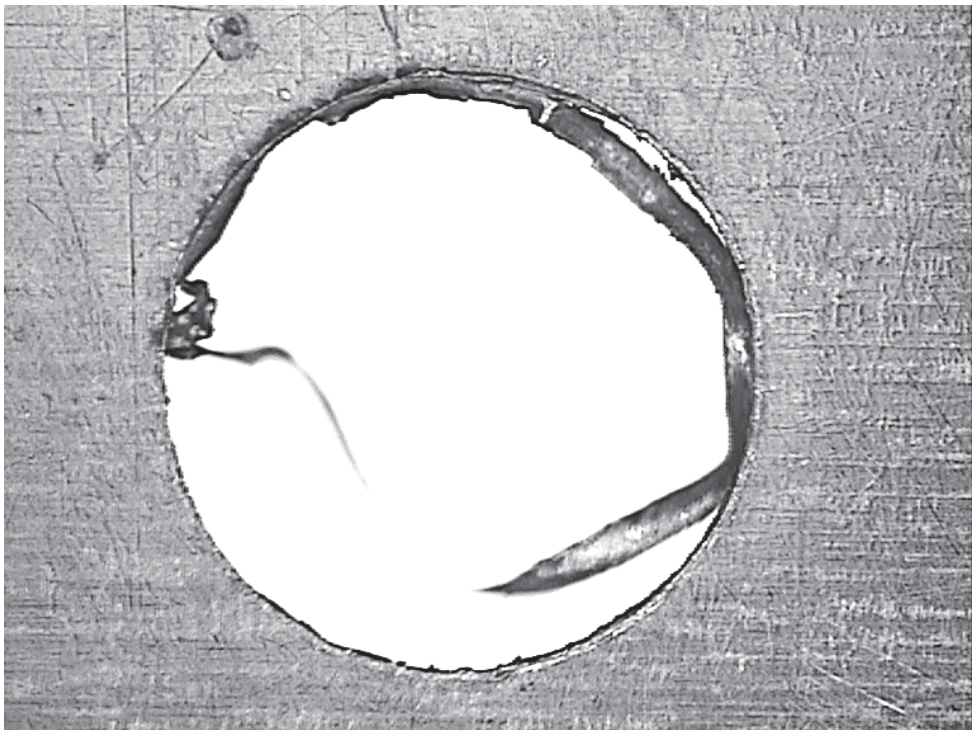

Figure 8.18: Hole exit drilled by Drill A ($v_c = 226\,\mathrm{m \cdot min^{-1}}$, $f = 0.073\,\mathrm{mm}$).

In spite of the most of drilled holes were not finished, advantageous burr formation was expected from Drill A due to double cone point geometry. The breakthrough force, as previously discussed in Chapter 8.5.1 dealing with force measurements, was much lower compared to other two fluted drills used, which is very favourable for less workpiece material to be formed into exit burr. The burr formation process can be seen from Figure 8.16, where crack separating drilling cap from burr was created at the corners of first cone at drill tip. There was still enough support material allowing ongoing cutting and less remaining material which undergo plastic deformation with following feed movement. Moreover, the resulting cutting force direct more to the surface material, due to sharp second point angle, which is less favourable for bending out of the remaining material and the drill cuts off the rest of the material by second cone grounded on drill point, leaving burr free edge (see Figure 8.19).

Exit burr heights

It is difficult to draw meaningful conclusion about hoe the drill geometries affect the exit burr formed, since the clamping system used is the predominant factor. Any defect in clamping system providing room for burr formation would be reflected in results and misrepresenting the influence of drill geometry itself.

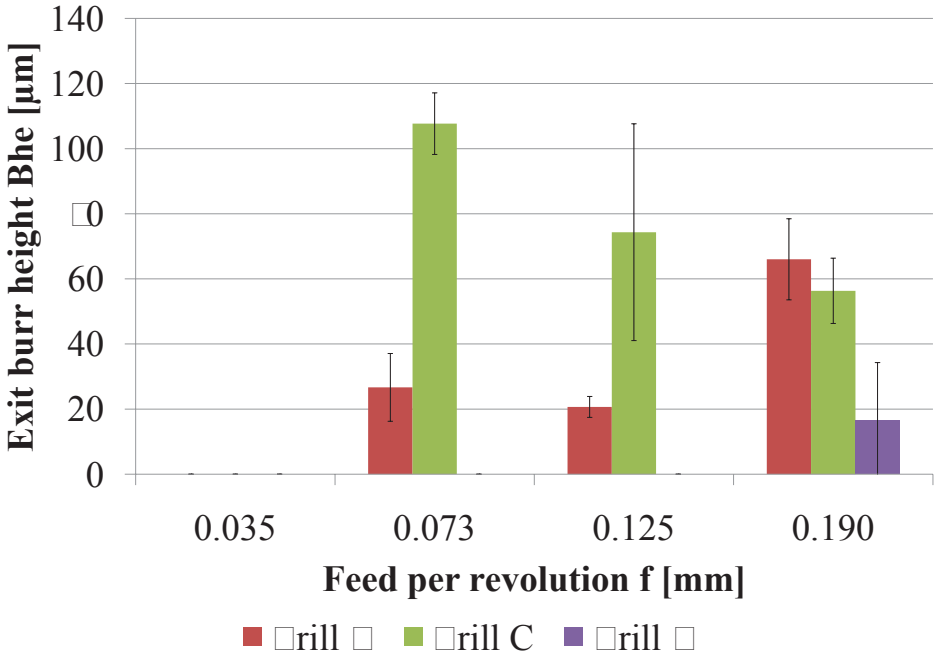

Figure 8.19: Comparison of exit burr heights resulting from four different drill geometries tested.

Measured exit burr heights resulting from Drill B, C and D used are shown in the graph in Figure 8.19. As seen, low feed resulted in burr free edges at hole exit for all the three drills evaluated. Drill D outperformed other drills tested and provided burr free edges at drill exit for all feeds used except the highest one, where small amount of burr was created at some portion of hole circumference. Drill B provided small volume of burr formed with higher feeds and increased with the greatest feed utilized. Drill C

created the biggest exit burr height as expected from maximal thrust force exerted at the drill breakthrough, previously discussed in force measurement results in Chapter 8.5.1.

Exit burr widths

As seen from the graph in Figure 8.20 and Figure 8.21, Drill D created the lowest burr widths and greatly outperformed other drills tested. This drill geometry provided burr free edges at the drill exit for all feeds tested, except the greatest one where small amount of burr was created. Other drills tested, Drill B and Drill C, shown increasing burr widths with increasing feed rate used.

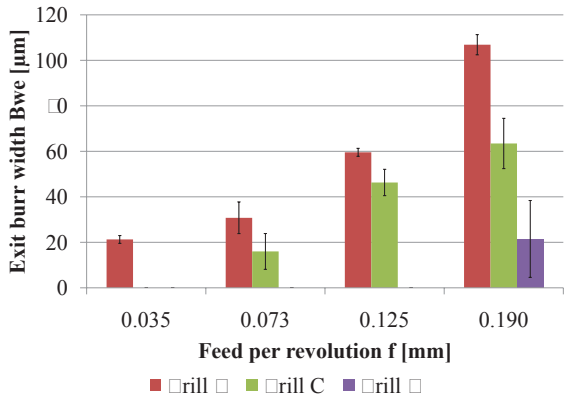

Figure 8.20: Comparison of exit burr widths resulting from four different drill geometries tested.

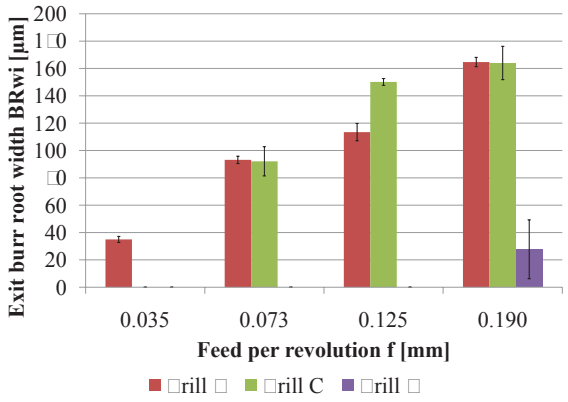

Figure 8.21: Comparison of exit burr root width resulting from four different drill geometries tested.

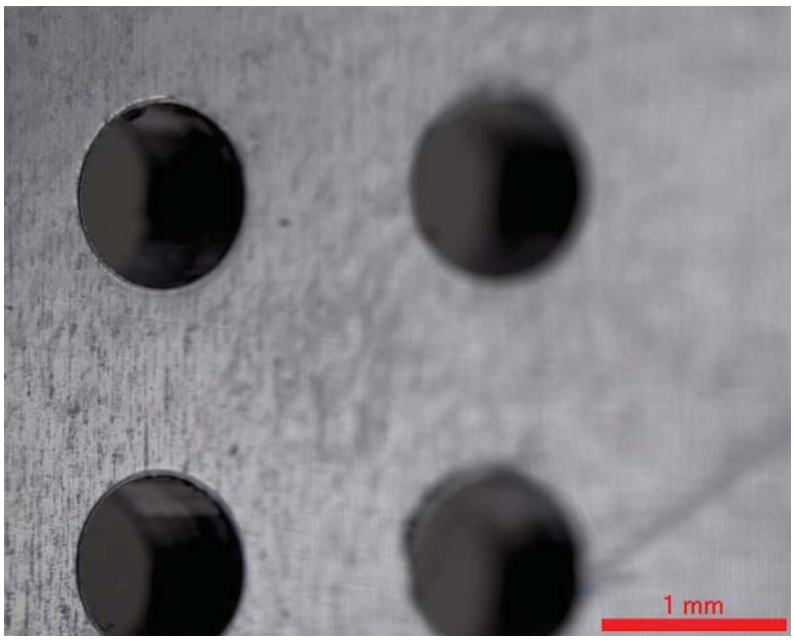

Figure 8.22: Photograph of hole exit burrs, Drill D, 1st setting ($v_c = 226\,\mathrm{m} \cdot \mathrm{min}^{-1}$, $f = 0.190\,\mathrm{mm}$).

8.5.3 Uniformity of drilled holes

Visual checking

All the drilled samples were visually checked for problems causing visual non uniformity in drilled holes. Drill exit side was free of any defects for all the sheet samples. Since the sheet workpieces were covered with protective foil on drill entry side, no scratches on entry side were revealed after removing of the foil. Hole entry problem previously discussed in Chapter 6.6.3 was seen to be present only with setting of the highest speed and very low feed (0.01 mm) for all drill geometries except Drill A providing excessive entry burrs. In this setting, slight shiny ring around entry hole circumference appeared at few holes drilled, caused by drill wandering at the sheet surface. With higher feed rates utilized, this defect was seen to be restricted due to stabilization of the drilling process by more advantageous ratio of uncut chip thickness to cutting edge radius resulting in a more favourable cutting process.

Cross-sectional metallographic samples

In order to gain better understanding of burr formations and structural changes in workpiece material caused by high speed cutting and high deformations, metallographic samples were investigated under microscope. Detailed investigation in structural changes was not of goals of present work, thus only two samples were chosen to be investigated as two opposing cases.

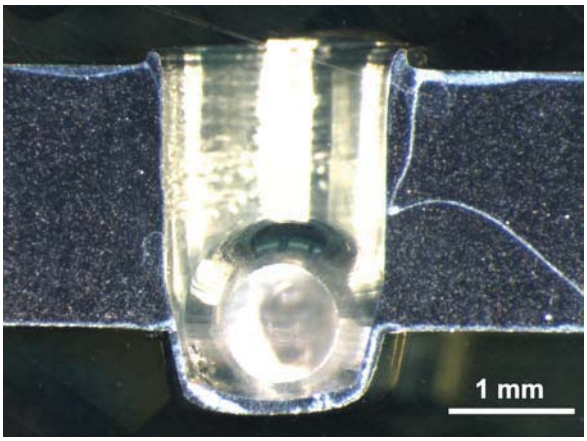

Figure 8.23: Cross-section view of incompletely drilled hole with double cone Drill A, aggressively fed ($v_c = 94\,\mathrm{m{\cdot}min^{-1}}$, $f = 0.457\,\mathrm{mm}$, setting A20).

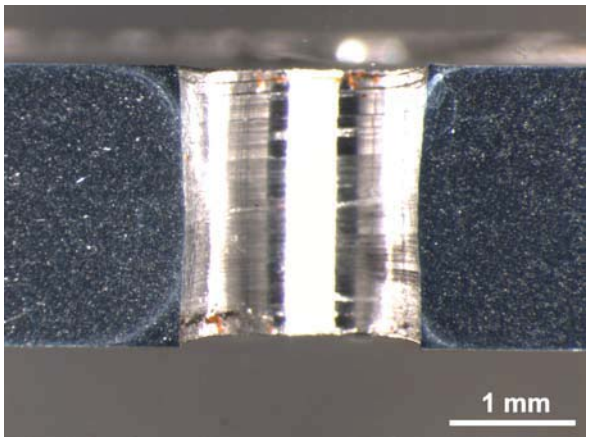

Figure 8.24: Cross-section view of hole drilled with Drill D, resulting in burr free edges ($v_c = 226\,\mathrm{m \cdot min^{-1}}$, $f = 0.190\,\mathrm{mm}$, setting D1).

The first sample chosen was incompletely drilled hole with double cone Drill A, when very aggressive feed rate was utilized ($v_c = 94\,\mathrm{m \cdot min^{-1}}$, $f = 0.457\,\mathrm{mm}$, setting A20). This setting resulted in an excessive entry burr (Figure 8.25) and workpiece material being formed into drilling cap and material to be cut off as swarf or sheared out into burr by subsequent feed movement of the drill at hole exit side (see Figure 8.26 and Figure 8.23 for entire cross-section of the hole drilled).

The second sample under investigation was hole drilled by Drill D, when setting providing the highest productivity was utilized ($v_c = 226\,\mathrm{m \cdot min^{-1}}$, $f = 0.190\,\mathrm{mm}$ —

maximum of the machine tool for long term production), resulting in burr free edges at hole exit (Figure 8.28) and very small amount of burr created at hole entry (Figure 8.25).

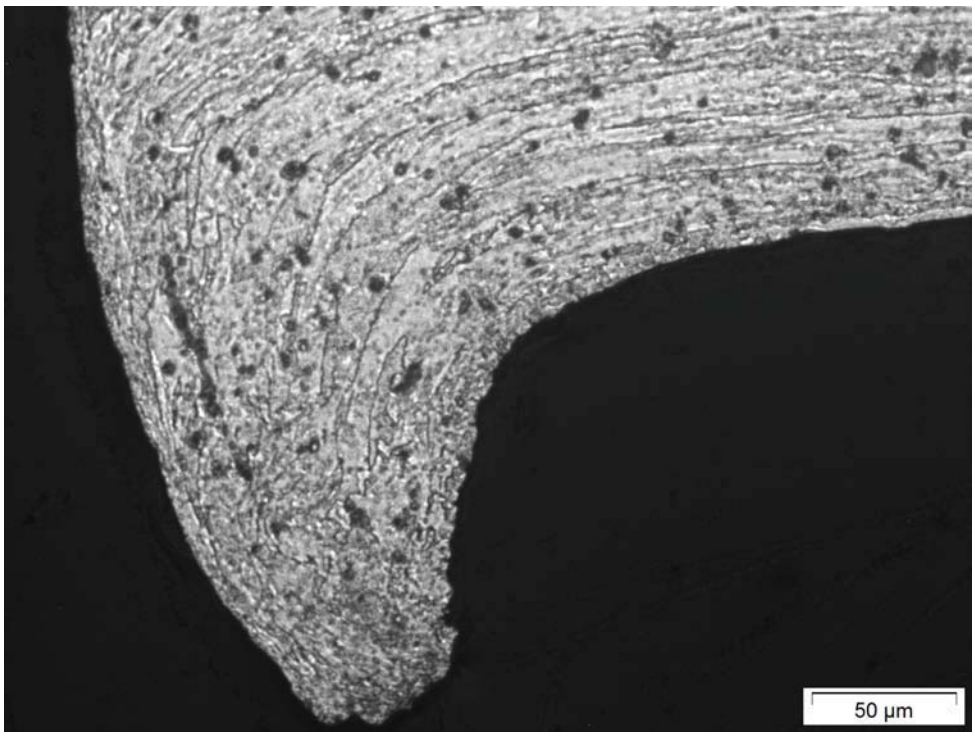

Figure 8.25: Etched cross-section view of entry burr, Drill A, zoomed on Figure 8.23.

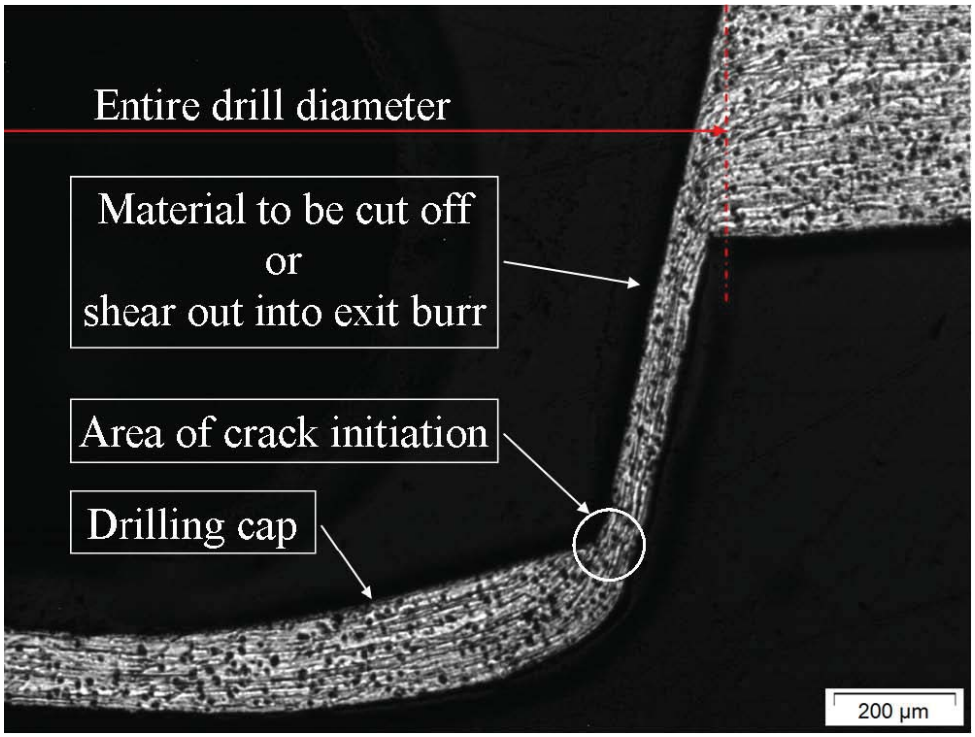

Figure 8.26: Etched cross-section view of exit burr, Drill A, zoomed on Figure 8.23.

From the photographs, aluminium grains oriented from rolling process of the sheet and of great size resulting from annealing process can be seen. In highly deformed areas as shown in Figure 8.26 the texture got denser due to work hardening, resulting in harder burr/swarf material.

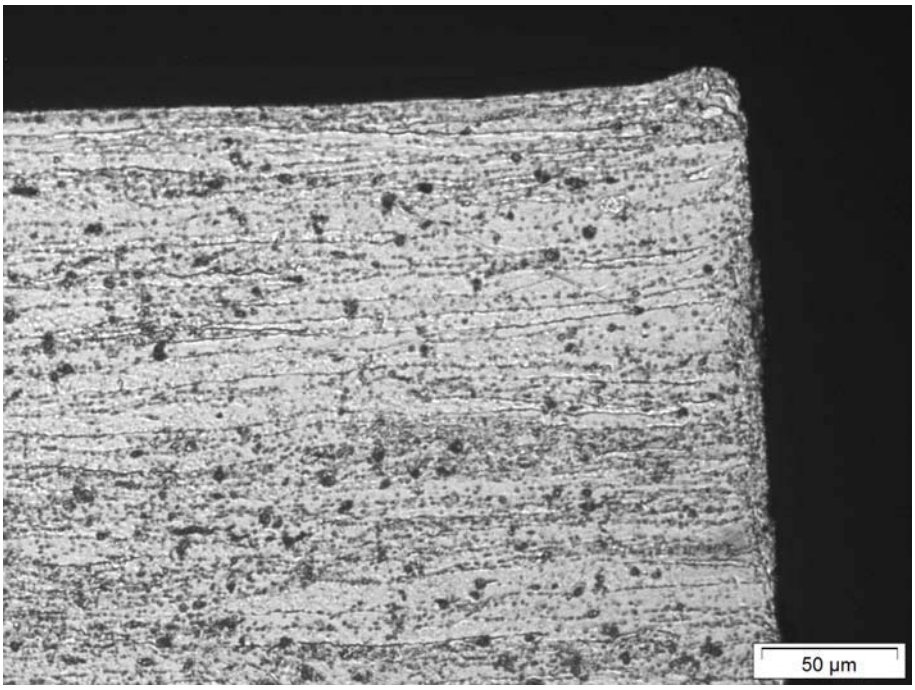

Figure 8.27: Etched cross-section view of hole entry edge, Drill D, zoomed on Figure 8.24.

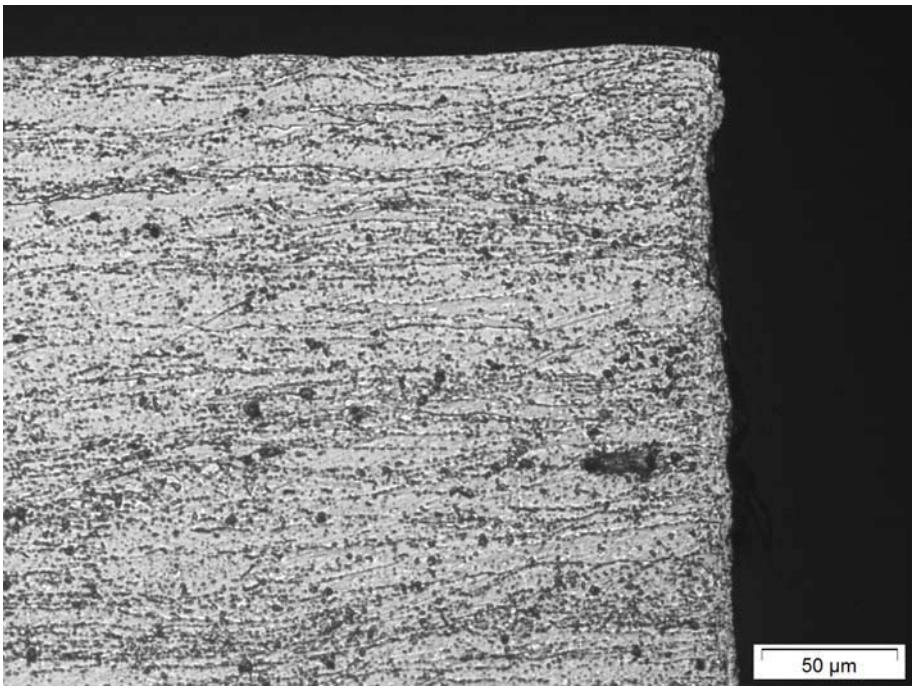

Figure 8.28: Etched cross-section view of hole exit edge, Drill D, zoomed on Figure 8.24.

8.6 Summary

The experimental work undertaken to find a drill geometry suitable for minimizing burrs at both entry as well as exit side of drilled holes, reaching high production productivity, and ensuring uniform appearance of drilled holes was done in the present chapter. Initially, four different drill geometries were selected for investigation, based on previous researches pertinent to the project goals. Subsequently, experimental drilling tests with wide ranges of cutting data tested and 200 holes drilled for each setting were performed. This was done in order to investigate influence of different drills on burr formation and occurrence of any errors causing non-uniformity in visual appearance of drilled holes. Special vacuum clamp fixture with using soft neoprene rubber vacuum seal, completely filling into the sealing grooves when clamped and providing no freeboard between the sheet plate and the clamp fixture, and dovetail shaped sealing grooves, in order to avoid any swarf or debris falling into the sealing grooves and to keep the sealing cord in place during the process of repeated changing of the sheet workpieces, was used during the test. With respect to project goals, burr reduction and high production productivity was required. Based on results from the preliminary test, where the highest cutting speed proved to be advantageous for both named requirements, it was of interest to investigate the highest cutting speed used for all drill geometries tested in detail. Since the error causing the so called "star effect at entry hole" was seen to be reduced with increasing feed and the burr volume tends to be greater with increasing feed rate, it was of interest to investigate different feed rates used and consequently find an optimal setting for the production. Therefore, the thrust force and burr measurements were performed for the highest cutting speed used (given by machine tool capability) with four levels of feed rate.

The results show that a 3 flute drill (Drill D) outperformed the other 2 flute drill geometries tested, requiring only approximately 50 % of thrust force, compared to the other drills tested, when the highest cutting speed together with the highest feed rate utilized, providing the highest productivity reachable with machine tool used. Therefore, less workpiece material underwent the plastic deformation, resulting in burr free hole exit. Average burr formed at hole entry was of small size 20 μm high and 60 μm wide, with root of the plastically deformed material into the entry burr 100 μm wide from drilled hole periphery. Other drills tested resulted in greater burr volume formed on both sheet sides. Even though that purchase costs of Drill B are five time less in comparison with other drills tested, a frequent problem with swarf clogging in the drill flutes was experienced and this drill is not recommended for production. The problem with clogged flutes can cause hole entry defects resulting from a drill cap stuck on a drill tip. A tool breakage due to insufficient chip flow or force overload during the drill retraction movement may occur when a drill clogged with swarf. This results in a tendency to pull the workpiece away from the vacuum clamp, which exerts an opposing force. Double cone Drill A provided excessive, non-permissible entry burrs and it's advantage in exit burr reduction due to less breakthroug thrust force could not be proved because of insufficient drill overrun used during the test. However, some of the holes resulted in burr free drill exit edge and optimization of such drill geometry is one possible topic for future study.

Defects causing so called "star effect at hole entry" was experienced only when very low feed rate used and was proven to be eliminated with increase in feed, using

short drill length, and drill points warranting good self-centering capability.

Chapter 9

Conclusions

The desired quality of the metal drilling process includes a minimal amount of burrs and a uniform appearance of the drilled holes. This is important in order to increase structural integrity and to possibly eliminate the needs for costly deburring operations. Three separate experiments were performed on a 2 mm sheets of wrought aluminium alloy Al99.7Mg0.5Cu-H24, using 1.6 and 2 mm diameter drills. The cutting conditions, the clamping conditions, and the drill geometry were varied in order to optimize the process and reach desired quality.

The first experiment revealed that the height and the width of the burr are reduced at both entry and exit sides of a metal sheet when a higher cutting speed was applied. With greater feed rates, the burr height and width increase on both sides, with the exception of the height of burrs on the entry side, which may be minimally decreased. Variation in burr dimensions was reduced when higher cutting speed was used, leading to process stabilization. The burr formed were uniform with a drilling cap. Measurements of the thrust force have shown the effect of material thermal softening, resulting in lower cutting forces required when the high cutting speed was used. Measurements of the drilling torque determined the maximum power output of high speed spindle to be insufficient for consequent tests. A defect causing the so called "star effect at hole entry" , represented by shiny ring around the hole periphery, determined as being caused by a conical defect at drill entry. This defect reflects light in different directions compared to other properly drilled holes, causing non-uniform hole appearance. This defect was caused by drill wandering on the workpiece surface when drilling was initiated. This phenomenon was eliminated through the use of a high feed rate and short drill length.

The measured data from the second experiment have shown that a properly designed vacuum clamp fixture can be used to significantly reduce exit-side burr formation. The vacuum seal implemented in the clamping device was not compressed enough to entirely fit into the groove, leaving no freeboard between the sheet and the fixture. This freeboard provided room for exit burr formation and stabilized exit burr height at about 250 μm. Defects in the form of scratches at the exit hole periphery appeared when high cutting speeds were used. This defect was caused by swarf rotated by the drill in between the aluminum sheet and the clamp fixture, causing radial scratches and torn exit burrs. This defect and exit burr formation can ideally be eliminated with a properly designed fixture that limits the amount of freeboard between the drilled

sheet and clamp fixture.

The third experimental test was performed using four different drill geometries. A 3-flute drill, Drill D, required only about 50 % of the thrust force in comparison with other 2-flute drill geometries tested, with the highest cutting speed and the highest feed rate set, providing the best possible productivity with the present machine tool used for the experiment. Due to the lower thrust force exerted, less workpiece material was subjected to plastic deformation, resulting in burr-free hole exit. The entry burr formed was of a small size, easily removable by a consequent anodizing process. Other drill geometries resulted in greater burr volume formed on both metal sheet sides. Although the purchase cost of Drill B is five times lower than of other drills tested, a frequent problem with swarf clogging in the drill flutes was experienced and this drill is not recommended for production. The problem with clogged flutes can cause hole entry defects resulting from a drill cap stuck on a drill tip. A tool breakage due to insufficient chip flow or force overload during the drill retraction movement may occur when a drill clogged with swarf. This results in a tendency to pull the workpiece away from the vacuum clamp, which exerts an opposing force. The trend in measured thrust force revealed advantageous reduction of breakthrough thrust force of a double cone point geometry of Drill A, which may result in less material volume formed into the exit burr. Though this could not be proven due to insufficient drill overrun used during the test, some of the holes resulted in burr-free drill exit and optimization of such drill geometry is one possible topic for future study. Conversely, this geometry resulted in an unacceptably large entry burr volume. Thus, it was decided not to repeat the test with proper drill overrun. Defects causing the so called "star effect at hole entry" were only experienced when a low feed rate was used. Its elimination was proven to be reachable with increase in feed, using short drill length, and drill points warranting good self-centering capability.

The three flute drill, Drill D, with a properly constructed vacuum fixture and the following cutting conditions were found to eliminate both entry and exit burrs: cutting speed $v_c = 226\,\mathrm{m} \cdot \mathrm{min}^{-1}$, 2 mm diameter drill, resulting in spindle rotations of $n = 36\,000\,\mathrm{min}^{-1}$, high feed of $f = 0.190\,\mathrm{mm}$, and flood coolant applied. The demand for the uniform appearance of drilled holes was fulfilled along with the high productivity requirement. Such optimized processes requires no additional deburring operations and result in a noticeable reduction in production cost.

9.1 Suggestions for future work

The investigations of the present work have provided a basis of knowledge in an effort to understand the causes of burr formation and variations in quality of drilled holes. Some suggestions for further research that may yield improvements of the production process are given bellow.

- Perform tool life tests with the tool proposed (Drill D) for the production process.
- An optimization of the double cone (chamfered) drill point geometry for drilling in aluminium. This geometry has proven to have an advantageous distribution of thrust force, minimizing the breakthrough thrust force responsible for the

amount of the workpiece material which undergo the plastic deformation at the drill exit. In contrast, the sharp point angle of the second cone resulted in an excessive entry burr.

- Simulation of the chip and the burr formation process. An extensive number of experimental studies would need to be performed in order completely optimize the drill geometry. This is due to the large number of variable geometry parameters. Moreover, other workpiece materials have different properties that affect these parameters and make the optimized results non-transferable to other materials..
- Improvements in clamping system. The tighter and closer the clamping force is applied in the vicinity of the hole drilled, the less space there is for burr formation.
- Reduction of vibrations and the drill wobbling. A wobbling drill causes a bigger hole diameter in the clamp fixture, resulting in room for burr formation when another hole with a smaller diameter is steadily drilled.

Bibliography

[1] Montgomery, D. C., *Design and Analysis of experiments*. John willey & Sons, Inc., 2005, 6th ed., ISBN 0-471-48735-X, 638 pp.

[2] BMW in the News. [online] [cit. 2011-04-19], URL `http://www.bmwinthenews.com/bmw-concept-features-bang-olufsen-sound-system/`.

[3] Aurich, J. C., et al., Burrs — Analysis, control and removal. *CIRP Annals — Manufacturing Technology*, vol. 58, no. 2, 2009, pp. 519–542.

[4] Cartype Inc. [online] [cit. 2011-04-19], URL `http://www.cartype.com/pages/400/audi_related_emblems`.

[5] Coromant, A. S., *Modern Metal Cutting — a practical handbook*. AB Sandvik Coromant, 1994, ISBN 91 - 97 22 99 - 0 - 3, XI-1–XI-61 pp.

[6] Thomas J. Drozda, C. W., *Tool and Manufacturing Engineers Handbook: Machining*. Society of Manufacturing engineers (SME), Dearborn, Michigan, 1983, ISBN 0872630854.

[7] S. Kalpakjian, S. R. S., *Manufacturing Engineering and Technology*. Prentice—Hall, Inc., 2001, 4th ed., ISBN 0201361310, 1148 pp.

[8] ISO 3002/1-2009 Basic quantities in cutting and grinding — Part 1 : Geometry of the active part of cutting tools — General terms, reference systems, tool and working angles, chip breakers.

[9] Forejt, M., Píška, M., *Teorie obrábění, tváření a nástroje (Metal cutting and forming theory, tools)*, vol. 1. Akademické nakladatelství Cerm, s.r.o. Brno, 2006, ISBN 80-214-2374-9, 223 pp.

[10] Shaw, M. C., *Metal Cuting Principles*. Oxfor University Press, New York, Oxford, 2005, 2nd ed., ISBN 0-19-514206-3, 651 pp.

[11] King, R. I., *Handbook of High-Speed Machining Technology*. Chapman and Hall, 1985, ISBN 0412008114, 471 pp.

[12] Melkote, S., et al., Interfacial Burr Formation in Drilling of Stacked Aerospace Materials. In *Burrs - Analysis, Control and Removal*, edited by Aurich, J. C., Dornfeld, D., Springer Berlin Heidelberg, 2010, ISBN 978-3-642-00568-8, pp. 89–98.

[13] ISO 13715:2000. Geometrical Product Specifications (GPS) – Technical drawings – Edges of undefined shape, vocabulary and indications, International Organization for Standardization, Geneve, Switzerland.

[14] Dornfeld, D., Min, S., A Review of Burr Formation in Machining. In *Burrs - Analysis, Control and Removal*, edited by Aurich, J. C., Dornfeld, D., Springer Berlin Heidelberg, 2010, ISBN 978-3-642-00568-8, pp. 3–11.

[15] Hashimura, M., Hassamontr, J., Dornfeld, D., Effect of In-plane Exit Angle and Rake Angles on Burr Height and Thickness in Face Milling Operation. *Journal of Manufacturing Science and Engineering*, vol. 121, no. 1, 1999, pp. 13–19.

[16] Gillespie, L. K., Blotter, P. T., The Formation and Properties of Machining Burrs. *Transactions of ASME Journal of Engineers for Industry*, vol. 98, 1976, pp. 66–74.

[17] Gillespie, L. K., Deburring, an Annotated Bibliography. *Technical Paper. Society of Manufacturing Engineers*, vol. III, no. MRR76-07, 1976, pp. 1–59.

[18] Gillespie, L. K., *Deburring and Edge Finishing Handbook*. Society of Manufacturing Engineers, 1999, ISBN 0872635015, 404 pp.

[19] Kim, J., Min, S., Dornfeld, D. A., Optimization and control of drilling burr formation of AISI 304L and AISI 4118 based on drilling burr control charts. *International Journal of Machine Tools and Manufacture*, vol. 41, no. 7, 5 2001, pp. 923–936.

[20] Ko, S.-L., Lee, J.-K., Analysis of burr formation in drilling with a new-concept drill. *Journal of Materials Processing Technology*, vol. 113, no. 1-3, 6/15 2001, pp. 392–398.

[21] Min, S., et al., Finite Element Modeling of Burr Formation in Metal Cutting. *Machining Science and Technology: An International Journal*, vol. 5, no. 3, 2001, pp. 307–322.

[22] Gillespie, L., The measurement of burrs. *SME Technical Paper*, vol. MR74-993, 1974.

[23] Schäfer, F., *Entgraten*. Krausskopf-verlag, 1975.

[24] Hoang, H., Ko, S., Burr Measurement Systemfor Drilled Hole at Inclined Exit Surface. In *Burrs - Analysis, Control and Removal*, edited by Aurich, J. C., Dornfeld, D., Springer Berlin Heidelberg, 2010, ISBN 978-3-642-00568-8, pp. 157–165.

[25] Leopold, J., Schmidt, G., Methods of Burr Measurement and Burr Detection. *VDI-Berichte 1860*, 2004, pp. 223–229.

[26] Schwenke, H., et al., Optical Methods for Dimensional Metrology in Production Engineering. *CIRP Annals - Manufacturing Technology*, vol. 51, no. 2, 2002, pp. 685–699.

[27] Gillespie, L., Inspecting for burrs. *Manufacturing Engineering*, vol. 120, no. 4, 1998, pp. 70–76.

[28] Link, R., *Gratbildung und Strategien zur Gratreduzierung*. Ph.D. thesis, RWTH Aachen, 1992.

[29] Pande, S. S., Relekar, H. P., Investigations on reducing burr formation in drilling. *International Journal of Machine Tool Design and Research*, vol. 26, no. 3, 1986, pp. 339–348.

[30] Lauderbaugh, L. K., Analysis of the effects of process parameters on exit burrs in drilling using a combined simulation and experimental approach. *Journal of Materials Processing Technology*, vol. 209, no. 4, 2/19 2009, pp. 1909–1919.

[31] Biermann, D., Heilmann, M., Burr Minimization Strategies in Machining Operations. In *Burrs - Analysis, Control and Removal*, edited by Aurich, J. C., Dornfeld, D., Springer Berlin Heidelberg, 2010, ISBN 978-3-642-00568-8, pp. 13–20.

[32] Sakurai, K., et al., High Feed Rate Drilling of Aluminum Alloy. *Material Science Forum*, vol. 331-337, 2000, pp. 625–630.

[33] Hamade, R. F., Ismail, F., A case for aggressive drilling of aluminum. *Journal of Materials Processing Technology*, vol. 166, no. 1, 7/15 2005, pp. 86–97.

[34] Elhachimi, M., Torbaty, S., Joyot, P., Mechanical modelling of high speed drilling. 2: predicted and experimental results. *International Journal of Machine Tools and Manufacture*, vol. 39, no. 4, 4 1999, pp. 569–581.

[35] Schey, J. A., Introduction to Manufacturing Processes. 2000.

[36] Alverio, J., Agapiou, J. S., Shen, C. H., High speed drilling of 390 aluminum. *Transactions of the North American Manufacturing Research Institution of SME 1990*, vol. Soc. Manufact. Eng., 1990, pp. 209–215.

[37] Kilickap, E., Modeling and optimization of burr height in drilling of Al-7075 using Taguchi method and response surface methodology. *The International Journal of Advanced Manufacturing Technology*, vol. 49, 2010, pp. 911–923, ISSN 0268-3768.

[38] Takazawa, K., The Challenge of Burr Technology and Its Worldwide Trends. *Japanese Society of Deburring and Surface Conditioning Technique*, vol. 22, no. 3, 1988, pp. 165–170.

[39] Min, S., *Modeling of Drilling Burr Formation and Development of Expert System*. Ph.D. thesis, University of California, Berkeley, 2001.

[40] Leitz, L., Franke, V., Aurich, J., Burr Formation in Drilling Intersecting Holes. In *Burrs - Analysis, Control and Removal*, edited by Aurich, J. C., Dornfeld, D., Springer Berlin Heidelberg, 2010, ISBN 978-3-642-00568-8, pp. 99–105.

[41] Sharma, N., *Preprocessing for Extracting Signal Buried in Noise Using LabVIEW*. Master's thesis, Thapar University, July 2010.

[42] M Seals, *O-ringe og tilbehør 005020.VER3.pdf*. [online] [cit. 2010-11-20], URL `http://www.m-seals.dk/en/download%20katalog`.

[43] Parker Hannifin Corporation, *Parker O-Ring Handbook*. [online] [cit. 2010-11-14], URL `http://www.logwell.com/tech/O-ring/Parker_Handbook.pdf`.

Nomenclature

Variable	Nomenclature	Unit
A	clamping area	[mm^2]
$A50$	elongation	[%]
A_D	transverse cross-sectional area of the undeformed chip	[mm^2]
Al	aluminum	
a_p	radial cutting depth	[mm]
b_D	undeformed chip width	[mm]
Bhe	exit burr height	[μm]
Bhi	entry burr height	[μm]
$BRwe$	exit burr root width	[μm]
$BRwi$	entry burr root width	[μm]
Bwe	exit burr width	[μm]
Bwi	entry burr width	[μm]
COV	coefficient of variation	[%]
Cu	cooper	
Cr	chromium	
d	diameter of primary hole	[mm]
D	drill diameter	[mm]
D_i	drill diameter of the tool point	[mm]
$EBhe$	excessive exit burr height	[μm]
f	feed per revolution	[mm]
F_{clamp}	clamping force	[N]
Fe	ferrum	
F_f	thrust force	[N]
f_m	minimal sampling frequency	[Hz]
f_n	nyquist frequency	[Hz]
f_s	sampling frequency	[Hz]
f_z	feed per tooth (edge)	[mm]
h_D	undeformed (uncut) chip thickness	[mm]
K_s	adjusted specific energy	[W $\cdot$ s $\cdot$ cm^{-3}]
L	total length of drill travel	[mm]
l	lenght of drilled hole	[mm]
l_a	length of approach	[mm]
l_o	lenght of overrun	[mm]
Mn	manganese	
Mg	magnesium	

Continued on the next page

Nomenclature continued from the previous page

Variable	Nomenclature	Unit
n	number of revolutions	$[\mathrm{min}^{-1}]$
p	pressure	[MPa]
P_f	assumed working plane	
Rm	ultimate tensile strength	[MPa]
$Rp0.2$	proof stress	[MPa]
Si	silicon	
STD	standard deviation	["as data"]
t	drilling time	[min]
T	torque	[Ncm]
t_0	initial drill contact with workpiece	[ms]
t_1	full drill diameter involved in cutting	[ms]
t_2	contact of the drill tip with bottom workpiece surface	[ms]
t_3	last drilling position — end of cutting	[ms]
Ti	titanium	
u	specific cutting energy	$[\mathrm{W \cdot s \cdot m}^{-3}]$
v_c	cutting speed	$[\mathrm{m \cdot min}^{-1}]$
$v_c i$	peripheral speed at the tool point	$[\mathrm{m \cdot min}^{-1}]$
v_e	resultant cutting speed	$[\mathrm{m \cdot min}^{-1}]$
v_f	feed speed	$[\mathrm{mm \cdot min}^{-1}]$
w	web thickness	[mm]
z	number or cutting edges of the tool	[-]
Zn	zinc	
α_n	tool normal clearance	[deg]
β_n	normal wedge angle	[deg]
γ_e	tool effective rake angle	[deg]
γ_n	tool normal rake angle	[deg]
δ	helix angle	[deg]
η	resultant cutting speed angle	[deg]
κ_r	cutting edge angle	[deg]
$2\kappa_r$	point angle	[deg]
λ_s	tool cutting edge inclination	[deg]
φ, ε	feed motion angle	[deg]
θ	an angular proportion of an excessive burr	[μm]

List of abbrevations

Abbrevation	Nomenclature
AW	wrought aluminium
BUE	built up edge
CAD	computer aided design
CNC	computer numeric control
DOE	design and analysis of engineering experiments
FFT	fast fourier transform
FIR	finite impulse response filter
NBR	nitrile butadiene rubber
RMS	measure root mean square